DOCTORAL THESIS

Properties of poly(lactic acid) in presence of cellulose and chitin nanocrystals

Shikha Singh

Wood and Bionanocomposites

This thesis is the result of a collaboration between Luleå University of Technology & Universitat Politècnica de Catalunya that aims toward a double degree (DocMASE)

UNIVERSITAT POLITÈCNICA DE CATALUNYA BARCELONATECH

LULEÅ TEKNISKA UNIVERSITET

Properties of poly(lactic acid) in presence of cellulose and chitin nanocrystals

A thesis submitted to Luleå University of Technology and Universitat Politècnica de Catalunya for double degree of Doctor of Philosophy (DocMASE) by

Shikha Singh

Department of Engineering Science and Mathematics at LTU and
Department of Materials Science and Engineering at UPC

Thesis supervisor: Prof. Kristiina Oksman and co-supervisors Dr. Shiyu Geng and Prof. Maria Lluïsa Maspoch Rulduà

October 2020

Principal Supervisor:

Professor Kristiina Oksman (Luleå Tekniska Universitet, Sweden)

Co-Supervisor:

Professor Maria Lluïsa Maspoch (Universitat Politècnica de Catalunya, Spain)

Co-Supervisor:

Dr. Shiyu Geng (Luleå Tekniska Universitet, Sweden)

Faculty Opponent:

Professor Alfonso Jimenez (Universitat d'Alacant, Spain)

Evaluation Committee:

Professor Mikael Skrifvars (Chalmers Tekniska Universitet, Sweden)

Associate Professor Giada Lo Re (Chalmers Tekniska Universitet, Sweden)

Professor Fabiola Vilaseca (Universitat de Girona, Spain)

Printed by Luleå University of Technology, Graphic Production 2020

ISSN
ISBN (print)
ISBN (pdf)

Luleå 2020

www.ltu.se

"If you want to walk fast, walk alone. But if you want to walk far, walk together"

~Rattan Tata

ACKNOWLEDGMENTS

The journey of Ph.D. has arrived on the verge of the completion and it would have not been possible to walk that long without the support and help of some of the wonderful persons. I would like to acknowledge the European Commission for the financial support of DocMASE programme (Project grant: 02-2015). Next, I would like to acknowledge and thank my alma maters, Luleå University of Technology (LTU), Sweden, and Universitat Politècnica de Catalunya (UPC), Spain for providing infrastructure and instrument support for conducting research. I would also like to acknowledge the University of Saarland (UdS), Germany for facilitating the funding for 3 years of my scholarships and Bio4Energy, strategic research program for funding the 4th year of the Ph.D.

The most important pillars of this voyage are the supervisors; therefore, firstly I would like to express my gratitude to my principal supervisor Prof. Kristiina Oksman for giving me an opportunity to work on this project. Her constructive ideas, honest and organized work approach, kind guidance and support provided during the Ph.D. have immensely helped me. She has inspired me in many ways. Her hard-working and perseverance nature would certainly create a positive impact on my future endeavours. Likewise, I am grateful to my co-supervisor Prof. Maria Lluïsa Maspoch Rulduà for her kindness, patience, care, very well organized work practice, and important advice. I am also thankful to my assistant supervisor and senior Dr. Shiyu Geng for her valuable suggestions, help, and providing the training for several laboratory equipments. I am lucky to have such an amazing persons who not only taught me the professional lessons but also the personal ones.

I would like to pay my utmost regards to Prof. Frank Mücklich, who was the preacher of this journey. He was the first person who informed me about the DocMASE programme and introduced to Dr.-Ing. Flavio Soldato, another kind, and humble person, whom I met in this journey. I am thankful to the whole DocMASE team for their generous supports and for making happy and informative summer school days. I enjoyed the DocMASE events. Thank you for organizing those meetings, workshop and conferences. It was a nice platform to meet new people across the globe and discuss research topics in the working hour and about language, culture, cuisine in leisure time.

I would like to extend my gratitude to Prof. Lennart Wallström for his unconditional help and fruitful suggestions. I am thankful to Johnny Grahn and Lars Frisk for the technical support during the experiments and interesting conversations about the

Swedish system and culture in the spare time. I would also like to thank the administrative staff of LTU, Birgitta Lidström, and Ihrene Niva-Strand for their assistance.

My sincere gratitude is given to all my former and present colleagues of wood and Bionanocomposites at LTU. Specifically, I would like to thank Dr. Maxime Nöel, Dr. Natalia Herrera, Dr. Anshu Anjali Singh, Dr. Shokat Sarmad, and Prof. Dip-Ing. Daniel Schwendemann and Dr. Helena Oliver Ortega for their valuable help. I would like to convey my sincere thanks to the friends and current colleagues of the wood and Bionanocomposites group; Dr. Linn, Dr. Gejo, Dr. Oisik, Simon, Annika, Mitul, Bony, Farida, and Luisa for the enjoyable time at the fika room and good support in the lab.

I would also like to convey my gratitude to all of my co-workers at CCP and UPC. I am grateful to Prof. Orlando Santana Perez for his valuable contributions and important discussions for the project work. I am also grateful to Prof. Christina Rodriguez for her contributions and help. Assistance provided by Prof. Miguel Sanchez-Soto and Dr. Tobis Abt is commendable and I am thankful for their help in the lab. My time in Spain would not have been that pleasant without friends and colleges. I am highly thankful to Dr. Noel León for helping and giving company to me for getting an extension of my visa in Spain. I would like to convey my regards to my all colleague of the UPC including Hakim, Daniel, Violeta, Magali, and Jonathan. I am also thankful to Irene-Perez, Anna Carreras, and Susana Ortiz for administrative help. I spent a joyful time because of these lovely and helpful people during my stay in Spain.

Apart from the professional world, I have some fantastic friends including Rashi, Thamali, Suchandra, Anuttam, Anvith, Reena, and many more who helped me in various ways and make this tough journey to a lighter and happier one. This is not the end; there are many friends and teachers, whose names must be included. They have continuously encouraged and helped me in the entire situation to every extent. Finally, I would like to thank God for blessing me with wonderful parents and siblings, who have always been a supportive pillar for me. Thank you my dear brother Vishal and loving sister Vaishali for giving me strength and happiness. I have no word to say about you; both mom and dad for your love, care, kindness, scarifies, what you have given to me those are unconditional and I am extremely thankful to God for giving you as my parents.

Shikha Singh

August 2020, Luleå, Sweden

LIST OF APPENDED PUBLICATIONS

PAPER I

Singh, S.; Maspoch, M. Ll; Oksman, K. Crystallization of triethyl-citrate-plasticized poly (lactic acid) induced by chitin nanocrystals, *Journal of Applied Polymer Science*, **2019**, 136 (36), 47936, DOI: 10.1002/app.47936

Contributions: Participated in planning, performed main experiments (prepared isothermally crystallized films, performed crystallization study including kinetics, and structural, thermal test) analyzed the data and played a lead role in writing the manuscript.

PAPER II

Singh, S.; Patel, M.; Schwendemann, D.; Zaccone, M.; Geng, S.; Maspoch, M. Ll; Oksman, K. Effect of chitin nanocrystals on crystallization and properties of poly(lactic)-based nanocomposites, *Polymers,* ***2020,*** 12 (3), 726***,*** DOI: 10.3390/polym1230726

Contributions: Participated in planning, performed main experiments including preparation of isothermally crystallized films of materials and their crystallization study, performed structural, thermal, optical, water barrier, water uptake and hydrolytic degradation test. Dr. Marta Zaccone performed oxygen barrier test and Mitul Patel and Daniel Schwendemann prepared nanocomposite materials using liquid assisted extrusion. Analysed the data of tested materials and played a lead role in writing the manuscript.

PAPER III

Singh, S.; Patel, M.; Schwendemann, D.; Geng, S.; Herrera, N.; Maspoch, M. Ll; Oksman, K. Effect of orientation on PLA/chitin nanocomposite films with a combination of melt and solid-state drawing (manuscript under preparation)

Contributions: Participated in planning, performed most of the experiments including solid-state drawing, structural, mechanical, thermal, optical test. Dr. Natalia Herrera prepared nanocomposites using liquid assisted extrusion process, Mitul Patel and Daniel Schwendemann performed melt-sate drawing of the nanocomposite. Analysed the data and played a lead role in writing the manuscript.

PAPER IV

Singh, S.; Rodriguez, C.; Santana, O.; Oksman, K.; Maspoch, M. Ll; Evaluation of Mechanical Properties of Poly (Lactic Acid)/Cellulose Nanocrystal Nanocomposites: A Comparative Study of Conventional Tensile Test and Small Punch Test, *eXRESS Polymer Letters*, **2020** (accepted manuscript), DOI: 10.3144/expesspolymlett.2020.92

Contributions: Participated in planning, performed main experiments including grafting of CNC, preparation of the materials and their films, birefringence, viscosity, thermal, mechanical, and structural tests. Small punch test was performed in collaboration with the co-authors. Analysed data and played a lead role in writing the manuscript.

CONFERENCE CONTRIBUTIONS

- Singh, S.; Oksman, K. Crystallization and trans-crystallization studies of PLA in the presence of chitin and cellulose nanomaterials, *International Materials Research Meeting (IMRM)*, 6-7 April **2017**, Saarbrücken, Germany (Oral presentation).

- Singh, S.; Oksman, K. PLA nanocomposites with polysaccharide as reinforcing agents, 4th International Conference on *Bio-Based Polymers and Composites (BioPoCo)*, 2-6 Sept **2018**, Balatonfüred, Hungary (Oral presentation).

- Singh, S.; Rodriguez, C.; Santana, O.; Oksman, K.; Maspoch, M. Ll; Evaluation of Mechanical Properties of Poly (Lactic Acid)/Cellulose Nanocrystal Nanocomposites: A Comparative Study of Conventional Tensile Test and Small Punch Test, 36th *Conference of the Spanish Group of Fracture* (GEF), 3-5 April, **2019,** Seville, Spain (Oral presentation).

LIST OF ABBREVIATIONS

AFM	Atomic force microscopy
CM	Compression molding
ChNCs	Chitin nanocrystals
CNCs	Cellulose nanocrystals
mCNC	Modified cellulose nanocrystals
DMF	N, N-dimethylformamide
DR	Draw ratio
DSC	Differential scanning calorimeter
FC	Film calendering
FTIR	Fourier transform infrared spectroscopy
G	Growth rate
GTA	Glycerol triacetate
HCl	Hydrochloric acid
H_m	Heat of melting
IC_{TEMP}	Isothermal crystallization temperature
IC_{TIME}	Isothermal crystallization time
IV	Intrinsic viscosity
K_g	Nucleation constant
kN	Kilo newton
M_n	Number average molecular weight
M_v	Viscosity average molecular weight
M_w	Weight average molecular weight
MSD	Melt-state drawing
μm	Micrometer
mm	Millimeter
nm	Nanometer
OP	Oxygen permeability
OTR	Oxygen transmission rate
OM	Optical microscopy
POM	Polarized optical microscopy
PLA	Poly(lactic acid)
TEC	Triehtyl citrate
SEM	Scanning electron microscopy
SPT	Small punch test
T_c	Crystallization temperature
T_{cc}	Cold crystallization temperature
T_g	Glass transition temperature

T_m	Melting temperature
SSD	Solid-state drawing
TGA	Thermo-gravimetric analysis
WVTR	Water vapor transmissions rate
WVP	Water vapor permeability
XRD	X-ray diffraction

ABSTRACT

Plastic based materials are widely used for industrial and domestic packaging application. However, disposal of such petroleum-based materials *e.g.* polyethylene (PE), polypropylene (PP), and polyethyleneterephthalate (PET) has become a huge threat to the environment. These materials are non-biodegradable and complex for waste management, which causes plastic-pollution in both land and marine eco-system. For a sustainable industrial and economic development, it is indeed an urgency to develop packaging materials, which are environmentally benign, easy for waste treatment and recycling, and less/non-toxic. However, developing suitable and efficient plastic-substituents needs multiple requirements to be fulfilled *viz.,* logistics and cost-effectiveness, good mechanical, thermal, optical and barrier properties, structural integrity of the constituents and morphological properties of the films. In this regard, utilizing bio-based polymers such as poly(lactic acid) (PLA), which originates from the natural resources, can be a viable and practical due to its low toxicity, biodegradability, and eco-friendly behavior. Moreover, it has good optical and mechanical properties, *e.g.* high stiffness (3-4 GPa) and strength (50-70 MPa), which are similar or comparable to the polymers used for packaging applications. However, pristine PLA poses few challenges to overcome before it finds real world applications. Especially, slow crystallization rate, low crystallinity, poor toughness (very brittle material) and, poor barrier properties (O_2 barrier) of PLA are particularly important aspects, which need to be modified and fine-tuned. Utilizing nano-reinforcements, such as nanocellulose and nanochitin, is a promising approach for modifying PLA because of raw materials abundancy; easily obtainable from forest-based and bio-waste, hence, utilizing such materials also help the sustainable bioeconomy. Chitin nanocrystals (ChNCs) and cellulose nanocrystals (CNCs) possess unique properties, such as, low density, biodegradability, low toxicity, good mechanical, and barrier properties; therefore, can act as suitable nano-reinforcements for PLA.

Homogeneous dispersion of the nano-reinforcements into the polymer matrix is crucial and challenging. To achieve good dispersion, primarily two methods were employed *viz.,* (a) liquid–assisted extrusion of PLA with ChNCs in the presence of plasticizers, and (b) surface modification of the CNC via grafting. First segment of the research was aimed to understand and gain an insight about the role of nano-reinforcements on the crystallization behavior of plasticized PLA *e.g.* crystallization kinetics including rate and temperature dependency, and morphology of the spherulites. ChNCs, due to large surface area, acted as better nucleating agent and improved the overall crystallization rate by reducing the crystallization time and size of the spherulites. Interestingly, rarely found neutral type of spherulites along with commonly occurring negative type, and multi ring-banded spherulites were observed at different crystallization time and temperature. Second part of the research was aimed to investigate the role of homogenously dispersed nano-reinforcements on the thermal, optical, barrier, and hydrolytic degradation properties of the nanocomposites. Noticeably, at a lower temperature (110°C), the highest rate of

crystallization achieved within 5 min. Furthermore, homogenous crystallization and smaller spherulite size (7 nm) of PLA achieved due to the good dispersion of ChNCs significantly improved the crystallinity, thermal, barrier, and hydrolytic degradation properties. Faster crystallization at lower temperature resulted in a smaller spherulites sizes, which improved the oxygen and moisture barrier properties by hindering permeation path of the gases. On the other hand, the synergistic effect of isothermal crystallization and ChNCs improves the rate of hydrolytic degradation. It is noticeable that nanocomposites showed better optical properties than the plasticized PLA even at same crystallization conditions. As mechanical properties play an important role in packaging applications. So, the third part of the research involved the study of mechanical properties of oriented films (PLA/ChNCs) achieved by a combination of solid-state and melt-state drawings. Melt state drawing of relatively higher amount (5 wt%) ChNCs with PLA was prepared to obtain oriented films. These oriented nanocomposites films exhibited excellent mechanical properties. For example, a tensile strength with 360%, elongation at break with 2400%, and the toughness with 9500% increment achieved as compared to un-oriented nanocomposite films. The degree of crystallinity of highly oriented nanocomposite films increased from 8% to 53% with respect to the un-oriented nanocomposite films and smaller crystallites sizes were observed. Drawing conditions including drawing temperature and speed had a strong impact on the properties. By utilizing this knowledge, materials with high strength and toughness can be produced. Finally, in the fourth part, mechanical properties of the surface modified PLA/CNCs nanocomposites were investigated by a conventional tensile test and compared with the small punch test. Surface modification of CNC facilitated better dispersion of CNC into PLA matrix and increased the elastic modulus of the PLA/CNC nanocomposites. Grafting induced crazing effect, which induced better ductility. Knowledge and results gained in this study demonstrate the potential path for the development of the PLA nanocomposites with higher properties for packaging applications.

Keywords: poly(lactic acid); chitin nanocrystals; cellulose nanocrystals; crystallization; orientation; nanocomposites; mechanical properties.

CONTENTS

1.1. Background

Plastics have become a crucial part of our life. We use plastics almost every day in every sector. For example, food items that we eat usually come in plastic packaging, electronic gadgets, household items, etc. [1]. The importance of plastics is visible from the chart (see Figure 1.1) that shows the data of the yearly production of plastic in word and Europe, and plastic demand of the European Union (EU) by different segments. Almost 40% of plastics demand for the packaging sector. Plastics are so demanding due to their lightweight, flexibility, durability, and low cost of production. Despite being an inevitable part of life and ample advantages, it has some drawbacks as well. For instance, the disposal of plastics leads to pollution of both terrestrial and aquatic ecosystems; therefore, it has become an environmental threat. Furthermore, the degradation of plastic is slow and challenging; it takes 500–1000 years for conventional plastics such as poly(styrene) (PS) and poly(ethylene) (PE) to degrade in the environment [2]. Moreover, during the degradation process, huge amount of CO_2 and many other toxic compounds were released. For example, burning 1 kg of plastic produces around 2.8 kg of CO_2 [3]. Every year thousands of tons of plastic waste goes to oceans and it has been expected to grow from 50 Mt in 2015 to 150 Mt by 2025 [4].

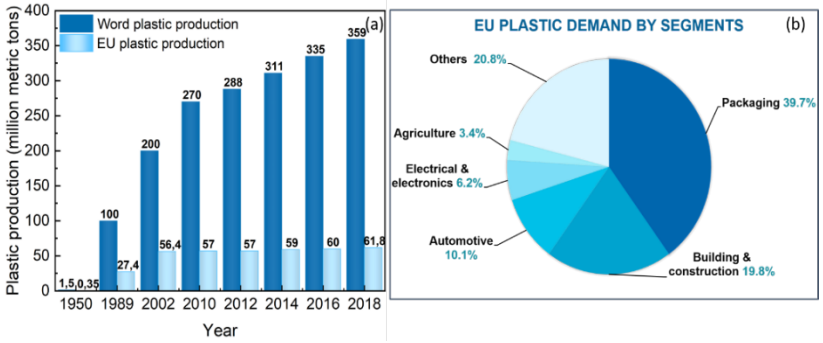

Figure 1.1. Chart showing (a) world and EU yearly plastic production and (b) EU plastic demand by segments (drawn from the data provided in reference [5,6])

In order to mitigate the problems caused by currently used petroleum-based polymers, the use of biopolymers and/or bio-based polymers, which either originate from the natural resources or synthesized from the natural materials will be a viable option. Biopolymers have immense potential to substitute or minimize the use of petroleum-derived polymers. Examples of some important biopolymers that can be useful for packaging are (1) polysaccharides: cellulose, hemicellulose, chitosan, chitin, and starch, (2) proteins: gelatin, casein, whey protein, corn protein, gluten, and soy protein, (3) other biopolymers/bio-based: poly(lactic acid) (PLA), poly(hydroxyalkanoates)(PHAs), etc.

1.2. Bio-based and biodegradable polymers

There is a fine difference between the bio-based and biodegradable polymers. Bio-based polymers are those polymers, which originates from the natural and renewable resources viz., cellulose, starch, vegetable oils. Biodegradable polymers are the polymers that can degrade into water, CO_2, and biomass over time with the help of microorganisms when exposed to temperature and/or moisture [7]. Bio-based polymers can be biodegradable or non-biodegradable depending on the molecular structure of the monomer units and origin [7]. For instance, poly(lactic acid) (PLA), which originates from corn and sugar beet, is a bio-based and biodegradable polymer. Contrary, poly(ethylene) (PE) that is synthesized from plant-based ethylene is a non-biodegradable polymer due to its linear structure [7]. Some more examples of the bio-based, biodegradable, petroleum-based, and non-biodegradable polymers are shown in Figure 1.2. Undoubtedly, biopolymers exhibits very interesting and potential properties that can compete with some of the conventional plastics. However, some biopolymers have limitations as well. For example, cellulose and starch possess very low water vapor permeability because of the hydrophilic nature that is also responsible for poor processing ability, and brittleness [7]. Poly(hydroxyalkanoates) (PHAs) exhibits stiffness, brittleness due to the high glass transition and melting temperature [7]. Poly(hydroxybutyrate) (PHB) has a melting temperature of 170-180°C, which is very close to the degradation temperature (generally around 270°C) that makes it difficult for the extrusion process [8]. Additionally, the high manufacturing cost of some the biopolymers is a problem for practical use.

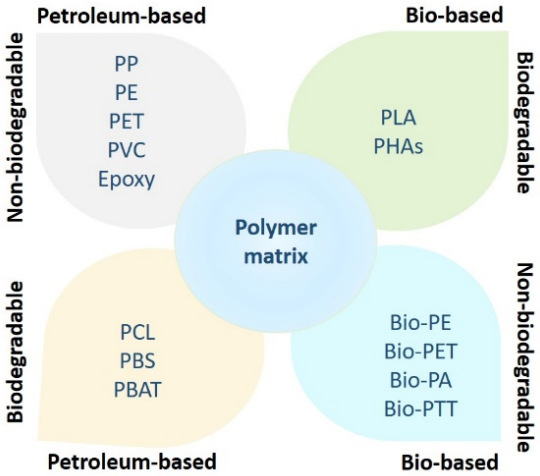

Figure 1.2. Schematic showing some of the examples of bio-based, biodegradable, petroleum-based and non-degradable polymer used as polymer matrix

1.3. Poly(lactic acid) (PLA)

PLA is a linear aliphatic, semicrystalline polymer mainly produced from natural sources

such as corn sugar, potato, sugarcane, and sugar-beet by polymerization of the monomer unit called lactic acid(2-hydroxy propionic acid) [9,10]. The schematic of the chemical structure and life cycle of the PLA is shown in Figure 1.3. Three types of polymerization techniques viz. (i) direct condensation polymerization, (ii) ring opening polymerization, and (iii) azeotropic dehydrative polycondensation are used for the polymerization of L-lactides [11]. Out of these, the ring-opening polymerization (ROP) is the most commonly used method to synthesize high molecular weight PLA at large scale [12]. Wallace Hume Carothers and co-workers [13] synthesized for first time PLA using ROP in 1932 and later on (1954) DuPont De Nemours and Ethicon, Inc. patented it. PLA exists in two enantiomeric forms viz. poly(L-lactic acid) (PLLA) and poly(D-lactic acid) (PDLA) due to the chiral nature of the lactic acid [12]. Commercially available PLA usually contains both forms. PLA can exist in either semicrystalline or amorphous form, based on the stereochemistry and chemical composition.

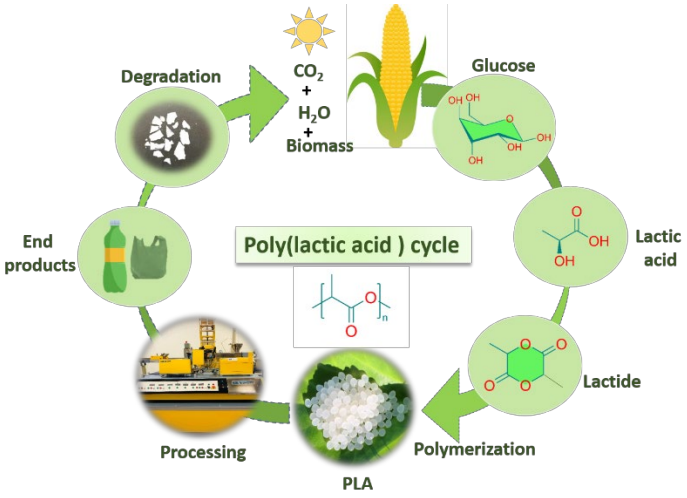

Figure 1.3. Schematic illustration of the chemical structure and life cycle of PLA; showing the source of origin of PLA, conversion of glucose to lactic acid, formation of PLA via polymerization of lactide, processing techniques, end products like plastic bottles, packaging bags, and finally their degradation into CO_2, H_2O and biomass

As a semicrystalline polymer, PLA exhibits a glass transition temperature (T_g) ranging from 35-60°C as well as a melting temperature (T_m) between 165-180°C [12]. PLA is a most suitable bio-based polymer for packaging application due to its inherent properties such as eco-friendly behavior including biodegradability and or/compostability (decomposes to H_2O, CO_2, and organic materials), low-toxicity, low energy consumption, and lower CO_2 emissions compared to the petroleum-based polymers [14]. Moreover, PLA is easier to process compared to some other biopolymers *viz.* poly(hydroxyl alkanoate) (PHA) and poly(ϒ-caprolactone) (PCl) and can be processed by extrusion, injection molding, thermoforming, and fiber spinning [15]. PLA has unique properties such as good mechanical properties including high stiffness (3000-4000 MPa) and high strength (50-70

MPa), good optical properties e.g., high transparency [16]. Due to its unique properties, PLA is widely used in various fields, from packaging and coating to agricultural products, medicine and surgery, pharmaceutical as well as disposable materials [17]. Despite various advantages, PLA has some challenges as well, which limits its use in practical applications. For instance, slow crystallization rate (low crystallinity), poor toughness (brittle material, less than 10% elongation at break), moderate barrier properties (to moisture and gas), high sensitivity to moisture, and low resistance to hydrolysis [16,18]. Moreover, due to its low thermal stability, the recycling of PLA has become a major problem [19]. As a slow crystallization rate [20] is a major drawback of PLA, hence next section will elaborate on the crystallization behavior of PLA, strategies on how to improve the crystallization rate, and the related publications.

1.4. Crystallization behavior of PLA

The study of the crystallization behavior of polymer is crucial because a high level of crystallinity is desirable in finished products as it can greatly influence the properties of polymer. For instance, the crystallinity of PLA can significantly enhance its hardness, stiffness, strength, chemical resistance, heat distortion temperature [15]. Therefore, in this work an emphasis has been given to the crystallization study of PLA. During the crystallization, the polymer molecular chains partially fold together and form highly ordered regions know as lamellae that compose a larger spheroidal structure called spherulites. Crystallization of polymer occurs via nucleation followed by crystal growth. PLA can be crystallized by a different method such as (i) slow cooling (ii) annealing of the polymer above its glass transition temperature, and/or (iii) strain-induced crystallization [21–23]. Depending on the method or crystallization conditions used, PLA exhibits mainly three types of crystals *viz.* α-form, β-form, and ϒ-form [24]. Recent studies have shown a new type of crystal, known as α'-form can also develop along with α-form [25]. Generally, α-form is the most common and stable form of crystal and it develops during the melt or solution crystallization at normal conditions, whereas β-form is produced by stretching of the α-form at a very high draw ratio and temperature [26].ϒ-form can be formed via epitaxial crystallization [27]. The crystallization behavior of PLA depends on various factors, for instance, on its molecular weight, degree of undercooling and its effect on morphology and crystal growth, the content of the isomer, processing temperature, and annealing time [28–30]. Furthermore, the thermal history has a high impact on the crystallinity and morphology of the PLA; therefore, more attentions have been given to study the crystallization kinetics of the PLA [28]. Researches have employed two methods: (1) Lauritzen-Hoffman theory [31] and (2) Avrami equation/model [32–34] to study the crystallization kinetics of PLA under isothermal conditions. Kalb and Pennings 1980 [35] elucidated crystallization behaviors of PLA from bulk and solutions using optical microscopy. They estimated the equilibrium melting temperature, dissolution temperature and investigated the lamellar crystals. Later on, Vasanthakumari *et al.* 1983 [28] studied crystallization kinetics, morphology and crystal growth of PLA from the melt as a function of undercooling and molecular weight with a hot stage microscopy. In 1997, Iannace *et al.* [30], studied isothermal crystallization of PLA with differential scanning calorimetry (DSC) in a temperature range of 90-135℃ and obtained a maximum crystallization at 105℃. Further, a transition from regime II to regime III was observed

around 115℃. In 1998, Miyata and Masuko [36] investigated the growth rate of spherulites (G) as a function of isothermal crystallization temperature (T_c) using optical microscopy, differential scanning calorimetry and a depolarized-light intensity method. Their T_c dependence of G exhibited a bell-shaped curve that indicated the crystallization temperature dependence of spherulite growth rates. Afterward, several other researcher also examined the crystallization behavior of PLA [37–40] and also observed the bell-shaped curves. Furthermore, the quest to increase the slow rate and explore more understating about the crystallization of PLA is still progressing.

The most popular method to improve the slow crystallization rate of PLA is the addition of nucleating agents. So far, several attempts have been made and a large variety of nucleating agents have been incorporated into the PLA. For example, clays [41,42], silicates [43–45], stereocomplex [46], carbon nanotubes [47], graphene [47], organic additives including aliphatic amide [48], hydrazide [49], inorganic additives, for instance, $CaCO_3$, TiO_2, $BaSO_4$ [50]. Several polysaccharides have also been used as a nucleating agents such as starch [51], cellulose [52] and lignin [53]. These nucleating agents reduce the surface free energy barriers for nucleation and thus initiates crystallization by increasing the number of primary nucleation sites at higher temperature upon cooling [54]. In this study, an attempt has been given to improve the crystallization rate of PLA by adding two nanoreinforcements; chitin nanocrystals, (ChNCs) and cellulose nanocrystals (CNCs) using isothermal crystallization. Therefore, the next section provides brief details about the origin, isolation, and properties of these two nanoreinforcements.

1.5. Cellulose nanocrystals (CNCs) and chitin nanocrystals (ChNCs)

Cellulose is the most abundant material and main structural component of different biomass *viz.* trees, plants, algae, bacteria and invertebrate animals like tunicates [55]. Chitin is the second most abundant materials after cellulose and generally found in the exoskeleton of arthropods (crustaceans and mollusks), the cell wall of fungi, and yeast. Cellulose is a linear macromolecule consists of a long unbranched chain of glucose units attached by (1→4)-β-glycosidic linkages [55] and chitin is of consisting long chain of β (1-4) linked N-acetyl-D-glucosamine units [56]. The schematics of the hierarchical structure of both cellulose and chitin is shown in Figure 1.4. The main function of the cellulose in plant and chitin in animal is to provide mechanical strength. Cellulose and chitin are the most promising materials that are used as reinforcement in polymer matrix due to their unique properties including low density, chemical reactivity, biocompatibility, biodegradability, and nontoxicity [55][57,58]. In addition to this, chitin possesses antibacterial [59] and antifungal [60] behaviour due to the presence of an additional functional group (-NH_2-CO-CH_3) in its structure, which is making it useful for several applications such as biomedical, agricultural, water treatment, biosensors and cosmetics [61]. Furthermore, the availability of additional functional group (-NH_2-CO-CH_3) enhances the chemical reactivity of the chitin as compared to the cellulose that further increases the scope of surface modifications.

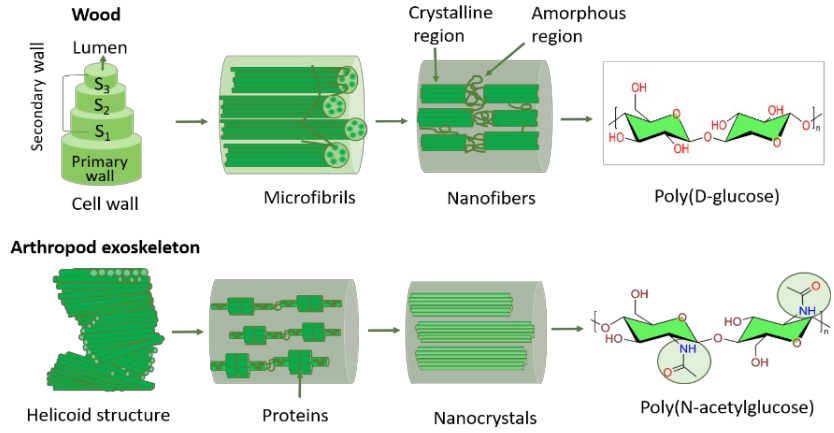

Figure 1.4. Hierarchical structure of wood and an arthropod exoskeleton. Cellulose made of a linear chain of β-(1, 4)-linked D-glucose units, and chitin consist of long chain of (1, 4)-β-N-acetylglucosamine polymers

From cellulose and chitin, nanocellulose and nanochitin can be isolated using a top-down approach due to their hierarchical structures. These nanomaterials can be separated from the wood and exoskeleton of the arthropods by different techniques such as mechanical treatments [62] and an acid hydrolysis method [63]. However, the most common method is acid hydrolysis. Two types of nanoreinforcements can be isolated from the cellulose and chitin sources *viz.* cellulose fibers (CNF), cellulose crystals (CNC), chitin nanofibers (ChNF), and chitin nanocrystals or whiskers (ChNC) [56]. Some of the characteristic properties of the CNCs and ChNCs are summarized in the Table1.1. By utilizing the inherent properties of the ChNCs and CNCs, some of the challenges of the PLA can be alleviated. Next section of the thesis will be focused on the PLA-based nanocomposites.

Table1.1 Properties of CNC and ChNC (adopted from reference [64])

Properties	CNC	ChNC
Shape	Needle shaped	Needle shaped
Diameter (nm)	5-30	6-60
Length (nm)	100-600	100-800
Aspect ratio(L/D)	10-100	10-55
Young's modulus (GPa)	150	150
Tensile strength (GPa)	10	10

1.6. PLA-based nanocomposites

PLA has several interesting properties as mentioned in the previous section but at the same time, it has some drawbacks as well. Many efforts have been made to overcome the limitations of PLA via different methods and modifications. For example, addition of plasticizers [65], nucleating agents [66], copolymers [67], and blends [68]. Furthermore,

the properties of PLA can be enhanced by using nanotechnology. The addition of nano-reinforcements into the PLA matrix, considered as a powerful tool to improve the properties of the PLA, because it combines the excellent properties of the polymer matrix with the intrinsic characteristics of the biopolymers like biodegradability and biocompatibility. Furthermore, it is necessary to understand the relationship between the properties of the polymer matrix and the nanoreinforcements, their interactions, compatibility, influences the manufacturing process, and on the final products, in order to maximize the benefits and versatility of the PLA [10]. In this section, the most relevant information and studies on the development of the PLA nanocomposites have been reviewed.

Earlier in 2003, Oksman and coworkers [69] studied flax fiber-reinforced PLA manufactured by twin-screw extrusion and observed that flax fibers (30 wt%) improved the stiffness of the PLA by 247%. Afterwards, in 2006, Oksman *et al.* [70] investigated a cellulose whisker (CNW) (pretreated before using) /PLA nanocomposites manufactured using liquid assisted extrusion and it was concluded that mechanical properties of the nanocomposites were increased; especially the elongation at break was increased by 800% as compared to the reference material. Later in 2010, Jonoobi *et al.* [71] investigated cellulose nanofiber (CNF) reinforced PLA using a batch process in a twin-screw extruder. They reported that the addition of 5 wt% of CNF, significantly improved the tensile modulus (increased from 2.9 to 3.5 GPa) and tensile strength (increased from 58 to 71 MPa) of the nanocomposites as compared to the reference materials. Fortunati *et al.* [72] prepared a nanocomposite with PLA/CNC by solvent casting. They investigated the effect of unmodified CNC and surface modified CNC (s-CNC) on the barrier properties; oxygen transmission rate (OTR) and water vapor permeability (WVP) of the PLA. It is worth mentioning that 5 wt% s-CNC reduced OTR by 48% and very good improvement in WVP of PLA films has been shown by all the nanocomposites, especially 1 wt% s-CNC reduced the WVP by 34%. These improved in barrier properties were ascribed be due to the better dispersion of modified s-CNC in the PLA matrix. Herrera *et al.* [73] prepared plasticized PLA films with cellulose and chitin based nanocomposites by liquid assisted melt extrusion followed with compression molding to films and studied light transmittance of films prepared with different cooling rates. The UV-Vis spectroscopy of the nanocomposite films revealed that fast cooling resulted in higher transparency compared to the slow cooling of the films. They also reported that compared to PLA/chitin, the PLA/cellulose nanocomposites were more transparent. Salaberria and co-workers [60] acetylated the surface of ChNC and processed PLA/ChNC nanocomposites via extrusion followed with compression molding to films. They demonstrated that the incorporation of both ChNC and modified ChNC slightly enhanced the hydrophobicity of the nanocomposites as well as improved the antifungal activity. Li *et al.* [74], reported that PLA nanocomposites synthesized with surface modified ChNC (5 wt%) significantly improved the mechanical properties of the nanocomposites. Tensile strength, tensile modulus, and fracture energy of the PLA/ChNC nanocomposites reached to 30.5 MPa, 1.4GPa, and 333.7 J/m^2 as compared to the neat PLA. This increment in the PLA nanocomposites implied to the better dispersion of the ChNC into the PLA due to the surface grafting of the ChNC. It can be concluded from the above studies that adding nanoreinforcements and use of liquid-assisted extrusion has affected the overall properties of PLA. The use of plasticizers during the processing of PLA-based nanocomposites have

facilitated the processing and influenced the final properties. Further, surface modification of nanoreinforcements has helped researcher to improve the properties of PLA. However, to achieve the practical applicability of the PLA-based nanocomposites, especially for food packaging application, some of the desired and important specifications [7] are listed below:

- Logistical practicality, cost-effectiveness, non-toxicity, eco-friendly and preferably recyclable, easy waste management, protective against the light and mechanical aggregation.
- Mechanically sustainable for easy transport, distribution, and storage without damaging the physical and chemical and/or biological nature of food. The structural and film integrity of the packaging materials is important. Transfer of toxic packaging additives and constituents must be prevented.
- Suitable gas barrier properties. Controlled moisture barrier or water vapour permeability to retain the aroma, prevent aerobic spoilage/degradation. Protect against oxygen barrier (oxygen transmission rate) to prevent aerobic and microbial degradation, maintain nutritional quality by preserving vitamins, proteins, lipids, etc. In addition, the barrier properties of CO_2, ethylene, NH_3, and other gases are also important in specific cases.
- Under any circumstances, the chemical, physical, biological constituents of the food must not be compromised or altered. In addition, packaging materials must prevent the development of pathogenic and microorganisms. In this context, various legislative directives *e.g.* various framework regulatory acts as outlined for FCM (Food contacting material) must be followed while developing and using various food-packaging materials.

These specifications provides further scopes of research to develop novel materials that can reduce and/or replace the use of conventional ones. Therefore, the next section of this thesis provides challenges and further scope of PLA-based nanocomposites for packaging applications.

CHAPTER 2: Challenges and objectives

2.1. Challenges of PLA-based nanocomposites

The challenges of developing PLA-based nanocomposites for an appropriate application lie in the optimization of various properties by suitable processing, characterization, and study of structure-property relationships. As it has already been mentioned in the previous part that although PLA presents a very significant commercial potential, some of the properties, including its slow crystallization rate, inherent brittleness, and moderate barrier properties, restricts its use in packaging applications. To solve these problems, in this study, the focus is given to increase the crystallization rate of PLA. Once the crystallization rate is optimized, subsequently, other properties, which depend on the crystallinity for instance, thermal, mechanical, barrier and degradation properties can be modified. Additionally, the brittleness of the PLA is certainly a challenge, which also seeks attention. Therefore, an attempt has also been given to fine-tune the brittle-to ductile behavior using a two-step orientation method.

The preparation of PLA-based nanocomposites using nanocellulose and nanochitin is challenging due to the functional groups (-OH and $-NH_2$-CO-) available on the surface of these nano-reinforcements as already reported in the literature. To mitigate this problem, different strategies have been employed in this study viz. surface modification of the nanoreinforcements, microsphere preparation, and film extrusion. A list of the specific objectives of the study is given below.

2.2. Objectives of the work

- To investigate the effect of ChNCs on the crystallization of PLA including crystallization rate, crystallization kinetics, and spherulite morphology developed during the crystallization process.
- Optimize the suitable isothermal crystallization conditions (crystallization temperature and time) to achieve homogenous crystallization and understand which parameters will be most suitable.
- Investigate the effect of crystallinity (developed by homogenous crystallization) on the final properties of the ChNC-based PLA nanocomposites.
- Achieve oriented nanocomposites films by a two-step process (melt and solid-state drawing) and evaluate its effect on the thermal, mechanical and microstructure properties.
- Improve dispersion of the CNC into PLA matrix by using a grafting method followed by microsphere preparation and its effect on the properties of the developed nanocomposites, especially mechanical properties.

CHAPTER 3: Materials and methods

3.1. Materials

In this section of the thesis, the focus has been given to the raw materials used for the preparation of the PLA-based nanocomposites using ChNC and CNC as reinforcements. The origin of the raw materials, visual appearance, their compositions in the nanocomposites and the coding of the materials have been presented.

Polymer matrix: Poly(lactic acid) was utilized as a polymer matrix for the preparation of all the nanocomposite materials prepared in this thesis. Three commercial grades of PLA were kindly provided by Futerro (Escanaffles, Belgium) and NatureWorks (4032D; Nebraska, USA and 4043D; Minnetonka, MN, USA). The technical details of the PLA are accumulated in Table 3.1. Photographs of the different grades of PLA are shown in Figure 3.1.

Figure 3.1. Photographs of the different grades of the PLA: (a) Futtero (b) 4032D and (c) 4043D used in the study

Table 3.1. Technical specification of the different grades of PLA: Futerro [75], Ingeo 4043D [76,77] and Ingeo 4032D [78]

PLA	D isomers % (%mol)	Mw ($Kg.mol^{-1}$)	MFI (g/10min)	X_c (%)	Involved papers
Futerro	1	211	8	6	I, III
Ingeo 4043D	2	168	6	7	II
Ingeo 4032D	2	181	6.4	40	IV

Nano-reinforcements: Both ChNCs and CNCs were used as reinforcing materials for the PLA matrix. ChNCs utilized in the paper I, was kindly prepared and purified at Pontific Catholic University of Chile (PUC) using chitin powder from crustacean waste via acid hydrolysis as reported by Salaberria *et al.* [79]. On the other hand, ChNCs used in the paper II and III were isolated from the chitin powder obtained from shrimp shell supplied by Sigma-Aldrich grade C7170, (Stockholm, Sweden) via the hydrochloride acid hydrolysis method as ascribed by Herrera *et al.* [80]. CNCs (2013-FPL-CNC-049) used in paper IV, were kindly provided by Forest Products Laboratory (FPL) (Madison, USA), in powdered form and it was prepared by sulfuric acid hydrolysis. The technical specification of the ChNC and CNC is gathered in Table 3.2.

Table 3.2. Specifications of the ChNCs and CNCs

ChNC/CNC	Diameter (nm)	Length (nm)	Aspect ratio (l/d)	X_c (%)	Involved papers
ChNC	7-25	314-1571	47-63	91	I,II,II
CNC	3-11	161-550	35-45	80	IV

Plasticizers and solvents: Two types of plasticizers viz. triethyl citrate (TEC, ≥99%, Mw: 276.3 g/mol) (paper I, II) and glycerol triacetate (GTA, ≥99%, Mw: 218 g/mol) (paper III) were added to the nanocomposites to facilitate the processing of the nanocomposites by the co-authors. Both plasticizers were used in liquid form and purchased from VWR and Sigma-Aldrich (Stockholm, Sweden), respectively. Various solvents were used for different purposes. For instance, HCl (ACS reagent, 37%) used for acid hydrolysis (paper II) was supplied by Merck (Darmstadt, Germany). Surface modification of CNC (paper IV) was carried out with the following reagents. Lactide, stannous octoate ($Sn(Oct)_2$, toluene, dichloromethane, chloroform ,and N, N-dimethylformamide (DMF) used for the grafting of CNC was purchased from Sigma Aldrich (St. Louis, USA). Ethanol (99.5%) was purchased from Solveco (Stockholm, Sweden). Some other solvents used for purification of the unreacted monomer after grafting (methanol, ethanol, and acetone) and dispersion 1, 4-dioxane) were supplied by WVR International (Stockholm, Sweden). Finally, by using the PLA, ChNC, CNC, TEC, and GTA different types of PLA nanocomposites processed using various techniques that will be elaborated in the next section. The achieved nanocomposites coded based on the compositions of the materials used in different papers are summarized in Table 3.3.

Table 3.3. Codes and compositions of the materials utilized in the study

Coding of the materials	Composition of the materials (wt%)		
Paper I	PLA	TEC	ChNC
PLA	100	0	0
PLA-TEC	80	20	0
PLA-TEC-ChNC	79	20	1
Paper II	PLA	TEC	ChNC
PLA	100	0	0
PLA-TEC	90	10	0
PLA-TEC-ChNC	89	10	1
Paper III	PLA	GTA	ChNC
PLA	100	0	0
PLA-GTA	80	20	0
PLA-GTA-ChNC	75	20	5
Paper IV	PLA	CNC	mCNC
PLA	100	0	0
PLA-CNC	99	1	0
PLA-mCNC	99	0	1

3.2. Methods

The present section of the thesis provides a detailed description of the various techniques that have been used to prepare PLA and its nanocomposites with ChNC and CNC. Moreover, the method that is used to improve the dispersion of the nanoreinforcements into the PLA matrix is also elaborated here. Further, different characterization techniques utilized for the PLA-based nanocomposites are summarized.

Preparation PLA and its nanocomposites (pellets or films) : PLA-based nanocomposites have been prepared using various techniques and an overview of all the methods used in different papers (I-IV) is shown in Figure 3.2. In the paper I, first pellets of PLA, PLA-TEC, and PLA-TEC-ChNC (79: 20:1 wt%) was extruded using liquid-assisted extrusion. Then, with the help of compression molding, amorphous films of the materials were prepared. In paper II, similar to paper I, PLA, PLA-TEC, and PLA-TEC-ChNC (89: 10: 1 wt%) pellets, were prepared with liquid-assisted extrusion. Further, compression molding is used to prepare amorphous and crystallized films of the extruded materials. In paper III, like the paper I and II, liquid-assisted extrusion was used to prepare pellets of PLA, PLA-GTA, and PLA-GTA-ChNC (75: 20: 5 wt%) followed by a compression molding to prepare amorphous films of the materials. Previously prepared pellets and amorphous films of the materials were further processed by film calendering and solid-state drawing to get oriented films. In paper IV, film calendering was used to produce oriented films of PLA and its nanocomposites with CNC and modified CNC followed by a post-treatment of the films by compression molding.

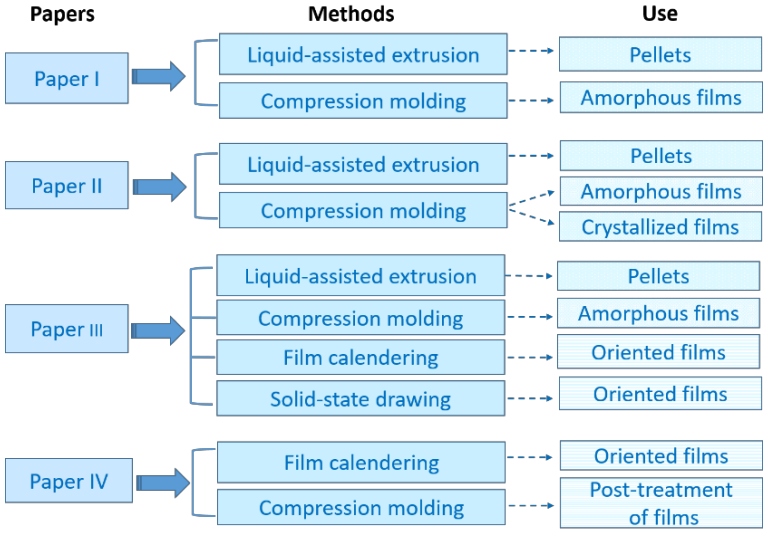

Figure 3.2. An overview the methods that have been used to prepare pellets and films of the materials in different papers of the thesis

Compression molding: Was utilized for two purposes; firstly, to prepare amorphous films of the extruded materials (paper I, II, III) and secondly, to produce isothermally crystallized films (paper I, II) with laboratory press LPC-300 Fontijne Grotnes (Vlaardingen, Netherlands). Pellets of the materials were first placed between Mylar (PET) films and then the Mylar covered materials were inserted between two metallic sheets. Materials were heated at 190°C for 2 min under contact pressure and then 1 min using a pressure of approximately 10 MPa. The films were subsequently, cooled to room temperature to obtain amorphous films. For isothermally crystallized films, materials were first cooled down to specific crystallization temperature, kept for the desired time interval, and then rapidly cooled to room temperature using a water cooling system. The schematics of the compression molding process is illustrated in Figure 3.3.

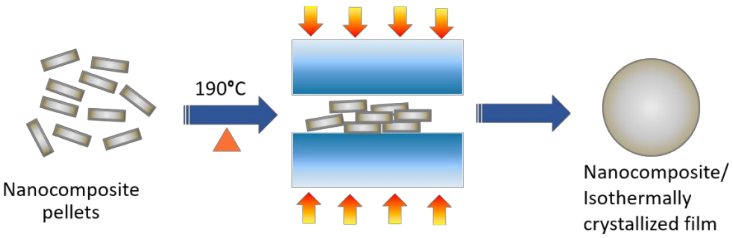

Figure 3.3. Schematic showing the compression molding techniques to prepare nanocomposites of PLA with ChNC

One more role of the compression molding technique in this study was to assure the better surface quality of the samples (paper IV). Extrusion-calendered films were stacked using 3 films (each has a thickness of 0.1 mm) to get a thickness of 0.3 mm. Materials were pressed using a compression molding machine (IQAP LAP PL-15; IQAP Masterbatch group SL, Barcelona, Spain) at a molding temperature of 190°C and using a pressure of 15 bars for 30s. Materials were kept under pressure for another 3 min and immediately cooled by immersing them in the ice water.

Film calendering: Was used to produce oriented nanocomposite films of PLA-GTA-ChNC (paper IV) by using a single screw extruder (Lab Tech Engineering Company Ltd., Samutprakan, Thailand) with an L/D ratio of 30:1. The schematic of the drawing process is given in Figure 3.4. Firstly, molten polymer extruded through a die (200°C) at a screw speed of 65 rpm and then produced extruded film immediately quenched on a casting roll. A post drawing performed on heating rollers at 60°C (Lab Tech Engineering Company Ltd., Thailand, and type LUMCR-50) by applying the tension between stripper rolls and haul-off rolls to prepare the oriented nanocomposite films. The oriented films were collected on the windup unit and draw ratio (DR) was measured. DR is defined as the ratio of the increased film length to the original film length produced during a specific time. Apart from this, film calendering also used to prepare nanocomposites of the CNC-based nanocomposites (IV). Microspheres of the materials poured in the hopper and temperature of the die, the barrel was set to 200 and 190°C, respectively, and the screw speed was set to 40 rpm. The films were produced by stretching the extruded materials between the rollers.

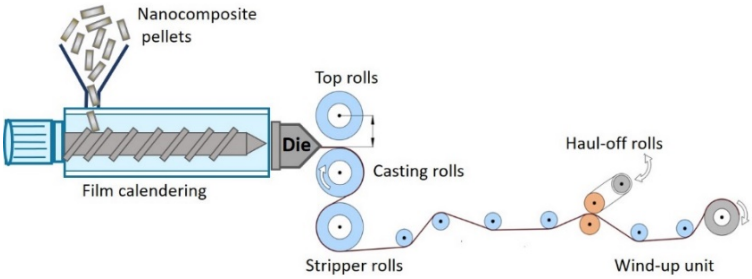

Figure 3.4. Schematic illustration of the film calendering process to orient the nanocomposites of PLA-GTA-ChNC

Melt-state drawing: To achieve the highly oriented films of the PLA, PLA-GTA ,and PLA-GTA-ChNC (paper III), melt-state drawing (MSD) was performed by the co-authors. Pre-orientation was performed on the same film-calendering machine as mentioned in the previous part in a similar manner. A detailed description of the process and parameters are mentioned in the appended paper III.

Solid-state drawing: PLA and its nanocomposites (paper III) were oriented using solid-state drawing (SSD) on a tensile testing machine; Shimadzu AG-X universal tensile tester (Kyoto, Japan) equipped with 5 kN load cell Tensile machine was connected to a chamber with a controlled temperature. The schematic of the SSD process is shown in Figure 3.5.

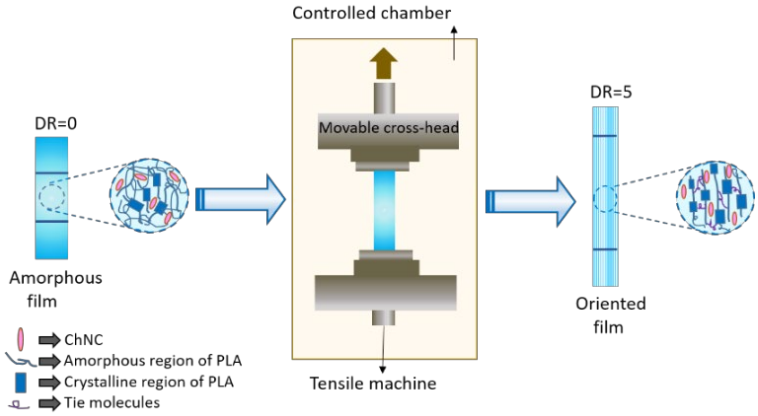

Figure 3.5. An illustration of the solid-state drawing process used to produce oriented films of the materials

It has been well documented in the literature that good orientation of polymer can be achieved by drawing the polymer between its glass transition and melting temperature [81]. Therefore, in this paper III orientation of materials was carried out at 60°C that was the best drawing temperature for PLA-GTA-ChNC nanocomposites. The highest draw ratio of 5 was achieved with a drawing speed of 100 mm/min. Rectangular shape samples

were cut from the original films with dimensions of 40 × 6 × 0.1 mm^3 and a gauge length of 10 mm was used. Samples were marked before the drawing to be able to calculate the draw ratio of the materials using the following equation (1).

$$Draw\ ratio\ (DR) = \frac{Final\ length\ of\ the\ ink\ mark\ (l)}{Original\ lenght\ of\ the\ ink\ mark\ (lo)} \qquad (\text{eq } 1)$$

SSD was performed to orient the films prepared by compression molding techniques and already pre-oriented films with melt-state drawing. Based on the processing techniques used for the orientation and draw ratio achieved, samples were coded as given in Table 3.4. Compression-molded samples named as CM and film calendered called as FC. Further, SSD added to these samples when the materials were further drawn with SSD. It was interesting that CM and FC nanocomposite films after SSD exhibited a maximum DR of 4. Contrary, SSD of pre-oriented nanocomposites that were already oriented with MSD (i.e. FC-2), a slightly higher DR was achieved (DR5).

Table 3.4. Coding of the nanocomposites based on the techniques used for the orientation and draw ratio (DR) obtained during the stretching

Codes	Process involved for orientation	DR	Name of sample
CM	Compression molding	N/A	Undrawn sample
FC	Film calendaring	N/A	----
FC-2	Film calendaring	2	Pre-drawn sample
CM-SSD-4	Compression molding / solid state drawing	4	Drawn sample
FC-SSD-4	Melt state drawing /solid state drawing	4	Drawn sample
FC-2-SSD-5	Melt state drawing/solid state drawing	5	Drawn sample

Liquid-assisted extrusion: Was used to prepare pellets of PLA and its nanocomposites (paper I, II, III) by co-authors. The schematic of the preparation of the process is depicted in Figure 3.6. In brief, first, an aqueous suspension of ChNCs was prepared as follows; initially, ChNC gel in water (18 wt%) was pre-dispersed in water/ethanol solvent mixture (1:5 weight ratio) for 2h using a magnetic stirrer and then this suspension was mixed with TEC (2.61 wt% solid content was incorporated to achieve 10 wt% of TEC, for example, paper II). Finally, the prepared suspension fed into the extruder by a peristaltic pump PD 5001 Heidolph (Schwalbach, Germany). The pellets of the materials (paper I, II, III) were prepared on a co-rotating twin-screw extruder ZSK-18 MEGALab, Coperion W&P (Stuttgart, Germany) length to diameter ratio of 40, connected with a K-Tron gravimetric feeder (Niederlenz, Switzerland).

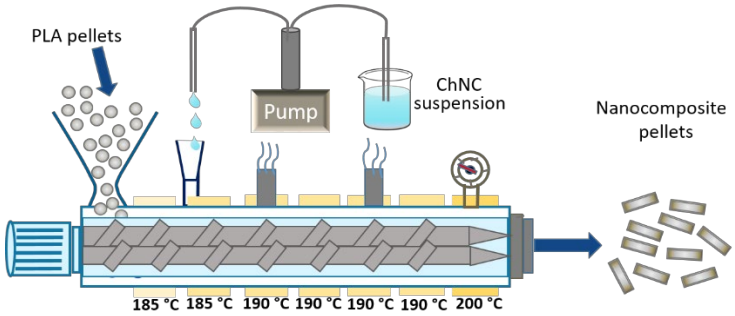

Figure 3.6. Picture depicts the process of liquid-assisted extrusion showing how materials are first melted in the melting in zone after that passed to the mixing zone and finally extruded through the die in the form of pellets

3.2.1. Surface modification technique

Grafting technique: As already mentioned in the introduction part that the dispersion of nanoreinforcements is very important and challenging to achieve. In this study (paper IV), to improve the dispersion, the surface of the CNC was modified by a grafting technique popularly known as "grafting from" via ring-opening polymerization of lactides and the schematic is shown in Figure 3.7. The same procedure employed as reported by Mujica-Garcia *et al.* [82]. In brief, properly dispersed aqueous suspension of CNC was solvent exchanged by a combination of solvents: acetone, dichloromethane, and toluene using a centrifugation and re-dispersion cycles. A three-neck round bottom flask, connected to the condenser taken. After that, L-lactide and dry toluene added into the flask. Once L-lactide was well dissolved in toluene, previously dispersed CNC poured into the reaction flask, and the temperature was set to 80°C. 0.2 g of catalyst, $Sn(oct)_2$ was added to the reaction flask ,and the reaction mixture was kept for 24 hr with a stirring speed of 150 rpm. After completion of the reaction, the reaction mixture was washed to remove the unreacted monomers.

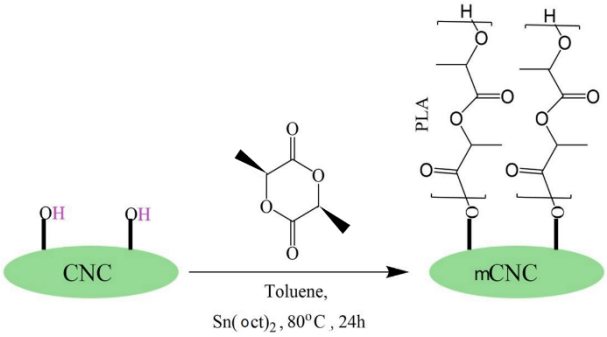

Figure 3.7. Schematic of the surface modification of CNC by ring opening polymerization. Lactide (monomer) polymerized to prepare PLA-grafted-CNC (i.e. mCNC)

Microsphere preparation: To achieve further dispersion, microspheres of the materials (paper IV) were prepared by dropping them into liquid nitrogen followed by freeze-drying. Schematics of the preparation of microspheres of PLA/CNC is shown in Figure 3.8. PLA/mCNC was also prepared in the same manner. Prior to prepare microspheres, 1 wt% of both CNC and PLA-grafted CNC (i.e., mCNC) were dispersed in DMF and at the same time PLA was also dissolved in the 1, 4-dioxane. The dispersion of the nanoreinforcements was confirmed with the flow birefringence test before mixing with PLA. Finally, well-dispersed CNC and mCNC and dissolved PLA mixed together and further, stirred for 2h at room temperature. Obtained suspension of PLA with CNC/mCNC utilized to prepare the microspheres. To compare the PLA/CNC and PLA/mCNC nanocomposites, microspheres of PLA were also made.

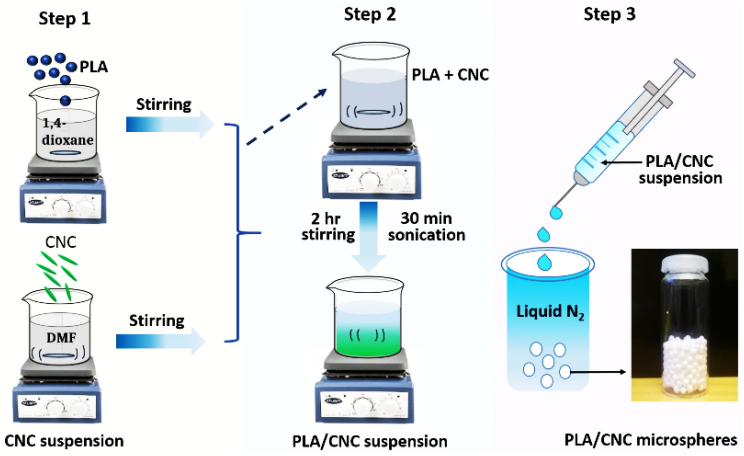

Figure 3.8. Schematic representation of the preparation of microspheres of PLA, PLA/CNC and PLA/mCNC

3.2.2. Characterization techniques

Characterization of the PLA-based nanocomposites is very important to understand both structural aspects of the materials as well as to gain knowledge of the structural-property correlations. For instance, crystallinity, mechanical, thermal, optical, and barrier properties are directly related to the molecular and microstructure of the materials [83]. In the context of PLA-based nanocomposites, understanding of molecular and microstructure is immensely helpful to decipher the extent of homogeneity of dispersions of nanoreinforcements into the PLA matrix and their orientations or alignments, various levels of interactions among the components that are responsible for the overall material properties [83]. In this study, numerous characterization techniques have been used to characterize the produced PLA-based nanocomposites and understand the relationship between the structure and properties. A detailed summary of all the utilized techniques is given in Table 3.5.

Table 3.5. Summary of the characterization techniques utilized in the study

Techniques	Characterization	Involved papers
Polarized optical microscopy (POM)	Study the crystallization behavior and surface morphology especially the birefringence	I,II,III
Optical microscopy (OM)	Study the surface morphology and dispersion of the nanomaterials	III,IV
Scanning electron microscopy (SEM)	Study the microstructure and dispersion of the nanomaterials	I-IV
Atomic force microscopy (AFM)	Analyse the size distribution and shape of the nanomaterials	I,II
Fourier transform infrared spectroscopy (FT-IR)	Study the interactions between the components in nanocomposites	I,II,III
X-ray diffractometer (XRD)	Study the crystallinity, crystal structure and crystal size	I,II,III
Differential scanning calorimetry (DSC)	Study the thermal properties and crystallinity	I,II,III,IV
Thermo-gravimetric analysis (TGA)	Determine the weight change of the materials as a function of temperature and/or time	II,III
Tensile testing	Study the mechanical properties	III,IV
UV-vis spectroscopy	Study transparency and dispersion of nanomaterials	II,III
Moisture uptake test	Measure the water uptake	II
Water vapor permeability test	Water vapor transmission rate (WVTR)	II
Degradation test	Hydrolytic degradation of the materials	II
Flow birefringence	Study nanomaterials dispersion in the used solvent	IV
Intrinsic viscosity (IV) test	Study degradation/ molecular weight of the PLA after processing	IV

Optical microscopy (OM) and polarized optical microscopy (POM): Dispersion of the nanomaterials into the plasticized PLA matrix confirmed by the OM (paper II and III). A Nikon Eclipse LV100POL (Kanagawa, Japan) POM was used to investigate the isothermal crystallization of the materials (paper I and II) connected with a hot stage and temperature controller. Materials were isothermally crystallized at different temperatures (135℃ to 110℃) and time intervals (5, 10, 15 min, and 30 min). For this, a thin film of the material was kept between two glass slides and then transferred to the hot stage, where it was heated at 200℃ to eliminate thermal history if any , and then cooled down to specific temperatures. Additionally, the spherulite morphology and size (paper I and II) of the materials were analyzed by POM. Furthermore, the effect of orientation on the microstructures of the materials as well as the birefringence behavior also observed under

cross-polarized conditions (paper III). The polarized optical micrographs of the materials were recorded by a charge-coupled device (CCD) camera. In addition to this, the transcrystallization study of ChNCs was also performed using POM ,and set-up was prepared similarly as reported by Gray [84]. Schematics of the set-up illustrated in Figure 3.9.

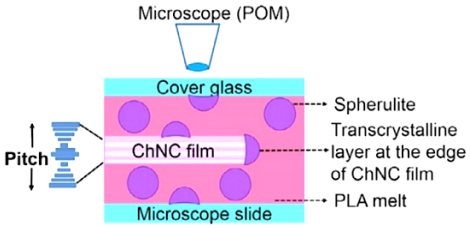

Figure 3.9. Schematic illustration of set-up to study the transcrystallization behavior of ChNCs

Atomic force microscopy (AFM): Veeco Multimode Nanoscope (Santa Barbara, USA) in tapping mode used to characterize the surface morphology and the size distribution of the ChNCs (paper I and II). The diameter and length of the ChNCs were analyzed by the Gwydion software version 2.55 (Czech Metrology Institute, Brno, and Czech).

Scanning electron microscopy (SEM): JEOL JSM-IT300, (Tokyo, Japan) was used to examine the lamellar arrangement of the spherulites and transcrystalline layers formed between the ChNCs and plasticized PLA (paper I) The samples were etched with sodium hydroxide and ethanol (1:2 by volume) solution followed by washing in distilled water two to three times. Additionally, fractured surfaces of the materials were also investigated with SEM (paper II, III). Prior to the study, the surface of the samples was sputter-coated (Leica EM ACE220, Wtzlar, Germany) with either gold or platinum to avoid charging effect. The acceleration voltage was kept at 5, 15 kV, and SEM micrographs were collected.

Fourier transform infrared spectroscopy (FT-IR): VERTEX 80 (Ettlingen, Germany) FT-IR spectrometer with a spectral range of 400-4000 cm^{-1} and a resolution of 128 scans was used to study the role of ChNCs into TEC-plasticized PLA (paper I) and to analyze the interactions developed between the TEC, ChNC, and PLA during isothermal crystallization (paper I and II). FTIR was also used to understand if the orientation of the materials has any influence on the molecular interactions between the various components of the nanocomposites (paper III).

X-ray diffractometer (XRD): PANalytical Empyrean X-ray diffractometer (Almo, Malvern, UK) was used to study the effect of crystallization rate on the overall crystallinity of the materials and to determine the crystal structure of the isothermally crystallized materials (paper I). With the help of XRD, crystallinity and crystallite size of the materials were calculated (paper I, II, and III) using Scherrer equation [85] as given below

$$Crystallite\ size\ = \frac{k\lambda}{\beta Cos\theta} \qquad \text{(eq 2)}$$

Differential scanning calorimetry (DSC): Mettler Toledo DSC 822e (Schwerzenbach, Switzerland) instrument was used to study the thermal properties of the materials including glass transition temperature (T_g), cold crystallization temperature (T_{cc}), melting temperature (T_m) and degree of crystallinity was determined by the (paper I, II, III, IV). Hydrolytic degraded and oriented films were also investigated (paper II, III). The percentage crystallinity was calculated by using the following equation(3) [86].

$$Crystallinity(\%) = \frac{\Delta H_m - \Delta H_{cc}}{\Delta H_m^0} \times \frac{100}{w} \qquad \text{(eq 3)}$$

where, ΔH_m, ΔH_{cc}, is the melting enthalpy and cold crystallization enthalpy, respectively. ΔH_m corresponds for 100% crystalline PLA and w is the weight fraction of PLA present in the samples.

Thermo-gravimetric analysis (TGA): TA instrument Q500 (New Castle, DE, USA) was used to characterize the thermal stability of the isothermally crystallized and oriented films (paper II and III). The investigation was made using a heating rate of 10°C/min in a temperature range of 0-600°C. The effect of isothermal crystallization on hydrolytic degradation was also evaluated using the TGA (paper II).

Intrinsic viscosity (IV) test: Used to investigate the possible thermal degradation effect of the post-extrusion process (paper IV). An Ubbelhode-type (1B) capillary viscometer (Comecta Sl., Barcelona, Spain) was used to measure the intrinsic viscosity of the materials (PLA, PLA/CNC, and PLA/mCNC) as shown in Figure 3.10. Total five concentrations (0, 0.2, 0.4, 0.6, 0.8 and 1 wt %) of all the materials were prepared. First, 1 wt% of the solution of the materials was prepared and then it was diluted to lower concentrations. Flow time was measured using a stopwatch. For better accuracy, the measurement was performed five times and the average values were reported.

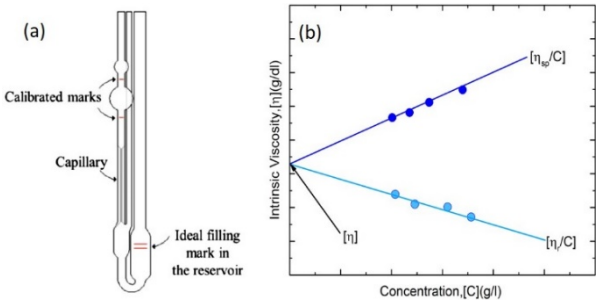

Figure 3.10. (a) Intrinsic viscosity measurement of PLA and its nanocomposites (with CNC and mCNC) by Ubbelohde-type viscometer (b) Schematic of the graph plotted between intrinsic viscosity and concentration for all of the investigated samples. Here, arrow represents the intrinsic viscosity value that was determined by the intercept between reduced and inherent viscosity plot

The molecular weights (Mn, Mv, Mw) of the materials were determined by the intrinsic viscosity method as reported by Hakim *et al.* [87]. First, a viscometer was inserted into the water bath at a homogenous temperature of 30°C. A blank solution (i.e. chloroform) was run through the viscometer and after that, the solution of the highest concentration (1 wt%) was passed through the viscometer (as shown in Figure 3.10a) followed by the other lower concentrations. To perform the test, the solution was first introduced into the reservoir up to the marked line and then it was sucked through the capillary and measuring bulb. After that, the solution was allowed to return to the reservoir and the flow time was measured by a stopwatch. The travel time taken by the solution to pass from one mark to another mark is a measure of its viscosity. This flow time was used to calculate the relative and specific viscosities. Finally, intrinsic viscosity was calculated by plotting a graph of reduced viscosity against the concentrations. The intercept of this determines the intrinsic viscosity. The relative viscosity [η_r] and specific viscosity [η_{sp}] of the prepared solutions were calculated from the flow time of the solution (t) with respect to the flow time of the blank or pure solvent (t_0) (i.e. chloroform) as mentioned in the following equations (4) and (5). Huggins [88] and Kraemer [89] expressions (eq 5 and 6) were used to calculating the intrinsic viscosities of all the materials. Here, intrinsic viscosity [η] is ideally the common intercept of the two equations and the schematic is shown in Figure 3.10(b).

$$\eta = \frac{t}{t_0} \qquad \text{(eq 4)}$$

$$\eta = \eta - 1 = \frac{t - t_0}{t_0} \qquad \text{(eq 5)}$$

$$\frac{\eta_{sp}}{C} = [\eta] + k_H\,[\eta]^2\,C \qquad \text{(eq 6)}$$

$$\frac{ln_{sp}}{C} = [\eta] + k_K\,[\eta]^2\,C \qquad \text{(eq 7)}$$

where C, is the concentration of the polymer solution, k_H and k_K are Huggins and Kraemer constants, respectively. The intrinsic viscosity can be related to average molecular weight (M) by using Mark–Houwink–Sakurada equation (8):

$$[n] = KM_v^{\alpha} \qquad \text{(eq 8)}$$

where K and α are constants for a given polymer–solvent–temperature system and its values for PLA are K = 2.21 x 10^{-4}; α = 0.77 as Mark-Houwink constants [90]. Subsequently M_n and M_w can be determined using equation (9) and (10), respectively.

$$M_n : M_v : M_w = 1 : (1 + \alpha) : 2 \qquad \text{(eq 9)}$$

$$\overline{M_n} = \left[\frac{\sum N_i\,M_i}{\sum N_i}\right] = \overline{M_v}\left[\frac{\sum N_i\,M_i^{(1+\alpha)}}{\sum N_i M_i}\right] = \overline{M_w}\left[\frac{\sum N_i M_i^2}{\sum N_i M_i}\right] \qquad \text{(eq 10)}$$

Mechanical testing: The mechanical properties of the materials including un-oriented, pre-oriented, and oriented nanocomposites (paper III) were tested using Shimadzu AG-X universal tensile tester (Kyoto, Japan) equipped with a 5 kN load cell. The materials were

tested at a crosshead speed of 2 mm/min and the distance between the grips was 20 nm. The tensile strength, tensile modulus, and elongation at break were determined from the recorded stress-strain curves and the toughness was calculated from the area under the stress-strain curve. Seven samples were tested for each material; average and standard deviation were calculated.

Further mechanical properties of the PLA/CNC and PLA/mCNC nanocomposite films (paper IV) were tested using a Galdabini Sun 2500 universal tensile tester (Galdabini, Cardano al Campo, Italy) combined with a 1 kN load cell. A dumbbell-shaped sample (ISO 527-2 type 1 BA) was prepared from the compression molded films using a ZCP 020 manual cutting press (Zwick, Ulm, Germany). The tensile tests were carried out at room temperature with a crosshead speed of 2 mm/min and the actual displacement of the calibrated zone was determined with a video extensometer (OS-65 D CCD, Minstron, Taipei, Taiwan), which was connected to a Windows-based software (Messphysik, Fürstenfeld, Austria). Prior to the test, tensile samples were subjected to a thermal treatment process called 'physical de-aging' (rejuvenating) as mentioned by Cailloux *et al.* [91]. The average values and corresponding standard deviation from five valid tests were calculated.

UV-Vis spectroscopy: UV-Vis spectrophotometer (GENESYS, 10 UV, Thermo-Scientific, Dreiech, Germany) was used to measure the transparency of the prepared films. In this study, the light transmittance of the materials was determined at a wavelength of 550 nm. Total three specimens of each samples were tested to calculate the average value (paper II, III).

Water vapor permeability test: To determine the water vapor transmission rate (WVTR) of the materials (paper II) a modified method according to ASTM E96 was used. Firstly, films were cut into circular discs with diameters of 0.04 m. Then the test samples were placed on a cup filled with silica gel. After that, these cups were placed in a chamber with controlled temperatures of 23°C and 50% relative humidity (RH). Finally, the weight of the cups was taken after specific time intervals and WVTR (g/m^2 day) was determined using the following equation (11) [25]:

$$\mathrm{WVTR} = \left[\frac{G/t}{A}\right] \qquad \text{(eq 11)}$$

where, G/t is the slope of the curve with increased weight gain (g) as a function of time (h) and A is the exposed area (m^2).

Degradation test: The test was performed according to the ASTM F163 on 30 mm × 30 mm × 0.1 mm films. At first, samples were dipped into distilled water and kept inside in an oven, set at 58°C and after that, the samples were taken out and gently wiped with tissue paper to remove water droplets present on the surface. After that, the samples were weighed and change in the physical appearance of the samples were regularly monitored until the samples were degraded into small fragments. Additionally, water uptake studies were carried out to determine the diffusion kinetics of PLA110, PLA–TEC110, and PLA–TEC–ChNC110. Thermal properties of the degraded samples were also tested for the

confirmation of degradation as discussed in the previous section.

Flow birefringence: Birefringence of CNCs in a liquid suspension is an indication that the nanocrystals are well separated and dispersed in the used liquid. In order to see the birefringence, the CNCs and PLA-grafted-CNCs were dispersed in DMF; the suspension was kept between cross-polarized filters connected with a lamp. Colorful birefringence was seen when the CNCs were aligned in the direction of flow and this confirmed that the prepared materials were in nanosize and dispersed in DMF.

CHAPTER 4: Results and discussions

This chapter summarizes the main results obtained during the doctoral research project. The discussion follows the summary of the paper vise results. Knowledge of isothermal crystallization behavior of PLA and plasticized PLA with ChNCs was explored (paper I). ChNC acted as an efficient nucleating agent and increased the crystallinity of the nanocomposites. This increased crystallinity affected the overall properties of the isothermally crystallized PLA-based nanocomposites (paper II). Further, the orientation of nanocomposites was performed (paper III) by a combination of two step-orientation methods and resulted in a drastic increase in the mechanical properties of the nanocomposites. Furthermore, surface modification of CNC was carried out (paper IV) that led to a homogenous dispersion of CNC into the PLA matrix and had some effect on the mechanical properties.

4.1. Effect of chitin nanocrystals (ChNCs) on isothermal crystallization of PLA and its nanocomposites

It is worth mentioning that most of the properties of PLA are strongly dependent on the degree of crystallinity. Hence, it is important to understand the isothermal crystallization behavior of the PLA. In this study (paper I), the effect of both plasticizer and ChNC was investigated. The idea was to understand and optimize the isothermal crystallization conditions of PLA with ChNC. To compare the role of ChNCs with plasticizer, isothermal crystallization of PLA-TEC and PLA-TEC-ChNC was performed at temperature range of 135-125°C for 30 min using POM connected to the hot stage. Prior to the isothermal crystallization study, ChNCs subjected to POM and AFM observations and micrographs are presented in Figure 4.1. It is seen in the Figure 4.1 (a) that ChNCs showed a colorful birefringence in POM and needle shape and dimensions (Figure 4.1 (b)) between 2-22 nm in height and 263-761 nm in length were measured in AFM images (Figure 4.1 b). Figure 4.1(c-d) shows a comparison of isothermal crystallization of PLA-TEC and PLA-TEC-ChNC at 125°C for 30 min. It is clearly visible that the addition of ChNCs into PLA-TEC has increased the crystallization rate as well as the nucleation density of PLA-TEC-ChNC. Further, due to the presence of ChNCs in PLA-TEC-ChNC, the size of the spherulites was also greatly reduced as compared to the PLA-TEC.

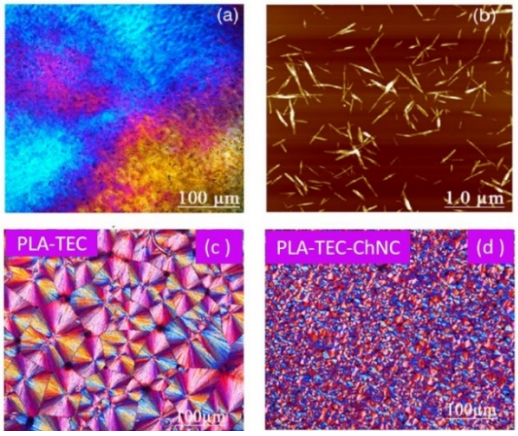

Figure 4.1. POM and AFM images of the ChNCs (a) showing birefringence (b) needle like shape of the ChNC. Comparison of isothermal crystallization of PLA-TEC and PLA-TEC-ChNC nanocomposites at 125℃ after 30 min. POM images clearly showed faster nucleation for PLA-TEC-ChNC and a reduced spherulites size compared to the PLA-TEC. Adopted from paper I

Transcrystallization study: Knowledge of transcrystallization behavior is important because the transcrystalline layer (TCL) enhances the interfacial adhesion between the two materials and eventually affects the physical and mechanical properties of the materials [92]. In this study, a transcrystallization study was performed to get better insights of the role of ChNCs at the interface of PLA-TEC and PLA-TEC-ChNC using POM at different temperatures (135℃, 130℃ ,and 125℃) and time intervals (5, 10, 15 min) and results are shown in Figure 4.2. Both isothermal crystallization temperature and time had a significant influence on the crystallization behavior of the materials. As it can be seen from Figure 4.2 that ChNC has acted as a nucleating agent and therefore, increased the bulk nucleation density of the PLA-TEC-ChNC films within 5 min of crystallization, resulting in a relatively more number of spherulites compared to the PLA-TEC. On lowering the isothermal crystallization form 135 to 125℃, the speed of nucleation further increased and some spherulites started developing at the interface of the materials. Once the crystallization time reached to 15 min, a very clear TCL appeared at the interface of PLA-TEC and PLA-TEC-ChNC. The nucleation ability of ChNC was extremely fast at 125℃; almost all the surface of the PLA-TEC-ChNC fully covered with the spherulites and size was reduced. However, very few and large size spherulites developed in the PLA-TEC at all the crystallization temperatures. Interestingly, at different temperatures, different morphology of the spherulites was observed. For example, 135℃, a typical 'Maltese-cross pattern spherulites' [35] with negative birefringence [93] were seen, contrary at 130℃, beautiful multi ring-banded spherulites appeared and 125 ℃, neutral spherulites were found along with negative ones. It is evident that TCL not only can improve the adhesion and stress-transfer between the interfaces but also can change the spherulite morphology on varying the crystallization conditions.

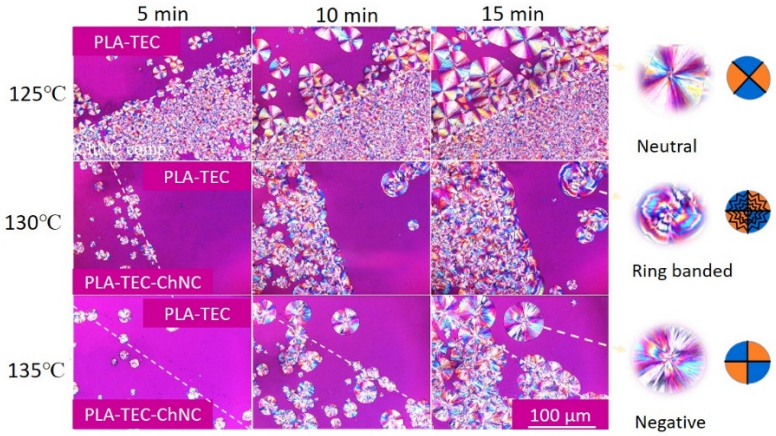

Figure 4.2. Comparison of transcrystallization behavior ChNCs at the surface of PLA-TEC and PLA-TEC-ChNC nanocomposite with isothermal crystallization temperatures of 135°C, 130°C, and 125°C and holding times of 5, 10, and 15 min. Dashed line shows the interface between the materials. Noticeably, on varying the isothermal crystallization temperatures; different spherulites morphology were observed; at 135°C negative spherulite; at 130°C ring banded spherulite and at 125°C neutral spherulites. As the crystallization time, reach to 10 min, a very sharp and clear TCL developed at both 130°C and 125°C of crystallization temperature. Adopted from paper I

To investigate the lamellar structure of the TCL and spherulites morphology developed during the crystallization study, SEM carried out. A fan-shaped TCL formed at the junction of PLA-TEC and PLA-TEC-ChNC as shown in Figure 4.3 (a). Further analysis revealed that lamellae were arranged differently for the spherulites. For example, radial growth of lamellae observed in Figure 4.3 (b), whereas a scattered lamellar pattern was seen in Figure 4.3 (c).

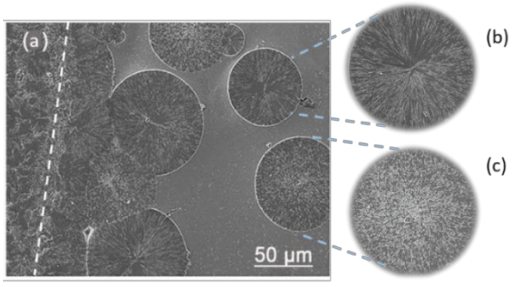

Figure 4.3. SEM micrographs (a) showing the lamellar structure of TCL developed at the interface between PLA-TEC and PLA-TEC-ChNC after isothermally crystallized at 125°C and different types of spherulites (b) banded and (c) spherulites with scattered lamellar pattern. Adopted from paper I

To investigate, the effect of ChNCs on the isothermal crystallization of PLA and PLA-TEC, films of all the materials were isothermally crystallized 125℃ for 30 min prior to XRD. Comparative XRD curves of PLA, PLA-TEC, and PLA-TEC-ChNC are shown in Figure 4.4 (a). The XRD peaks confirmed the presence of three different crystals of the PLA. A strong diffraction peak appeared at 16.7° assigned to α-form of the PLA [94]. Some weak diffraction peaks observed at 24°, 24.9° and 29.3° were assigned to the α'-form [95] and β-form of the PLA, respectively [96]. This confirms that both isothermal crystallization conditions and ChNCs have affected the crystal structure of PLA. The crystallite size of the materials was determined from the XRD curves and a decrease in the crystallite size observed in PLA-TEC-ChNC.

DSC measurements performed for PLA, PLA-TEC, and PLA-TEC-ChNC after isothermal crystallization at 125℃ for 30 min. DSC studies helped to understand the role of ChNC on the thermal behavior of the isothermally crystallized PLA-TEC-ChNC films. It was noticed from Figure 4.4 (b) that TEC reduced the T_g, T_{cc}, and T_m of the PLA-TEC (from 62℃, 101℃, 174℃ to 34℃, 68℃, 163℃, respectively) compared to the PLA. In a study, Muller *et al.* [97] used poly(ethylene glycol) (PEG) as a plasticizer and found that PEG influenced crystallization as well as the melting behavior of the PLA. They concluded that PEG interacted with the PLA lattice that led to a decrease in the melting temperature of PLA by 5℃.

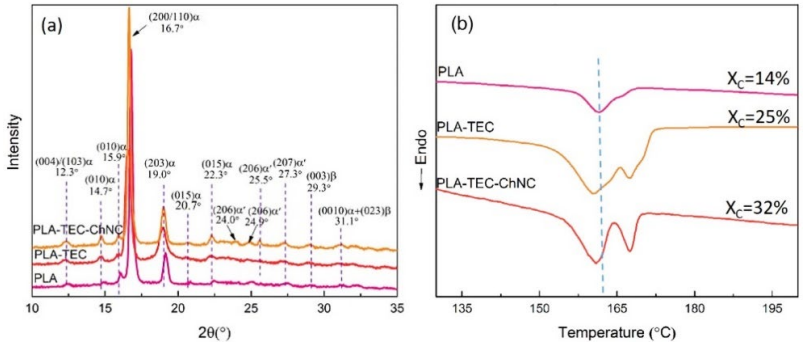

Figure 4.4. (a) XRD graphs and (b) 2nd DSC heating scans of PLA, PLA-TEC and PLA-TEC-ChNC after isothermally crystallized at 125℃ for 30 min. Adopted from paper I

It is well known that plasticizer increases the chain flexibility of the polymeric chains and shows a reduction in the thermal behavior of the polymers, especially T_g and T_{cc} [98]. However, the presence of ChNC in PLA-TEC has strongly affect thermal behavior and slightly higher values of T_g (37℃), T_{cc} (73℃), and T_m (166℃) seen in the PLA-TEC-ChNC due to the good nucleation ability of the ChNC. It can be seen from the DSC curves (Figure 4.4 (b)) that a double melting peak is observed in the PLA-TEC. The addition of 1wt% ChNC into PLA-TEC has not only affected the crystallization behavior but also had a strong effect on the melting behavior. Consequently, double melting peaks became sharper and shifted towards lower temperatures. Formation of double melting

peaks ascribed to the different crystal morphology of the PLA [99]. Shifting of melting peaks in PLA-TEC and PLA-TEC-ChNC revealed the occurrence of some interactions between the PLA, TEC, and ChNC. Furthermore, a higher degree of crystallinity was obtained in PLA-TEC-ChNC (32%) as compared to PLA-TEC (25%) and PLA (14%) which further confirmed the importance of ChNC.

Shapes and intensities of peaks are susceptible to the temperature that use to collect the spectra. In this study, to elucidate the role of ChNC on isothermal crystallization, FTIR performed. Figure 4.5 (a) illustrates the FT-IR spectra of the isothermally crystallized PLA, PLA-TEC and PLA-TEC-ChNC. The peaks at 2997 cm^{-1}, 2945 cm^{-1} and 2881 cm^{-1} ascribed to asymmetric, symmetric, and –CH stretching of CH_3, respectively PLA [100]. All samples exhibited peaks at 1759 cm^{-1} and 1188 cm^{-1}, assigned to –C=O, -C-O-C- stretching of PLA, respectively [100]. Here, the intensities and shape of the carbonyl peaks of PLA were less and broad. Conversely, the intensities of peaks were much higher, peaks became sharper in PLA-TEC, and PLA-TEC-ChNC compared to PLA due to the better crystallization efficiency. Some weak bands at 1658 cm^{-1} and 1619 cm^{-1} attributed to the amide I band of the acetamide group (NH_2-CO-CH_3) of chitin present in the PLA-TEC-ChNC and the peak at 1558 cm^{-1} ascribed to amide II (-NH bending) of the acetamide group [101]. The band at 3265 cm^{-1} and 3110 cm^{-1} attributed to –NH stretching [102]. The peak at 3504 cm^{-1} attributed to –OH group of the PLA shifted to the lower wavenumber in PLA-TEC and PLA-TEC-ChNC. This shifting of the peaks towards and higher intensities in the PLA-TEC-ChNC evident the occurrence of the H-bond interactions between the components of the nanocomposites and schematics of the H-bond developed during the crystallization of the PLA-TEC-ChNC depicted in Figure 4.5 (b). Two types of H-bond interactions including –NH-O=C- and –OH-O=C, can possibly occur due to the type functional groups available on the structure of the PLA, TEC, and ChNC. These interactions are expected to the reason for the improved crystallization of the PLA-TEC in the presence of ChNC, which also supported by the DSC and POM results.

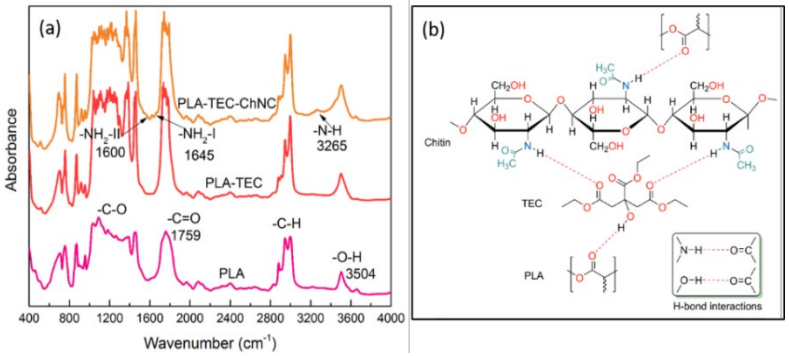

Figure 4.5. (a) FT-IR spectra of PLA, PLA-TEC, and PLA-TEC-ChNC and (b) schematic illustration of mechanism and interactions developed between the components of PLA-TEC-ChNC after the isothermal crystallization. Adopted from paper I

4.2. Effect of isothermal crystallization on properties of PLA and its nanocomposites

The knowledge gained about isothermal crystallization of materials from the paper I, further explored and investigated to understand how this isothermal crystallization in the presence of ChNC can affect the overall properties of PLA and its nanocomposites in a larger scale. In this study, relatively less amount of plasticizer (only 10 wt%) was used compared to paper I (20 wt%) to thoroughly investigate the effect of ChNC. Nanoreinforcements have the potentials to improve the properties of the polymers without compromising with transparency [103]. As noticed in the paper I that homogenous dispersion of ChNC played an important role to achieve homogenous crystallization. Therefore, in the study dispersion and distribution were investigate prior to isothermal crystallization. The dispersion and distribution of the nanocrystals in the polymer matrix is a function of the nanocrystals/polymer matrix compatibility and of the manufacturing method. To confirm the dispersion and distribution of the ChNC in PLA-TEC matrix, photographs and optical micrographs of the prepared films were taken. It can be seen from Figure 4.6, after the processing (liquid-assisted extrusion followed by compression molding) very clean and highly transparent films of the all the materials including neat PLA, PLA-TEC, and PLA-TEC-ChNC (89:10: 1wt%), which is attributed to fast cooling process during the compression molding led to low crystallinity in all three samples. It is further evident that ChNCs were well dispersed in the PLA-TEC and no agglomerates were visible in the optical micrographs of PLA-TEC-ChNC.

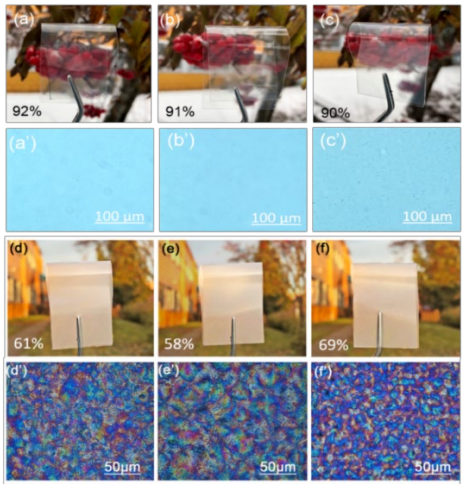

Figure 4.6. Visual appearance (a-c) and optical micrographs (a'-c') of neat PLA, PLA-TEC, and PLA-TEC-ChNC, respectively. High transparency and well dispersion are seen in PLA-TEC-ChNC. Photographs and POM images of isothermally crystallized PLA110 (d, d'), PLA-TEC110 (e, e') and PLA-TEC-ChNC110 (f, f'), respectively, showing the effect of isothermal crystallization on percentage transmittance and spherulites sizes of the materials. Adopted from paper II

After the confirmation of dispersion, materials were subjected to isothermal crystallization. Photographs and polarized optical micrographs of the films isothermally crystallized at 110℃ presented in Figure 4.6. Spherulites developed during the isothermal crystallization have affected the transparency of the materials resulted in a reduction in the transparency of all materials as compared to the neat films as shown in Figure 4.6 (e-f). The POM was used to observe the isothermal crystallization as well as to determine the spherulite size of these three samples (Figure 4.6. e'-f'). The size of the PLA, PLA-TEC, and PLA-TEC-ChNC were 49, 56, and 23 μm, respectively. As size of the spherulites of PLA-TEC-ChNC was lower compared to the PLA and PLA-TEC, therefore, the percentage transmittance of the PLA-TEC-ChNC was relatively higher (69%).

Thermal properties, crystallinity and crystallite size: Effect of isothermal crystallization and ChNCs on the thermal properties were determined using DSC and comparative curves of first heating scans of all their materials are shown in Figure 4.7 (a). As reported earlier, in this study also, plasticizer reduced T_g of PLA-TEC and PLA-TEC-ChNC to 45℃ and 37℃ as compared to PLA (62℃). However, there was no significant change in T*cc* and T*m* of all the three materials. Due to the higher nucleation ability of the ChNC in PLA-TEC-ChNC, the T*cc* peak was not visible and 47.5% of crystallinity achieved within 5 min of crystallization. Contrary, it took 40 min for PLA and PLA-TEC to reach a similar level of the degree of crystallinity. Further, XRD was carried out to measure the crystallite size of all three materials, and results are presented in Figure 4.7 (b). All samples exhibited diffraction peaks at 14.8º, 16.6º, 18.9º, and 22.2º, assigned to the (220/110), (203), and (015) planes of the PLA. It was noticeable that lowering the isothermal crystallization temperature to 110℃ resulted in very small crystallite size. The crystallite size of the PLA, PLA-TEC, and PLA-TEC-ChNC were in the order; 12 nm, 14 nm, and 8 nm, respectively, which further supports the DSC, POM as well as transparency results. It also confirmed the good nucleation ability of the ChNC.

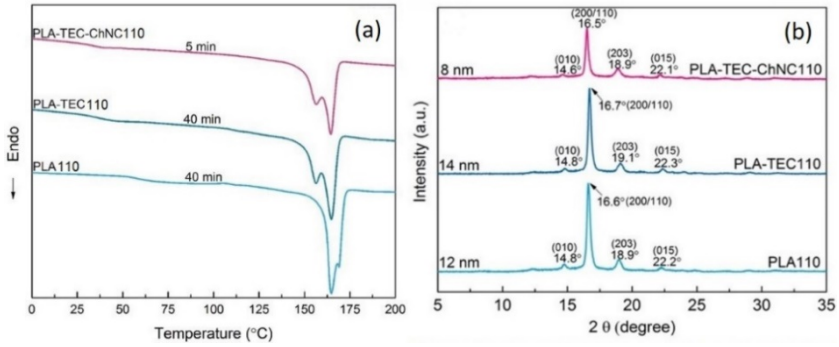

Figure 4.7. (a) DSC thermograms and (b) XRD graphs of isothermally crystallized PLA110, PLA-TEC110, and PLA-TEC-ChNC110. Adopted from paper II

Barrier properties: It is already mentioned in the previous section of the thesis that crystallinity greatly influences the properties of the PLA. Therefore, to elucidate it, the barrier properties of the isothermally crystallized films of PLA-TEC110 and PLA-TEC-

ChNC110 measured and comparative barrier properties of the materials are given in Figure 4.8. It can be seen from the chart that smaller spherulite and crystallite sizes of the PLA-TEC and PLA-TEC-ChNC has reduced the WVTR and OTR of the materials. Additionally, the presence of a very less amount of (1 wt%) ChNC in PLA-TEC-ChNC has decreased its WVTR and OTR values to 36% and 32%, respectively as compared to the PLA-TEC. Gas transport properties of the polymer composites are affected by various factors such as shape and aspect ratio of the reinforcements, degree of orientation, and loading of the reinforcements, interface, and degree of crystallinity [104–106]. Trifol *et al.* [107] studied how nanocellulose and nanoclays affected the barrier properties of PLA and they concluded that nanocellulose resulted in better barrier properties than nanoclays due to the variation in shape, size and a higher degree of crystallinity. In this present study, this increment in the barrier properties of the PLA-TEC-ChNC can be attributed to the good dispersion and distribution of the ChNCs resulted in the smaller spherulites size, which must have inhibited the permeation of the gas molecules within the PLA-TEC matrix.

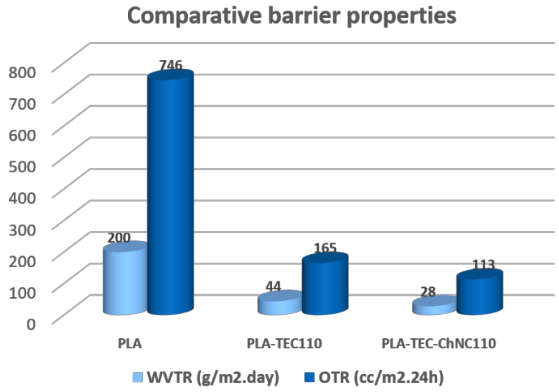

Figure 4.8. A comparative chart showing the WVTR and OTR of PLA, PLA-TEC110 and PLA-TEC-ChNC110. Isothermal crystallization has significantly decreased the WVTR and OTR of PLA-TEC110, and PLA-TEC-ChNC110

Hydrolytic degradation: Herein, the effect of crystallinity and ChNC on the hydrolytic degradation of the PLA-TEC-ChNC was examined. Figure 4.9 (a) shows the photographs of the hydrolytic degraded and disintegrated samples of PLA, PLA-TEC, and PLA-TEC-ChNC within 18 days. The weight loss of the materials during the hydrolytic test was measured and data is shown in Figure 4.9 (b). Initially, the degradation of all the three samples was very slow but it significantly increased after one week. Noticeably PLA-TEC-ChNC showed relatively improved degradation to that of PLA-TEC, possibly due to the smaller spherulites size. Paul *et al.* [108] investigated the effect of various types of montmorillonites (MMTs) on the hydrolytic degradation of PLA. It was observed that MMT accelerated the degradation of PLA. The authors concluded that composite structure as well as relative hydrophilicity played vital roles in the hydrolytic degradation of PLA. Similarly, here ChNC has promoted the degradation of PLA due to the functional

groups present in its structure.

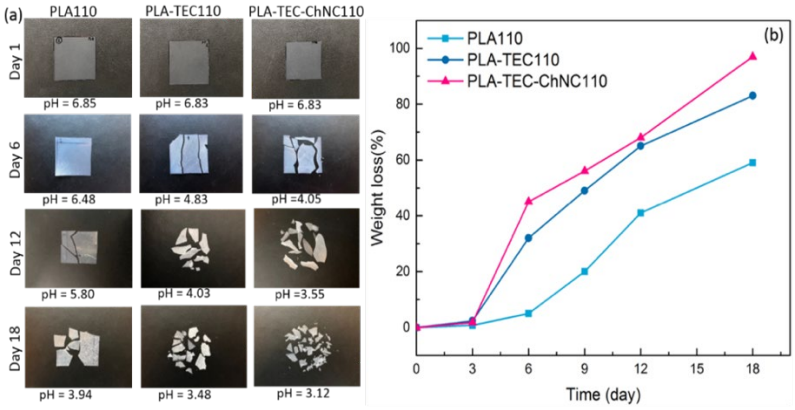

Figure 4.9. Images showing the visual changes in the PLA110, PLA-TEC110, and PLA-TEC-ChNC110 after hydrolytic degradation (form day 1 to day 18) (a) showing that the degradation has influenced the pH of the materials (b) chart depicting the change in a percentage weight loss of the material during the hydrolytic degradation. Adopted from paper II

Further, this hydrolytic degradation of the materials was confirmed with DSC and TGA. Samples were tested both before and after hydrolytic degradation. It can be seen from the DSC curves of the materials (Figure 4.10) that before degradation, double melting peaks were observed and after the degradation, only single peaks were seen in the DSC curves. Additionally, T_g peaks were also diminished after degradation. It is worth mentioning that the degree of crystallinity of the materials was increased after the degradation and it was in the following order, PLA110; 61%, PLA-TEC; 69%, and PLA-TEC-ChNC; 64%.
TGA curves show (Figure 4.10 (c)) that materials were very stable (up to 285℃) before the hydrolytic degradation. Water has greatly influenced the thermal stability of the materials and therefore, after degradation thermal stability reduced to 220℃. Moreover, DTG peaks were also affected by the water and resulting in a very sharp double DTG peak after the degradation. In the case of PLA-TGA-ChNC100, the hump of the peaks were very prominent as compared to the PLA110 and PLA-TEC110. It further evident the fast degradation of the materials with ChNC.

PLA undergo degradation in aqueous media by chain scission of the ester bonds [109] Firstly, the high molecular weight PLA chain break down into lower molecular weight chains. Then these lower molecular weight chains further undergo disintegration and cleaved into lactic acid and finally into water and CO_2. In this study, the chain scission of the PLA was carried out by the acid hydrolysis mechanism, and schematics of the mechanism is depicted in Figure 4.11.

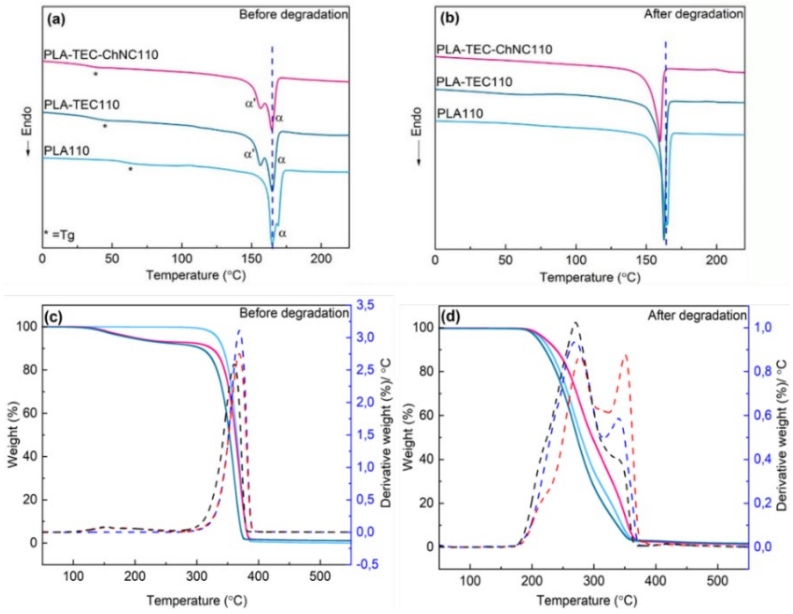

Figure 4.10. DSC (a, b) and TGA (c, d) curves of PLA110, PLA-TEC110, and PLA-TEC-ChNC110 before and after hydrolytic degradation

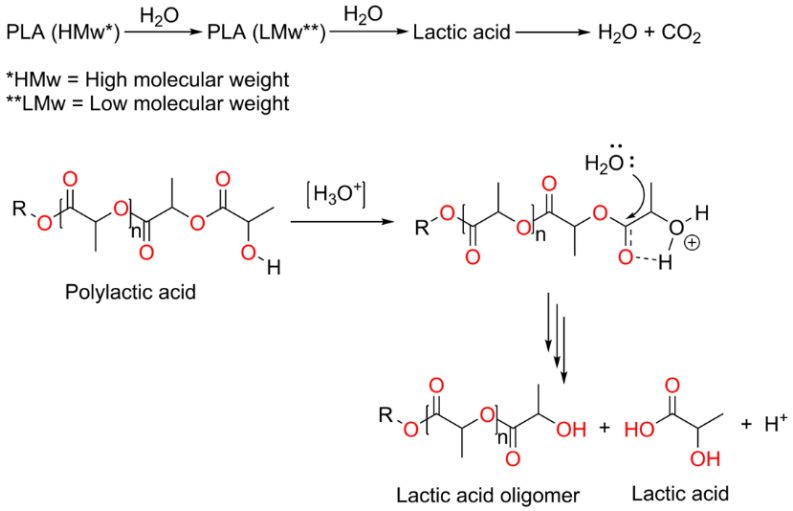

Figure 4.11. Schematic illustration of the mechanism of hydrolytic degradation of PLA into lactic acid and other oligomers. Adopted from paper II

4.3. Effect of orientation on properties of PLA nanocomposites

The orientation of polymers improves the overall mechanical properties of the polymers especially tensile strength and toughness [110]. Melt-state drawing [111] and/or solid-state drawing [112] are the commonly used methods to achieve the orientation of the polymers [112]. Different factors affect the orientation of the polymers such as draw temperature, draw ratio, and draw speed. Inspired from the previous research work of our group on the solid-state drawing (SSD), in this work (paper IV), a combination of melt-state (MSD) and SSD techniques were employed to orient the nanocomposites of PLA-GTA-ChNC (79:20:5 wt%). A pre-orientation performed using MSD and its effect on the mechanical properties were investigated. The mechanical properties of undrawn nanocomposites prepared by compression molding (CM) compared with drawn samples obtained by a two-step orientation (MSD and SSD) (FC-2-SSD-5) and results are shown in Figure 4.12. It can be seen from the stress-strain curves (Figure 4.12 (a)) and chart (Figure 4.12 (b)) that the orientation has greatly influenced the overall mechanical properties of the drawn samples. Consequently, all the tensile properties increased including tensile modulus, tensile strength, elongation at break, and toughness of the drawn (FC-2-SSD-5) nanocomposites, by 74%, 360%, 2400%, and 9500%, respectively to that of undrawn nanocomposites. This increment in the mechanical properties is due to the alignment of the molecular chains of PLA and ChNC in the FC-2-SSD-5 samples.

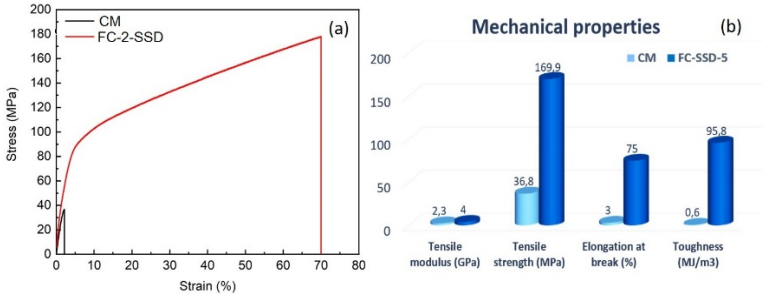

Figure 4.12. Mechanical properties of the undrawn (CM) and drawn (FC-2-SSD-5) nanocomposites (a) stress-strain curves of the CM and FC-2-SSD-5 (b) comparative chart of the mechanical properties of CM and FC-2-SSD-5

After tensile testing, photographs of the samples were taken for visual analysis (Figure 4.13) and it can be visible from the pictures (Figure 4.13 (b)) that after SSD, FC-2-SSD-5 samples have become opaque/white due to the stretching as compared to the CM (Figure 4.13 (a)), where the image was very transparent. In the drawn sample, some fibrils like structure are also seen. Further, drawing has reduced the thickness of the films resulted in a very thin cross-section of the films as shown by white arrows in the SEM micrographs of the FC-2-SSD-5, which evidence that the molecular chains aligned after orientation. DSC results also showed an increase in the degree of crystallinity of FC-2-SSD-5 (from to 53%) that further supports the alignment of the PLA as well as ChNC chains. Moreover, the T_{cc} of the drawn samples were also decreased to 63°C to that of undrawn (100°C), which again confirmed the transformation of the amorphous phase owing to the

orientation.

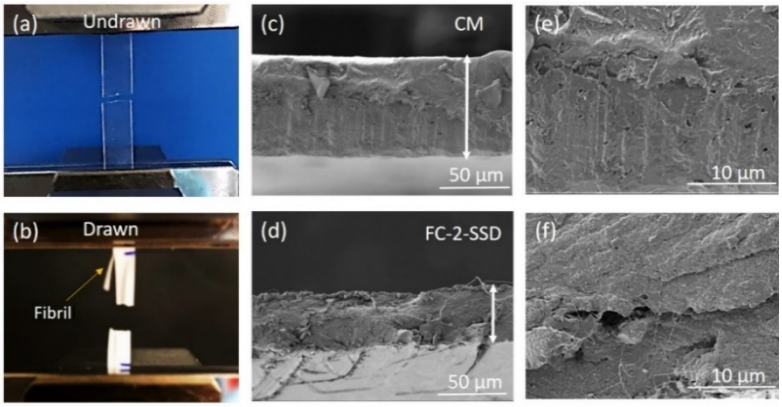

Figure 4.13. Fractured samples of (a) CM and (b) FC-2-SSD-5 after the tensile test. SEM micrographs of the tensile fractured samples of (c) CM and (d) FC-2-SSD showing a reduction in cross-section are of FC-2-SSD due to orientation. Adopted from paper III

The significant effect of orientation on the mechanical properties of nanocomposites encouraged us to investigate the possible reasons for the improvements. Figure 4.14 (a, a') shows the POM images of the undrawn and drawn samples. After drawing the nanocomposites (FC-2-SSD-5) showed strain-induced birefringence under POM at 45° to the direction of the cross-polarizer. This evident the higher degree of alignment of the molecular chains due to the drawing of the nanocomposites [113].

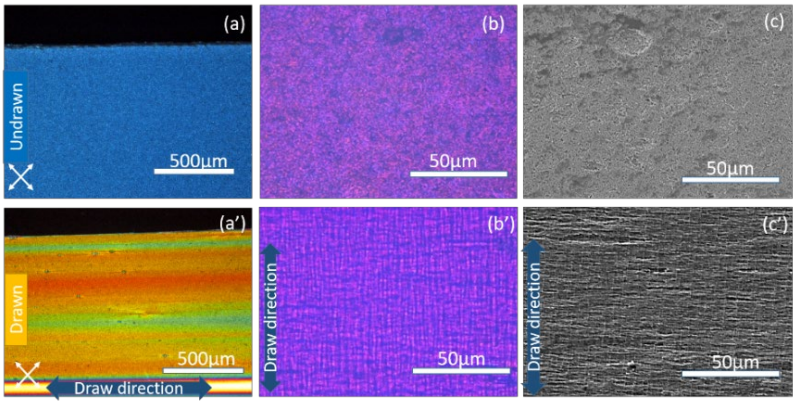

Figure 4.14. POM images of the (a) undrawn (CM) and (b) drawn FC-2-SSD-5 indicating the stain-induced birefringence behavior and a high degree of orientation. POM and SEM micrographs of the CM (b-b') and FC-2-SSD-5 (c-c') samples after etching the surface. Adopted from paper III

Noticeably, drawn samples showed a very homogenous birefringence that ascribed to the good dispersion and distribution of the ChNC into the GTA-PLA matrix. Both undrawn and drawn samples etched for further study. The etching was performed to remove the amorphous part from the nanocomposites to understand the orientation. After etching POM and SEM micrographs were taken as shown in the Figure 4.14 (b,b') and Figure 4.14 (c, c'), respectively and a clear orientation can be seen in the drawn samples due to the high draw ratio, which helped the molecule chains to align in the direction of the drawing. After etching, shish-kebab morphology formed that led to a cross-patterned structure in the drawn samples. Shish-kebab morphology develops due to the folding of the polymeric chains [114].

Figure 4.15 shows the schematic of the ordering of the molecular chains developed during the orientation. In this study, the PLA chain must have folded together during the MSD and formed some spherulites as depicted in Figure 4.15 (a-b). It is worth mentioning that in this study MSD followed by SSD (at 60°C), therefore during the stretching some tie molecules would have developed in the PLA nanocomposites, especially in the amorphous part. These tie-molecules must be responsible for the good mechanical properties of the drawn nanocomposites especially the toughness and strength because tie molecules can be attached to the crystalline lamellae and improve the flexibility of the nanocomposites. As mentioned in the earlier part of the thesis that nanochitin exhibits $-NH_2-CO-$ group in its molecular structure, which can form some hydrogen bond interaction with the polymer (PLA) and plasticizer (GTA) that would have led to the formation of tie-molecules in the drawn nanocomposites.

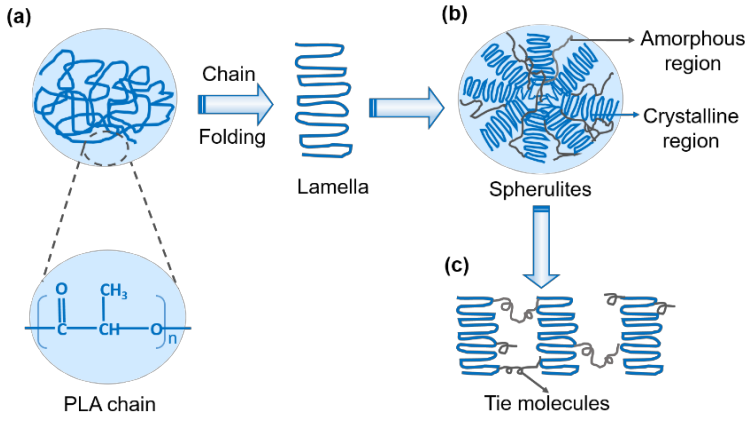

Figure 4.15. Schematic illustration showing how polymer chains arrange during the orientation of the nanocomposites (a) arrangement of the molecular chains to form the ordered lamella (b) demonstrates the amorphous and crystalline part of the PLA (c) formation of tie molecules in the amorphous part owing to the orientation. Adopted from paper III

4.4. Effect of surface modification of CNCs on properties of PLA

In paper IV, only 1 wt% CNCs was used as nanoreinforcement in the PLA matrix without using any plasticizer to observe the overall effect of CNC. As discussed in the introduction part that CNCs tend to agglomerate, which makes it difficult to disperse in PLA. Surface modification of the nanoreinforcements helps to improve the compatibility between polymer and reinforcement that eventually affects the properties of nanocomposites [115]. Therefore, the surface of the CNC was modified via ring-opening polymerization (ROP) to enhance the dispersion and compatibility of the CNC into the PLA matrix. The effectiveness of grafting verified by FT-IR and comparative spectra of L-lactide, CNC, and mCNC is presented in Figure 4.16 (a). A sharp and intense band at 1739 cm^{-1} in mCNC spectra attributed to the carbonyl stretching frequency of the PLA that was absent in the CNC, which evident the grafting. Moreover, the characteristic bands of L-lactide (1212 and 1296 cm^{-1}) were not present in the mCNC, which confirmed that unreacted monomer washed away during the purification process. As expected well dispersed nanoreinforcements speed up the crystallization process. Hence, POM was used to investigate both dispersion and crystallization behavior of the CNC and mCNC in PLA matrix. The nanocomposites crystallized at 125℃ for 10 min and micrographs were recorded. Figure 4.16 (b, c) shows the POM images of the crystallized PLA/CNC and PLA/mCNC. As expected, mCNC has not only improved the dispersion as well as the rate of crystallization of PLA/mCNC. Subsequently, very homogenous spherulites were seen within 3 min of crystallization in PLA/mCNC, which confirmed the good nucleation ability of the mCNC. Conversely, PLA, and PLA/CNC took a longer time (10 min) to crystalize and larger spherulites were developed.

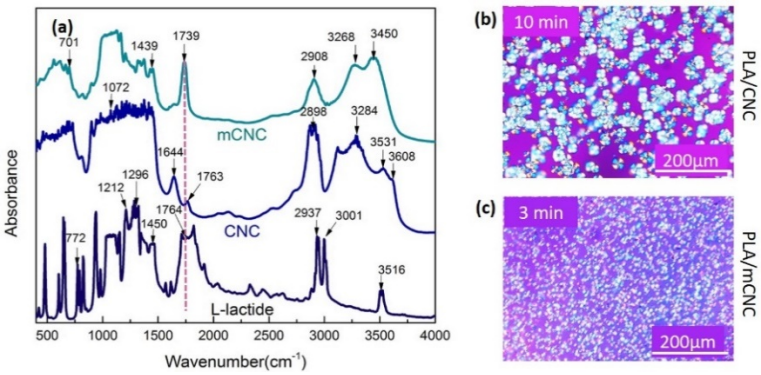

Figure 4.16. (a) FTIR spectra of L-lactide, CNC, and mCNC. A clear and sharp peak at 1739 cm^{-1} observed in mCNC is indicative of the grafting (b) POM images of the isothermally crystallized (at 125℃) CNC films (c) showing the enhanced crystallization due to surface modification of mCNC resulted an increased number of spherulites, decreased crystallization time and spherulite size. Adopted from paper IV

Nanocomposites of PLA with 1 wt% CNC and mCNC were prepared by film calendaring followed by post-processing using compression molding. Prior to prepare

nanocomposites of PLA/CNC and PLA/mCNC, dispersion of the nanomaterials were confirmed by flow birefringence. As it can see from, Figure 4.17 that mCNC showed very intense flow colors compared to the CNC during flow birefringence indicating that the modification has increased the dispersion of mCNC.

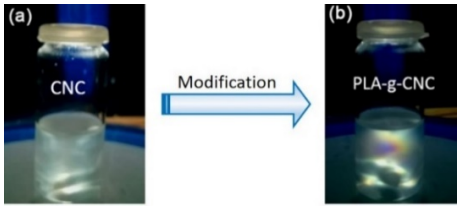

Figure 4.17. Flow birefringence images of (a) CNC and (b) mCNC dispersed in DMF solution

In order to evaluate possible thermos-degradation effects of this post-extrusion protocol, the molecular weights such as Mv, Mn and Mw of all the materials were estimated through the determination of the intrinsic viscosity (IV) and obtained results are presented in Table 4.1. The intrinsic viscosities values of PLA films and PLA plates were reduced by 21% and 22%, respectively, compared to neat PLA pellets. However, IV of PLA/CNC and PLA/mCNC films and plates were similar to the PLA film and plates. Average molecular weights (Mv, Mn, and Mw) of the PLA/CNC and PLA/mCNC were also similar to the PLA films and plates. It indicates that the average molecular weights of the PLA nanocomposites were not affected by both the processing techniques; including extrusion calendering and compression molding. Results evident that the processing causes a maximum loss of 8%, which confirmed that different processing has no significant effect on the degradation.

Table 4.1. Effect of addition of CNC and mCNC on intrinsic viscosity of PLA and estimation of molecular weight of the PLA and its nanocomposites

Materials name	Processing method	Intrinsic viscosity [η] (g/dl)	Average molecular weight (kg/mol)		
			Mv*	Mn*	Mw*
PLA pellets	Supplier	1.4	91.4	48.4	96.7
PLA film	Calendering	1.1	67.0	35.5	70.9
PLA film	Compression molding	1.1	65.5	34.7	69.3
PLA/CNC film	Calendering	1.1	64.0	33.8	67.7
PLA/CNC film	Compression molding	1.1	59.6	31.5	63.0
PLA/mCNC film	Calendering	1.1	67.8	35.9	71.7
PLA/mCNC film	Compression molding	1.1	64.8	34.3	68.6

***Mv** =Viscosity average molecular weight; were calculated using Mark Houwink-Sakurada equation
***Mn=**Number average molecular weight; were calculated based on the Mn=Mv/1.89
***Mw=** Weight average molecular weight; were calculated by using equation (10)

Thermal properties of the prepared PLA and its nanocomposites with CNC and mCNC were tested to investigate the effect of modification on the glass transition temperature (T_g), cold crystallization temperature (T_{cc}), and melting temperature (T_m) and DSC curves are shown in Figure 4.18. The first heating scan shows that CNC has slightly reduced the T_g of PLA from 64.4 to 64.0°C. However, T_g was comparatively increased by the modified CNC and it was the same as the neat PLA (64.4°C). Sung *et al.* [116] also observed a decrease in T_g of PLA after the addition of 1 wt% CNC (T_g decreased from 61.4 to 61.1°C). Figure 4.18 (a, c) showed a double melting peak in the DSC curves of PLA. It assigned to a melting/re-crystallization/ re-melting mechanism [117]. T_m of the PLA decreased from 168.8 to 167.3 and 167.6°C with CNC and mCNC, respectively. This reduction of T_m can be due to the (i) lowering of cold crystallization temperature which generally leads to smaller lamellae thickness [118] and/ or (ii) the presence of CNC and modified CNC might have restricted the chain mobility of the PLA. The addition of CNC and modified CNC reduced T_{cc} of PLA from 111.4 to 103.6 and 101.3°C, respectively. Similar results can be seen from the second heating scan; here the T_{cc} of PLA was decreased from 111.7 to 104. 2°C with CNC and with modified CNC; it was further decreased to 98.9°C. This shift of the T_{cc} peak of PLA in PLACNC and PLAmCNC towards lower temperatures is seen in Figure 4.18 (a, c). It indicates that the addition of CNC and mCNC favors the recrystallization of PLA [119]. The cooling scan also shows a decrease in T_c of PLA from 96.8 to 95.0 and 92.5°C with CNC and modified CNC, respectively. Lizunida *et al.* [120], reported a decrease in T_{cc} of PLA during the heating scan, grafted CNC decreased the T_{cc} of PLA by 10°C. This decrease in T_{cc} during heating scans indicates a faster rate of crystallization. The degree of crystallinity of PLA, PLACNC, and PLA/mCNC calculated from the first and second heating cycles. PLA an amorphous behavior with a degree of crystallinity of 2%. This low degree of crystallinity of PLA was attributed to the slow crystallization kinetics of the PLA. The addition of CNC and mCNC slightly increases the crystallinity of PLA from 2-12% and 18%, respectively.

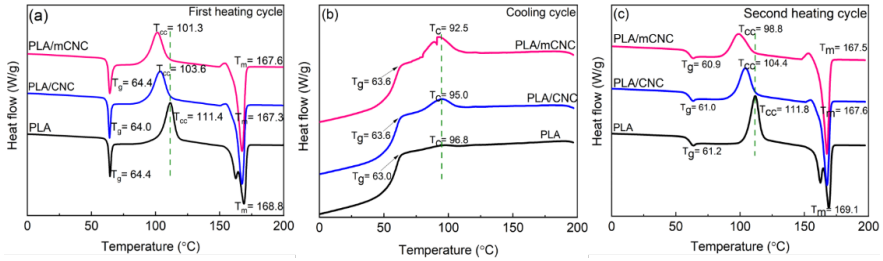

Figure 4.18. DSC curves of PLA, PLA/CNC and PLA/mCNC obtained from (a) first heating cycle (b) cooling cycle, and (c) second heating cycles showing T_g, T_{cc}, T_c, and T_m of the materials

The mechanical properties of the unmodified (PLA/CNC) and modified (PLA/mCNC) nanocomposites were tested by two different techniques *viz*, tensile test, and small punch test to evaluate the effectiveness of the modification. It is worth mentioning that the

tensile test was carried out in a uniaxial mode whereas SPT performed in a biaxial loading mode. The SPT was performed with the help of co-authors. Therefore, the details of only the tensile test have been discussed here. The mechanical properties of the tensile test were calculated from the engineering stress-strain curve and the results are shown in the Figure 4.19. All the materials exhibited three types of behavior based on the stress-strain traces. PLA showed a 'ductile' behavior, PLA/CNC represents a 'Ductile with cold drawing' behavior and due to addition of modified CNC, a typical 'brittle' behavior observed in PLA/mCNC. These behaviors were analyzed using OM and micrographs of the samples are depicted in Figure 4.19 (ii). A visual inspection of the tested materials exhibited no necking around the broken zone of the samples. However, crazes were observed, which are a much-localized phenomenon and confined to a small volume of the material [121]. The decline in engineering stress observed in the curves of materials (Figure 4.19 (i)) because of the decrease in the load-bearing part of the specimen was owing to the formation of crazes. These structures are depicted as a whitening area after adjusting the angle of incidence of the light beam on the fracture surface in Figure 4.19 (ii). Massive crazing on the fractured surfaces of the PLA and PLA/CNC was observed, whereas the surface of the PLA/mCNC looks much transparent. It evident that the surface modification of the CNC has drastically decreased the number of crazes due to the greater interaction between PLA and mCNC. Conversely, in the PLA/CNC, where a great number of crazes appeared with respect to the PLA. It can be because of the poor adhesion between the PLA matrix and CNC. Therefore, the particles of CNC, which may not have adhered to the matrix, may have acted as stress concentrators and would have promoted the number of crazes with a smaller size as compared to the neat PLA. This enhances the volume of plastic deformation that involved in the deformation process and thus providing a slight gain in the ductility of the material.

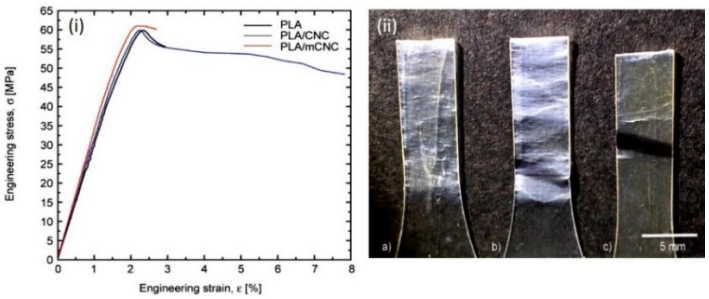

Figure 4.19. (i) Engineering stress-strain curves of PLA, PLA/CNC and PLA/mCNC (ii) optical micrographs of (a) PLA, (b) PLA/CNC, and (c) PLA/mCNC showing the crazing behavior of the samples. Adopted from paper IV

Figure 4.20 depicts the results of mechanical properties of PLA, PLA/CNC, and PLA/mCNC. Figure (a) and (b) shows some improvements of tensile modulus and strength of the PLA/mCNC as compared to the PLA and PLA/CNC. On the other hand, there is an increase of 11% in the elastic modulus of the PLA was observed by the addition of mCNC into this, whereas no significant change was observed with CNC. This may be related to the better matrix-mCNC interactions promoted by the mCNC.

The yield strain of PLA was decreased with CNC and mCNC as shown in Figure (c).Figure (d) demonstrates an increase of 167% in the elongation break of the PLA/CNC, which further confirm the ductile nature of the nanocomposites.

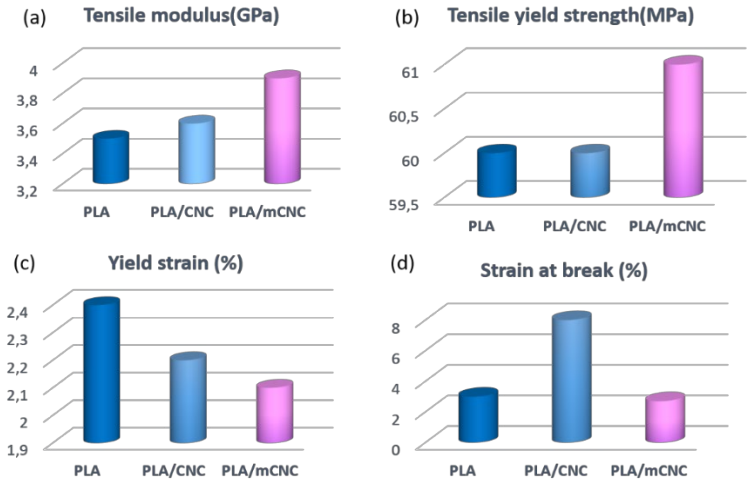

Figure 4.20. A comparative chart showing the mechanical properties of the PLA, PLA/CNC, and PLA/mCNC after the tensile test. Adopted from paper IV

CHAPTER 5: Conclusions and future scopes

5.1. Conclusions

In the context of developing alternative materials for sustainable and futuristic growth, PLA-based nanocomposites are highly promising. In this study, attempts have given to alleviate some of the challenges of the PLA-based nanocomposites. Focus has been given to slow crystallization rate and brittleness. The present thesis is an account for the processing of the ChNC/CNC reinforced-PLA nanocomposites, their structure, and properties closely relevant for packaging applications. The following conclusions can be drawn based on the results achieved in this thesis.

- Dispersion and distribution of the ChNC improved by the melt-extrusion process, which is attributed to the better compatibility between the PLA and or plasticized PLA and nanoreinforcements. The Effect of this well dispersed and distributed ChNC on crystallinity and properties of PLA-based nanocomposites have been investigated.
- ChNCs have acted as good nucleating agents and it was confirmed by microscopic studies (POM, SEM), and supported by DSC and XRD results. Additionally, the Lauritzen-Hoffman nucleation theory also confirmed the good nucleation ability of the ChNCs. Plasticizers have certainly facilitated the crystallization process. However, the addition of only a very small amount of ChNCs (1 wt%) into plasticized PLA has immensely improved the crystallization rate by reducing the crystallization time and crystallite size. Furthermore, the effect of ChNCs on crystallization and transcrystallization have studied and microscopic results revealed that rarely found neutral type of spherulites were observed along with common negative type. Interestingly at 130°C, ring-banded spherulites appeared. Crystallization conditions (temperature and time) have resulted in the different lamellar structures of the spherulites.
- This improved crystallization rate led to a very high degree of crystallinity of the plasticized PLA nanocomposites (PLA-TEC-ChNC110) (48%) as confirmed by DSC, which ascribed to the good dispersions. Additionally, it reduced the spherulite size to 23μm as compared to the PLA110 (49μm). This reduction in the size of the spherulites has affected the optical and barrier properties. Due to the smaller spherulites size of the PLA-TEC-ChNC110, light could easily be passed through the samples and hence higher light transmittance observed (69%). Barrier properties (WVTR and OTR) were significantly reduced. Further, increased crystallinity has strongly affected the hydrolytic degradation behavior of the PLA-based nanocomposites.
- Orientated PLA-GTA-ChNC nanocomposites films achieved by combining a melt-state and solid-state process. This two-step orientation has led to a multifold increment in the overall properties of the nanocomposites. For examples, all mechanical properties including tensile modulus (2 fold), tensile strength (5 fold), elongation at break (25 fold), and toughness (96 fold) were greatly improved due

to the alignment of the molecular chains of the ChNCs and PLA.

- Grafting of PLA chains on the surface of CNC has improved the dispersion of CNC in the PLA matrix resulted in reduced crazing behaviour observed during the tensile test, which demonstrates better adhesion between modified CNC and PLA. Furthermore, well-dispersed mCNC increased the crystallization rate of the PLA/mCNC by reducing the overall crystallization time form 10 min to 3 min as compared to the PLA/CNC.

5.2. Future scopes

In future, more focus will be given to developing integrated studies to understand the process-structure-property relationships of the PLA-based nanocomposites. Although promising results have been achieved in this study, some further investigated can be done to increase the applicability of the developed nanocomposites.

For example, the use of green solvents (instead of toluene) for the modification of the nanoreinforcements will be helpful to develop materials for a sustainable economy. Modified CNC has shown interesting results in SPT. Therefore, in the future, it will be interesting to produce PLA/mCNC with a high content of mCNC to enhance the applicability of the SPT. It is possible that on increasing the mCNC content more effect on the mechanical properties will be observed due to the greater reinforcing effects. As the addition of ChNC has shown great improvement in the overall properties of the nanocomposites, therefore it will be interesting to use ChNC (with various wt%) based nanocomposite for SPT.

Since isothermal crystallization has influenced the hydrolytic degradation behaviour of the PLA-GTA-ChNC nanocomposites. A further study on soil degradation and or composite testing will be interesting. Critical evaluation of the functional properties; especially biodegradation of the PLA-based packaging is required before it can be launched in the market at the commercial level. Full understanding of the effect of incorporation of nanoreinforcements on food safety needs to be studied to prevent the migration of these materials into the food products. Some tests related to the toxicity of the prepared nanocomposites also need to be carried out.

References:

1. Hottle, T.A.; Bilec, M.M.; Landis, A.E. Sustainability assessments of bio-based polymers. *Polym. Degrad. Stab.* **2013**, *98*, 1898–1907.
2. Sinclair, R.G. The case for polylactic acid as a commodity packaging plastic. *J. Macromol. Sci.-Pure Appl. Chem.* **1996**, *33*, 585–597.
3. Burgos, N.; Valdés, A.; Jiménez, A. Valorization of agricultural wastes for the production of protein-based biopolymers. *J. Renew. Mater.* **2016**, *4*, 165–177.
4. Jambeck, J.R.; Geyer, R.; Wilcox, C.; Siegler, T.R.; Perryman, M.; Andrady, A.; Narayan, R.; Law, K.L. Plastic waste inputs from land into the ocean. *Science (80),* **2015**, *347*, 768–771.
5. *https://www.statista.com/statistics/282732/global-production-of-plastics-since-1950/*.
6. Plastics-the Facts **2019**, *https://www.plasticseurope.org/application/files*
7. Plackett, D. *Biopolymers-New Materials for Sustainable Films and Coatings*, First Edition, **2011**, John Wiley & Sons, Ltd., ISBN: 9780470683415.
8. Arrieta, M.P.; Fortunati, E.; Dominici, F.; Rayón, E.; López, J.; Kenny, J.M. Multifunctional PLA-PHB/cellulose nanocrystal films: Processing, structural and thermal properties. *Carbohydr. Polym.* **2014**, *107*, 16–24.
9. Castro-Aguirre, E.; Iñiguez-Franco, F.; Samsudin, H.; Fang, X.; Auras, R. Poly(lactic acid)-Mass production, processing, industrial applications, and end of life. *Adv. Drug Deliv. Rev.* **2016**, *107*, 333–366.
10. Murariu, M.; Dubois, P. PLA composites: From production to properties. *Adv. Drug Deliv. Rev.* **2016,** *107*, 17–46.
11. Garlotta, D. A literature review of poly(lactic acid). *J. Polym. Environ.* **2001**, *9*, 63–84.
12. Lim, L.T.; Auras, R.; Rubino, M. Processing technologies for poly(lactic acid). *Prog. Polym. Sci.* **2008**, *33*, 820–852.
13. Carothers, W.H.; Borough, G.L.; Natta, F.J. Studies of polymerization and ring formation. X. The reversible polymerization of six-membered cyclic esters. *J. Am. Chem. Soc.* **1932**, *54*, 761–772.
14. Drumright, R.E.; Gruber, P.R.; Henton, D.E. Polylactic acid technology. *Adv. Mater.* **2000**, *12*, 1841–1846.
15. Farah, S.; Anderson, D.G.; Langer, R. Physical and mechanical properties of PLA, and their functions in widespread applications-A comprehensive review. *Adv. Drug Deliv. Rev.* **2016,** *107*, 367–392.
16. Raquez, J.M.; Habibi, Y.; Murariu, M.; Dubois, P. Polylactide (PLA)-based nanocomposites. *Prog. Polym. Sci.* **2013**, *38*, 1504–1542.
17. Nampoothiri, K.M.; Nair, N.R.; John, R.P. An overview of the recent developments in polylactide (PLA) research. *Bioresour. Technol.* **2010**, *101*, 8493–8501.
18. Rasal, R.M.; Janorkar, A. V.; Hirt, D.E. Poly(lactic acid) modifications. *Prog. Polym. Sci.* **2010**, *35*, 338–356.
19. Fan, Y.; Nishida, H.; Shirai, Y.; Tokiwa, Y.; Endo, T. Thermal degradation

behaviour of poly(lactic acid) stereocomplex. *Polym. Degrad. Stab.* **2004**, *86*, 197–208.
20. Pantani, R.; De Santis, F.; Sorrentino, A.; De Maio, F.; Titomanlio, G. Crystallization kinetics of virgin and processed poly(lactic acid). *Polym. Degrad. Stab.* **2010**, *95*, 1148–1159.
21. Sánchez, F.H.; Mateo, J.M.; Colomer, F.J.R.; Sánchez, M.S.; Ribelles, J.L.G.; Mano, J.F. Influence of low-temperatue nucleation on the crystallization process of poly(L-lactide). *Biomacromolecules* **2005**, *6*, 3283–3290.
22. Kokturk, G.; Piskin, E.; Serhatkulu, T.F.; Cakmak, M. Evolution of phase behavior and orientation in uniaxially deformed polylactic acid films. *Polym. Eng. Sci.* **2002**, *42*, 1619–1628.
23. Rangari, D.; Vasanthan, N. Study of strain-induced crystallization and enzymatic degradation of drawn poly(l-lactic acid) (PLLA) films. *Macromolecules* **2012**, *45*, 7397–7403.
24. Vestena, M.; Gross, I.P.; Müller, C.M.O.; Pires, A.T.N. Nanocomposite of poly(lactic acid)/cellulose nanocrystals: Effect of CNC content on the polymer crystallization kinetics. *J. Braz. Chem. Soc.* **2016**, *27*, 905–911.
25. Kawai, T.; Rahman, N.; Matsuba, G.; Nishida, K.; Kanaya, T.; Nakano, M.; Okamoto, H.; Kawada, J.; Usuki, A.; Honma, N.; Nakajima, K.; Matsuda, M. Crystallization and melting behavior of poly (L-lactic acid). *Macromolecules* **2007**, *40*, 9463–9469.
26. Eling, B.; Gogolewski, S.; Pennings, A.J. Biodegradable materials of poly(l-lactic acid): 1. Melt-spun and solution-spun fibres. *Polymer (Guildf).* **1982**, *23*, 1587–1593.
27. Nagarajan, V.; Zhang, K.; Misra, M.; Mohanty, A.K. Overcoming the fundamental challenges in improving the impact strength and crystallinity of PLA biocomposites: Influence of nucleating agent and mold temperature. *ACS Appl. Mater. Interfaces* **2015**, *7*, 11203–11214.
28. Vasanthakumari, R.; Pennings, A.J. Crystallization kinetics of poly(l-lactic acid). *Polymer (Guildf).* **1983**, *24*, 175–178.
29. Androsch, R.; Schick, C.; Di Lorenzo, M.L. Kinetics of nucleation and growth of crystals of poly(L-lactic acid). In *Advances in Polymer Science*; **2018**, 279, 235–272.
30. Iannace, S.; Nicolais, L. Isothermal crystallization and chain mobility of poly(L-lactide). *J. Appl. Polym. Sci.* **1997**, *64*, 911–919.
31. Lauritzen, J.I.; Hoffman, J.D. Theory of formation of polymer crystals with folded chains in dilute solution. *J. Res. Natl. Bur. Stand. Sect. A Phys. Chem.* **1960**, *64A*, 73-102.
32. Avrami, M. Kinetics of phase change. I: General theory. *J. Chem. Phys.* **1939**, *7*, 1103–1112.
33. Avrami, M. Kinetics of phase change. II Transformation-time relations for random distribution of nuclei. *J. Chem. Phys.* **1940**, *8*, 212–224.
34. Avrami, M. Granulation, phase change, and microstructure kinetics of phase change. III. *J. Chem. Phys.* **1941**, *9*, 177–184.

35. Kalb, B.; Pennings, A.J. General crystallization behaviour of poly(l-lactic acid). *Polymer (Guildf).* **1980**, *21*, 607–612.
36. Miyata, T.; Masuko, T. Crystallization behaviour of poly(L-lactide). *Polymer (Guildf).* **1998**, *39*, 5515–5521.
37. Sarasua, J.R.; Arraiza, A.L.; Balerdi, P.; Maiza, I. Crystallization and thermal behaviour of optically pure polylactides and their blends. *J. Mater. Sci.* **2005**, *40*, 1855–1862.
38. Di Lorenzo, M.L. Crystallization behavior of poly(l-lactic acid). *Eur. Polym. J.* **2005**, *41*, 569–575.
39. Kumar S., R.; Maiti, S.N.; Ghosh, A.K. Crystallization, Morphological, and Mechanical Response of Poly(Lactic Acid)/Lignin-Based Biodegradable Composites. *Polym. - Plast. Technol. Eng.* **2016**, *55*, 475–485.
40. Yuryev, Y.; Wood-Adams, P.; Heuzey, M.C.; Dubois, C.; Brisson, J. Crystallization of polylactide films: An atomic force microscopy study of the effects of temperature and blending. *Polymer (Guildf).* **2008**, *49*, 2306–2320.
41. Fukushima, K.; Tabuani, D.; Dottori, M.; Armentano, I.; Kenny, J.M.; Camino, G. Effect of temperature and nanoparticle type on hydrolytic degradation of poly(lactic acid) nanocomposites. *Polym. Degrad. Stab.* **2011**, *96*, 2120–2129.
42. Ouchiar, S.; Stoclet, G.; Cabaret, C.; Gloaguen, V. Influence of the Filler Nature on the Crystalline Structure of Polylactide-Based Nanocomposites: New Insights into the Nucleating Effect. *Macromolecules* **2016**, *49*, 2782–2790.
43. Nam, J.Y.; Sinha Ray, S.; Okamoto, M. Crystallization behavior and morphology of biodegradable polylactide/layered silicate nanocomposite. *Macromolecules* **2003**, *36*, 7126–7131.
44. Shi, X.; Zhang, G.; Phuong, T.V.; Lazzeri, A. Synergistic effects of nucleating agents and plasticizers on the crystallization behavior of Poly(lactic acid). *Molecules* **2015**, *20*, 1579–1593.
45. Xiao, H.; Yang, L.; Ren, X.; Jiang, T.; Yeh, J.T. Kinetics and crystal structure of poly(lactic acid) crystallized nonisothermally: Effect of plasticizer and nucleating agent. *Polym. Compos.* **2010**, *31*, 2057–2068.
46. Tsuji, H.; Takai, H.; Saha, S.K. Isothermal and non-isothermal crystallization behavior of poly(l-lactic acid): Effects of stereocomplex as nucleating agent. *Polymer (Guildf).* **2006**, *47*, 3826–3837.
47. Xu, J.-Z.; Chen, T.; Yang, C.-L.; Li, Z.-M.; Mao, Y.-M.; Zeng, B.-Q.; Hsiao, B.S. Isothermal Crystallization of Poly(l-lactide) Induced by Graphene Nanosheets and Carbon Nanotubes: A Comparative Study. *Macromolecules* **2010**, *43*, 5000–5008.
48. Nam, J.Y.; Okamoto, M.; Okamoto, H.; Nakano, M.; Usuki, A.; Matsuda, M. Morphology and crystallization kinetics in a mixture of low-molecular weight aliphatic amide and polylactide. *Polymer (Guildf).* **2006**, *47*, 1340–1347.
49. Kawamoto, N.; Sakai, A.; Horikoshi, T.; Urushihara, T.; Tobita, E. Nucleating agent for poly(L-lactic acid)-An optimization of chemical

structure of hydrazide compound for advanced nucleation ability. *J. Appl. Polym. Sci.* **2007**, *103*, 198–203.
50. Liao, R.; Yang, B.; Yu, W.; Zhou, C. Isothermal cold crystallization kinetics of polylactide/nucleating agents. *J. Appl. Polym. Sci.* **2007**, *104*, 310–317.
51. Li, H.; Huneault, M.A. Crystallization of PLA/Thermoplastic Starch Blends. *Int. Polym. Process.* **2008**, *23*, 412–418.
52. Frone, A.N.; Panaitescu, D.M.; Chiulan, I.; Nicolae, C.A.; Vuluga, Z.; Vitelaru, C.; Damian, C.M. The effect of cellulose nanofibers on the crystallinity and nanostructure of poly(lactic acid) composites. *J. Mater. Sci.* **2016**, *51*, 9771–9791.
53. Kovalcik, A.; Pérez-Camargo, R.A.; Fürst, C.; Kucharczyk, P.; Müller, A.J. Nucleating efficiency and thermal stability of industrial non-purified lignins and ultrafine talc in poly(lactic acid) (PLA). *Polym. Degrad. Stab.* **2017**, *142*, 244–254.
54. Battegazzore, D.; Bocchini, S.; Frache, A. Crystallization kinetics of poly(lactic acid)-talc composites. *Express Polym. Lett.* **2011**, *5*, 849–858.
55. Dufresne, A. *Nanocellulose:From Nature to High Performance Tailored Materials*, **2012,** Walter de Gruyter Gmbh, ISBN: 9783110254563.
56. Naseri, N. Porous materials based on nanopolysaccharides for medical applications: Effect of crosslinking on pore structure and mechanical performance, Luleå tekniska universitet: Material Science, Department of Engineering Sciences and Mathematics, Luleå University of Technology, PhD Thesis, **2016**.
57. Klemm, D.; Kramer, F.; Moritz, S.; Lindström, T.; Ankerfors, M.; Gray, D.; Dorris, A. Nanocelluloses: A new family of nature-based materials. *Angew. Chemie-Int. Ed.* **2011**, *50*, 5438–5466.
58. Salaberria, A.M.; Labidi, J.; Fernandes, S.C.M. Chitin nanocrystals and nanofibers as nano-sized fillers into thermoplastic starch-based biocomposites processed by melt-mixing. *Chem. Eng. J.* **2014**, *256*, 356–364.
59. Wei, J.; Liu, J.; Qiang, J.; Yang, L.; Wan, Y.; Wang, H.; Gao, W.; Ko, F. Antibacterial performance of chitin nanowhisker reinforced Poly(lactic acid) composite nanofiber membrane. *Adv. Sci. Lett.* **2012**, *10*, 649–651.
60. Salaberria, A.; H. Diaz, R.; Andrés, M.; Fernandes, S.; Labidi, J. The Antifungal Activity of Functionalized Chitin Nanocrystals in Poly (Lactid Acid) Films. *Materials (Basel).* **2017**, *10*, 546.
61. Zeng, J.B.; He, Y.S.; Li, S.L.; Wang, Y.-Z. Chitin Whiskers: An Overview. *Biomacromolecules* **2012**, *13*, 1–11.
62. Fan, Y.; Saito, T.; Isogai, A. Preparation of chitin nanofibers from squid Pen β-chitin by simple mechanical treatment under acid conditions. *Biomacromolecules* **2008**, *9*, 1919–1923.
63. Goodrich, J.D.; Winter, W.T. α-Chitin nanocrystals prepared from shrimp shells and their specific surface area measurement. *Biomacromolecules* **2007**, *8*, 252–257.
64. Abdul K. H.P.S.; Bhat, A.H.; Ireana Yusra, A.F. Green composites from sustainable cellulose nanofibrils: A review. *Carbohydr. Polym.* **2012**, *87*, 963–

979.
65. Ljungberg, N.; Wesslén, B. Preparation and properties of plasticized poly(lactic acid) films. *Biomacromolecules* **2005**, *6*, 1789–1796.
66. Li, H.; Huneault, M.A. Effect of nucleation and plasticization on the crystallization of poly(lactic acid). *Polymer (Guildf).* **2007**, *48*, 6855–6866.
67. Nampoothiri, K.M.; Nair, N.R.; John, R.P. Bioresource Technology An overview of the recent developments in polylactide (PLA) research. *Bioresour. Technol.* **2010**, *101*, 8493–8501.
68. Carrasco, F.; Santana, O.O.; Cailloux, J.; Sánchez-Soto, M.; Maspoch, M.L. Poly(lactic acid) and acrylonitrile−butadiene−styrene blends: Influence of adding ABS−g−MAH compatibilizer on the kinetics of the thermal degradation. *Polym. Test.* **2018**, *67*, 468–476.
69. Oksman, K.; Skrifvars, M.; Selin, J.F. Natural fibres as reinforcement in polylactic acid (PLA) composites. *Compos. Sci. Technol.* **2003**, *63*, 1317–1324.
70. Oksman, K.; Mathew, A.P.; Bondeson, D.; Kvien, I. Manufacturing process of cellulose whiskers/polylactic acid nanocomposites. *Compos. Sci. Technol.* **2006**, *66*, 2776–2784.
71. Jonoobi, M.; Harun, J.; Mathew, A.P.; Oksman, K. Mechanical properties of cellulose nanofiber (CNF) reinforced polylactic acid (PLA) prepared by twin screw extrusion. *Compos. Sci. Technol.* **2010**, *70*, 1742–1747.
72. Fortunati, E.; Peltzer, M.; Armentano, I.; Torre, L.; Jiménez, A.; Kenny, J.M. Effects of modified cellulose nanocrystals on the barrier and migration properties of PLA nano-biocomposites. *Carbohydr. Polym.* **2012**, *90*, 948–956.
73. Herrera, M.A.; Sirviö, J.A.; Mathew, A.P.; Oksman, K. Environmental friendly and sustainable gas barrier on porous materials: Nanocellulose coatings prepared using spin and dip-coating. *Mater. Des.* **2016**, *93*, 19–25.
74. Li, C.; Liu, H.; Luo, B.; Wen, W.; He, L.; Liu, M.; Zhou, C. Nanocomposites of poly(l-lactide) and surface-modified chitin whiskers with improved mechanical properties and cytocompatibility. *Eur. Polym. J.* **2016**, *81*, 266–283.
75. Herrera, N.; Salaberria, A.M.; Mathew, A.P.; Oksman, K. Plasticized polylactic acid nanocomposite films with cellulose and chitin nanocrystals prepared using extrusion and compression molding with two cooling rates: Effects on mechanical, thermal and optical properties. *Compos. Part A Appl. Sci. Manuf.* **2016**, *83*, 89–97.
76. Backes, E.H.; Pires, L. de N.; Costa, L.C.; Passador, F.R.; Pessan, L.A. Analysis of the Degradation During Melt Processing of PLA/Biosilicate® Composites. *J. Compos. Sci.* **2019**, *3*, 52.
77. Qahtani, M.; Wu, F.; Misra, M.; Gregori, S.; Mielewski, D.F.; Mohanty, A.K. Experimental design of sustainable 3d-printed poly(lactic acid)/biobased poly(butylene succinate) blends via fused deposition modeling. *ACS Sustain. Chem. Eng.* **2019**, 7, 14460–14470.
78. Cailloux, J.; Santana, O.O.; Franco-Urquiza, E.; Bou, J.J.; Carrasco, F.;

Gámez-Pérez, J.; Maspoch, M.L. Sheets of branched poly(lactic acid) obtained by one step reactive extrusion calendering process: Melt rheology analysis. *Express Polym. Lett.* **2012**, 7, 304–318.
79. Salaberria, A.M.; Labidi, J.; Fernandes, S.C.M. Chitin nanocrystals and nanofibers as nano-sized fillers into thermoplastic starch-based biocomposites processed by melt-mixing. *Chem. Eng. J.* **2014**, *256*, 356–364.
80. Herrera, N.; Singh, A.A.; Salaberria, A.M.; Labidi, J.; Mathew, A.P.; Oksman, K. Triethyl citrate (TEC) as a dispersing aid in polylactic acid/chitin nanocomposites prepared via liquid-assisted extrusion. *Polymers (Basel).* **2017**, *9*, 9, 406.
81. Walker, J.; Melaj, M.; Giménez, R.; Pérez, E.; Bernal, C. Solid-State Drawing of Commercial Poly(Lactic Acid) (PLA) Based Filaments. *Front. Mater.* **2019**, *6,* 280.
82. Mujica-Garcia, A.; Hooshmand, S.; Skrifvars, M.; Kenny, J.M.; Oksman, K.; Peponi, L.; Berglund, L.A.; Kenny, J.M. Poly(lactic acid) melt-spun fibers reinforced with functionalized cellulose nanocrystals. *RSC Adv.* **2016**, *6*, 9221–9231.
83. Mittal, V. *Characterization Techniques for Polymer Nanocomposites*; **2012**, Wiley-VCH Verlag & Co. KGaA, ISBN: 9783527328789.
84. Gray, D.G. Transcrystallization of polypropylene at cellulose nanocrystal surfaces. *Cellulose* **2008**, *15*, 297–301.
85. Langford, J.I.; Wilson, A.J.C. Scherrer after sixty years: A survey and some new results in the determination of crystallite size. *J. Appl. Crystallogr.* **1978**, *11*, 102–113.
86. Mathew, A.P.; Oksman, K.; Sain, M. The effect of morphology and chemical characteristics of cellulose reinforcements on the crystallinity of polylactic acid. *J. Appl. Polym. Sci.* **2006**, *101*, 300–310.
87. Hakim, R.H.; Cailloux, J.; Santana, O.O.; Bou, J.; Sánchez-Soto, M.; Odent, J.; Raquez, J.M.; Dubois, P.; Carrasco, F.; Maspoch, M.L. PLA/SiO_2 composites: Influence of the filler modifications on the morphology, crystallization behavior, and mechanical properties. *J. Appl. Polym. Sci.* **2017**, *134,* 40, 45367.
88. Huggins, M.L. The viscosity of dilute solutions of long-chain molecules. iv. dependence on concentration. *J. Am. Chem. Soc.* **1942**, *64*, 2716–2718.
89. Kraemer, E.O. Molecular Weights of Celluloses. *Ind. Eng. Chem.* **1938**, *30*, 1200–1203.
90. Hyon, S.H.; Jamshidi, K.; Ikada, Y. Synthesis of polylactides with different molecular weights. *Biomaterials* **1997**, *18*, 1503–1508.
91. Cailloux, J.; Santana, O.O.; Franco-Urquiza, E.; Bou, J.J.; Carrasco, F.; Maspoch, M.L. Sheets of branched poly(lactic acid) obtained by one-step reactive extrusion-calendering process: Physical aging and fracture behavior. *J. Mater. Sci.* **2014**, *49*, 4093–4107.
92. Zafeiropoulos, N.E.; Baillie, C.A.; Matthews, F.L. A study of transcrystallinity and its effect on the interface in flax fibre reinforced composite materials. *Compos. Part A Appl. Sci. Manuf.* **2001**, *32*, 525–543.

93. Wang, Y.; Mano, J.F. Banded spherulites in poly(L-lactic acid): Effects of the crystallization temperature and molecular weight. *J. Appl. Polym. Sci.* **2007**, *105*, 6, 3500-3504.
94. Pluta, M.; Galeski, A. Crystalline and supermolecular structure of polylactide in relation to the crystallization method. *J. Appl. Polym. Sci.* **2002**, *86*, 1386–1395.
95. Chen, X.; Kalish, J.; Hsu, S.L. Structure evolution of α′-phase poly(lactic acid). *J. Polym. Sci. Part B Polym. Phys.* **2011**, *49*, 1446–1454.
96. Sawai, D.; Takahashi, K.; Sasashige, A.; Kanamoto, T.; Hyon, S.-H. Preparation of Oriented β-Form Poly(l-lactic acid) by Solid-State Coextrusion: Effect of Extrusion Variables. *Macromolecules* **2003**, *36*, 3601–3605.
97. Muller, J.; Jiménez, A.; González-Martínez, C.; Chiralt, A. Influence of plasticizers on thermal properties and crystallization behaviour of poly(lactic acid) films obtained by compression moulding. *Polym. Int.* **2016**, *65*, 970–978.
98. Maiza, M.; Benaniba, M.T.; Massardier-Nageotte, V. Plasticizing effects of citrate esters on properties of poly(lactic acid). *J. Polym. Eng.* **2016**, *36*, 371–380.
99. Su, Z.; Li, Q.; Liu, Y.; Hu, G.H.; Wu, C. Multiple melting behavior of poly(lactic acid) filled with modified carbon black. *J. Polym. Sci. Part B Polym. Phys.* **2009**, *47*, 1971–1980.
100. Krikorian, V.; Pochan, D.J. Crystallization behavior of poly(L-lactic acid) nanocomposites: Nucleation and growth probed by infrared spectroscopy. *Macromolecules* **2005**, *38*, 6520–6527.
101. Chen, C.; Li, D.; Hu, Q.; Wang, R. Properties of polymethyl methacrylate-based nanocomposites: Reinforced with ultra-long chitin nanofiber extracted from crab shells. *Mater. Des.* **2014**, *56*, 1049–1056.
102. Mathew, A.P.; Laborie, M.P.G.; Oksman, K. Cross-linked chitosan/chitin crystal nanocomposites with improved permeation selectivity and pH stability. *Biomacromolecules* **2009**, *10*, 1627–1632.
103. Alexandre, M.; Dubois, P. Polymer-layered silicate nanocomposites: preparation, properties and uses of a new class of materials. *Mater. Sci. Eng. R Reports* **2000**, *28*, 1–63.
104. Fortunati, E.; Rinaldi, S.; Peltzer, M.; Bloise, N.; Visai, L.; Armentano, I.; Jiménez, A.; Latterini, L.; Kenny, J.M. Nano-biocomposite films with modified cellulose nanocrystals and synthesized silver nanoparticles. *Carbohydr. Polym.* **2014**, *101*, 1122–1133.
105. Sanchez-Garcia, M.D.; Gimenez, E.; Lagaron, J.M. Morphology and barrier properties of solvent cast composites of thermoplastic biopolymers and purified cellulose fibers. *Carbohydr. Polym.* **2008**, *71*, 235–244.
106. Martino, V.P.; Ruseckaite, R.A.; Jiménez, A.; Averous, L. Correlation between composition, structure and properties of poly(lactic acid)/polyadipate-based nano-biocomposites. *Macromol. Mater. Eng.* **2010**, *295*, 551–558.

107. Trifol, J.; Plackett, D.; Sillard, C.; Hassager, O.; Daugaard, A.E.; Bras, J.; Szabo, P. A comparison of partially acetylated nanocellulose, nanocrystalline cellulose, and nanoclay as fillers for high-performance polylactide nanocomposites. *J. Appl. Polym. Sci.* **2016**, *133, 14, 43257*.
108. Paul, M.A.; Delcourt, C.; Alexandre, M.; Degée, P.; Monteverde, F.; Dubois, P. Polylactide/montmorillonite nanocomposites: Study of the hydrolytic degradation. *Polym. Degrad. Stab.* **2005**, *87*, 535–542.
109. De Jong, S.J.; Arias, E.R.; Rijkers, D.T.S.; Van Nostrum, C.F.; Kettenes-Van Den Bosch, J.J.; Hennink, W.E. New insights into the hydrolytic degradation of poly(lactic acid): Participation of the alcohol terminus. *Polymer (Guildf).* **2001**, *42*, 2795–2802.
110. Penning, J.P.; Grijpma, D.W.; Pennings, A.J. Hot-drawing of poly(lactide) networks. *J. Mater. Sci. Lett.* **1993**, *12*, 1048–1051.
111. Xu, R.; Xie, J.; Lei, C. Influence of melt-draw ratio on the crystalline behaviour of a polylactic acid cast film with a chi structure. *RSC Adv.* **2017**, *7*, 39914–39921.
112. Mai, F.; Tu, W.; Bilotti, E.; Peijs, T. The influence of solid-state drawing on mechanical properties and hydrolytic degradation of melt-spun poly(lactic acid) (PLA) tapes. *Fibers* **2015**, *3*, 523–538.
113. Wang, Z.; Ciselli, P.; Peijs, T. The extraordinary reinforcing efficiency of single-walled carbon nanotubes in oriented poly(vinyl alcohol) tapes. *Nanotechnology* **2007**, *18, 45, 455709*.
114. Somani, R.H.; Yang, L.; Zhu, L.; Hsiao, B.S. Flow-induced shish-kebab precursor structures in entangled polymer melts. In Proceedings of the Polymer; **2005**, *46*, 8587–8623.
115. Eriksson, M.; Hamers, J.; Peijs, T.; Goossens, H. The Influence of Graft Length and Density on Dispersion, Crystallisation and Rheology of Poly(ε-caprolactone)/Silica Nanocomposites. *Molecules* **2019**, *24,* 11, 2106.
116. Sung, S.H.; Chang, Y.; Han, J. Development of polylactic acid nanocomposite films reinforced with cellulose nanocrystals derived from coffee silverskin. *Carbohydr. Polym.* **2017**, *169*, 495–503.
117. Ma, P.; Shen, T.; Lin, L.; Dong, W.; Chen, M. Cellulose-g-poly(D-lactide) nanohybrids induced significant low melt viscosity and fast crystallization of fully bio-based nanocomposites. *Carbohydr. Polym.* **2017**, *155*, 498–506.
118. Tsuji, H.; Tezuka, Y.; Saha, S.K.; Suzuki, M.; Itsuno, S. Spherulite growth of l-lactide copolymers: Effects of tacticity and comonomers. *Polymer (Guildf).* **2005**, *46*, 4917–4927.
119. Fortunati, E.; Armentano, I.; Zhou, Q.; Iannoni, A.; Saino, E.; Visai, L.; Berglund, L.A.; Kenny, J.M. Multifunctional bionanocomposite films of poly(lactic acid), cellulose nanocrystals and silver nanoparticles. *Carbohydr. Polym.* **2012**, *87*, 1596–1605.
120. Lizundia, E.; Fortunati, E.; Dominici, F.; Vilas, J.L.; León, L.M.; Armentano, I.; Torre, L.; Kenny, J.M. PLLA-grafted cellulose nanocrystals: Role of the CNC content and grafting on the PLA bionanocomposite film

properties. *Carbohydr. Polym.* **2016**, *142*, 105–113.

121. Legrand, D.G. Crazing, yielding, and fracture of polymers. I. Ductile brittle transition in polycarbonate. *J. Appl. Polym. Sci.* **1969**, *13*, 2129–2147.

Appended Publications

PAPER I

Crystallization of triethyl-citrate-plasticized poly (lactic acid) induced by chitin nanocrystals

Shikha Singh, Maria Lluïsa Maspoch, Maspoch, Kristiina Oksman

Journal of Applied Polymer Science, **2019**, 136 (36), 47936

DOI: 10.1002/app.47936

Journal of Applied Polymer Science

Crystallization of triethyl-citrate-plasticized poly(lactic acid) induced by chitin nanocrystals

Shikha Singh[1,2] **Maria Lluisa Maspoch**[2] **Kristiina Oksman**[1,3,4]

[1]Division of Materials Science, Luleå University of Technology, SE-97 187, Luleå, Sweden
[2]Centre Català del Plàstic (CCP), Universitat Politècnica de Catalunya Barcelona Tech (EEBE-UPC), C/Colom, 114, Terrassa 08222, Spain
[3]Fibre and Particle Engineering, University of Oulu, FI-90014, Oulu, Finland
[4]Mechanical and Industrial Engineering (MIE), University of Toronto, Toronto M5S 3G8, Ontario, Canada
Correspondence to: K. Oksman (E-mail: kristiina.oksman@ltu.se)

ABSTRACT: The aim of this study was to gain a better understanding of the crystallization behavior of triethyl-citrate-plasticized poly(lactic acid) (PLA–TEC) in the presence of chitin nanocrystals (ChNCs). The isothermal crystallization behavior of PLA–TEC was studied by polarized optical microscopy, scanning electron microscopy, differential scanning calorimetry, and X-ray diffraction (XRD). Interestingly, the addition of just 1 wt % ChNCs in PLA–TEC increased the crystallization rate in the temperature range of 135–125 °C. The microscopy studies confirmed the presence of at least three distinct types of spherulites: negative, neutral, and ring banded. The ChNCs also increased the degree of crystallinity up to 32%, even at a fast cooling rate of 25 °C min^{-1}. The XRD studies further revealed the nucleation effect induced by the addition of ChNCs and thus explained the faster crystallization rate. To conclude, the addition of a small amount (1 wt %) of ChNC to plasticized PLA significantly affected its nucleation, crystal size, and crystallization speed; therefore, the proposed route can be considered suitable for improving the crystallization behavior of PLA. © 2019 Wiley Periodicals, Inc. J. Appl. Polym. Sci. **2019**, *136*, 47936.

KEYWORDS: chitin nanocrystals; isothermal crystallization; microstructure; plasticizer; poly(lactic acid)

Received 10 November 2018; accepted 16 April 2019
DOI: 10.1002/app.47936

INTRODUCTION

Poly(lactic acid) (PLA) is a promising biobased, biodegradable, nontoxic, and commercially available thermoplastic polymer that is manufactured from natural resources (e.g., corn and sugar beets).[1] Furthermore, PLA has good mechanical properties (high stiffness and tensile strength), good optical properties (high transparency), and moderate barrier properties. However, PLA is brittle, and it has a low melt strength and slow crystallization rate.[1] The mechanical and barrier properties of PLA are highly dependent on its morphology and crystallinity.[2] The slow crystallization rate of PLA results in low crystallinity, which consequently limits its use in industrial applications.[3] Therefore, studies on improving the crystallization are crucial and fundamental aspect, which need to be addressed.

One approach to enhance the crystallization of PLA is through the addition of plasticizers.[4] Plasticizers promote the growth rate of crystallites[5] and act as processing aids[6]; they also enhance the flexibility and ductility of polymer materials.[4] Triethyl citrate (TEC) is a biodegradable, nontoxic, and efficient plasticizer for PLA.[7] However, TEC also has some drawbacks is that it degrade the thermal,[8] optical,[9] and mechanical properties[10] of PLA.

Another approach is to use nanosized additives and reinforcements; because of their large surface area, they can act as effective nucleating agents and promote the crystallization of polymers.[11] Several inorganic additives/reinforcements such as clays (e.g., montmorillonite,[12] silica,[13] and halloysite nanotubes[14]) and carbon-based materials (e.g., carbon nanotubes[2] and graphene[15]) have been widely used in nanocomposites. However, the poor biodegradability and toxicity of some of these materials restrict their use in food packaging applications. Therefore, the use of polysaccharide-based reinforcements would be more beneficial not only because of their biodegradable nature, low toxicity, low cost, and easy availability[16] but also because of their role as better nucleating agents. The most commonly used nanosized additives are nanocelluloses[17] and starch nanoparticles.[18] For example, Mathew *et al.*[17] studied the crystallization of PLA in the presence of three different types of cellulose reinforcements:

Additional Supporting Information may be found in the online version of this article.

microcrystalline cellulose, cellulose fibers, and wood flour. They found that the crystallization temperature influences both the number and size of the spherulites. Gray[19] investigated the crystallization of polypropylene (PP) on the surface of cellulose nanocrystals (CNCs); in the study, he employed CNC that acted as a nucleating agent and a transcrystalline layer (TCL) of PP was formed around the CNC film. The CNCs were found to increase the crystallization of PP. Pei *et al.*[11] studied the crystallization of PLA in the presence of CNCs. The CNCs were functionalized with silane to improve their dispersion in the PLA matrix, and their role as nucleating agents was explained. The results showed that the crystallization rate was improved by the addition of 1 wt % silane-functionalized CNCs (SCNCs); this improvement was attributed to their stronger nucleating ability compared to that of nonmodified CNCs. The degree of crystallinity improved from 14% (PLA) to 30% (PLA–SCNCs). Sullivan *et al.*[20] investigated the crystallization of PLA films prepared by melt compounding with different CNC contents (1, 2, and 3 wt %). They found that the crystallinity of the PLA film improved from 11 to 30% by the addition of 3 wt % CNCs. Trifol *et al.*[21] studied acetylated cellulose nanofibers (CNFs), CNCs, and clay (C30B) as additives for PLA nanocomposites. They observed that the addition of just 1 wt % CNFs and 1 wt % CNCs significantly improved the crystallization kinetics of PLA without affecting its transparency. They explained that the improved crystallinity could be a result of better nucleation abilities of the CNFs and CNCs than that of the nanoclay. Furthermore, the added CNCs provided better crystallinity than the added CNFs.

The crystallization of PLA in the presence of various natural nanomaterials has been studied; however, the potential use of chitin nanocrystals (ChNCs) for this crystallization improvement has been explored to a lesser extent than that of CNCs. ChNCs are natural polymers that are generally found in the exoskeleton of arthropods (crustaceans and mollusks).[22] ChNCs have low density, nontoxicity, biodegradability, and biocompatibility.[22] In addition to possessing good mechanical and thermal properties, ChNCs exhibit antimicrobial properties; as a result, they can possibly be used as nanoreinforcements in packaging applications, especially blow molded bags.

In the present study, the isothermal crystallization of plasticized PLA in the presence of ChNCs was studied. The main objective was to study the nucleation abilities of ChNCs and their effects on the crystallization rate and spherulite morphology of PLA films which could be used for packaging applications. Thin films of neat PLA, plasticized PLA, pure ChNCs, and PLA–TEC–ChNC nanocomposites were prepared and their crystallization kinetics, crystallinity, and crystal size, as well as the spherulite morphology, were examined by differential scanning calorimetry (DSC), X-ray diffraction (XRD), polarized optical microscopy (POM), and scanning electron microscopy (SEM).

EXPERIMENTAL

Materials

High-molecular-weight PLA in the form of pellets, which was provided by FUTERRO (Escanaffles, Belgium), was used as a matrix polymer in the composites and as a reference material for the crystallization studies. The melt flow index of the received PLA was 8 g/10 min (190 °C, 2.16 kg) and its L-isomer content was 99%, according to the supplier. TEC in liquid form (≥99% with Alfa Aesar, Thermo Fisher GmbH, Kandel, Germany), molecular weight of 276.3 g mol^{-1}, purchased from VWR, Sweden, was used as the plasticizer.

Table I. Sample Codes and Compositions of Prepared Materials (wt %)

Materials	PLA	TEC	ChNC
PLA	100	0	0
PLA–TEC	80	20	0
PLA–TEC–ChNC	79	20	1

ChNCs were used as the nanoadditive in the plasticized PLA; these nanocrystals were expected to affect the crystallization rate of PLA. PLA–ChNC nanocomposites were prepared using TEC as a processing aid for the compounding process as well as to enhance the dispersion of the ChNCs in the PLA matrix; further details of this preparation have been provided in our previous study.[23] Taking into the account of previous results of our group, the best results of the PLA–TEC–ChNC were obtained with 1 wt % of ChNC.[23] That is why we have chosen 1 wt % for this work. The material compositions and sample codes are listed in Table I.

The composition of the PLA–TEC–ChNC nanocomposite material (in wt %) was 79:20:1. PLA–TEC–ChNC nanocomposites have been described in detail in our previous studies.[7,24] In brief, the ChNCs were prepared by acid hydrolysis of a purified chitin powder, this process is described in detail elsewhere.[23] The ChNCs were subjected to POM and atomic force microscopy (AFM) observations. POM image shows the birefringence of ChNCs and the AFM image shows the dimensions of the ChNCs. The size distribution of the ChNCs was calculated from the height image; the obtained data are shown in Figure 1(b,c). For this calculation, a line was drawn across the height image by using the Gwyddion software and the peak profiles of the crystals were extracted. Several lines were drawn to include as many as crystals visible in the image as possible. Then, histograms of the size distributions were plotted and the ChNC dimensions were calculated. The height and length of the ChNCs were 2–22 nm and 263–761 nm, respectively.

Pure ChNC films were prepared by solution casting, after which the aqueous suspension of ChNCs (19.5 wt %) was evaporated and dried overnight in an oven at 80 °C. The thickness of the obtained films was measured using a digital micrometer (Mitutoyo Scandinavia Upplands Väsby, Sweden); it was in the range of 20–40 μm. These films were used to better understand transcrystalline transformation. In order to observe this transformation, the films were positioned as reported in the study of Gray.[19] A thin film of ChNCs was inserted between PLA films and observed by POM, as shown in Figure 2.

Pellets of neat PLA, PLA–TEC, and the PLA–TEC–ChNC nanocomposite were compression molded between steel plates to obtain films. Small amounts (2 g) of the pellets were first kept at 190 °C for 2 min under contact pressure, and after they melted,

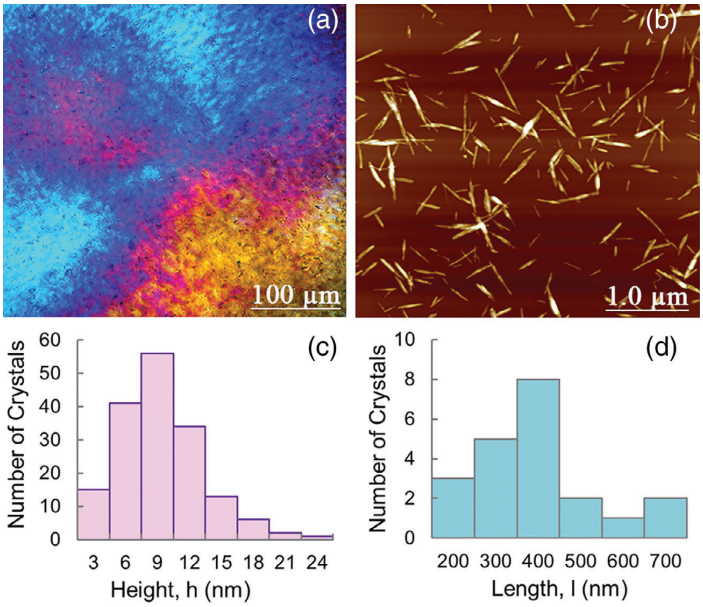

Figure 1. (a) POM image of ChNCs, showing their birefringence, (b) AFM image of ChNCs, showing their needle-like structure, and (c) average height and (d) length of used ChNCs. [Color figure can be viewed at wileyonlinelibrary.com]

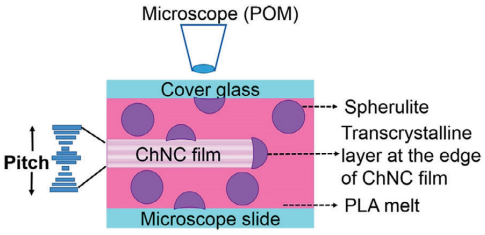

Figure 2. Schematic representation showing manner of insertion of ChNC film between PLA films. [Color figure can be viewed at wileyonlinelibrary.com]

the pressure was increased from 0 to 10 MPa in 1 min. The films were subsequently cooled in air. The film thickness ranged between 20 and 40 µm.

Characterization

The Nikon Eclipse LV100 POL (Kanagawa, Japan) POM equipped with the Linkam TH600 (Tadworth, UK) hot stage and temperature controller was used for examining the isothermal crystallization of the prepared materials. Objectives with 10× and 20× magnifications were used. A piece of the film was squeezed between two glass slides and transferred to the hot stage. Prior to crystallization, the sample was heated to 200 °C to eliminate any previous thermal history and then cooled at a rate of 25 °C min^{-1} to three specific temperatures, 135, 130, and 125 °C; finally, the sample was isothermally crystallized for 30 min. These temperatures were selected because PLA shows a rapid transition in this temperature range (135–125 °C).[25] The POMs of the sample were recorded using a charge-coupled device camera at various time intervals.

The size distribution of the ChNCs films prepared was determined by AFM; a Veeco MultiMode Scanning Probe (Santa Barbara, CA) with TESPA tips (Bruker, Camarillo, CA) in tapping mode. The length and height of the ChNCs were analyzed by the Gwyddion software.

The lamellar arrangement of the TCL and the spherulites formed in the presence of the ChNC films and PLA–TEC–ChNC films were examined using a SEM apparatus (JSM-IT300; JEOL, Tokyo, Japan) after the isothermal crystallization processes. To examine the transcrystalline morphology of the materials, the samples were etched with sodium hydroxide and ethanol (1:2 by volume). The etched surface was washed with distilled water. The film was rinsed two to three times with distilled water. The surfaces of these etched samples were then coated with gold by sputtering, and the acceleration voltage was kept at 5 kV.

The Mettler Toledo DSC 822e (Schwerzenbach, Switzerland) instrument was used to study how the addition of TEC and ChNCs affected the thermal properties and crystallization of PLA–TEC. Samples were placed in an aluminum pan, and then, the analysis was performed under a nitrogen atmosphere. The materials were isothermally crystallized in the following steps.

1. The sample was heated from −20 to 200 °C at a heating rate of 10 °C min^{-1} and kept for 5 min in order to eliminate any previous thermal history.
2. The sample was cooled to the isothermal crystallization temperature (e.g., 125 °C) at a cooling rate of 25 °C min^{-1}.

3. Isothermal crystallization was performed for 30 min.
4. The sample was reheated from 125 to 200 °C at a heating rate of 10 °C min^{-1} in order to measure the melting endotherm.

The glass-transition temperature (T_g), melt temperature (T_m), cold crystallization temperature (T_{cc}), and heat of melting (H_m) of all the samples were determined, and the percentage crystallinity corresponding to each curve was calculated. The percentage crystallinity was determined using the following empirical equation[17]:

$$\text{Crystallinity}\,(\%) = \frac{\Delta H_m - \Delta H_c}{93.1} \times 100 \quad (1)$$

where ΔH_m is the melting enthalpy, ΔH_c is the cold crystallization enthalpy, and the constant 93.1 (unit: J g^{-1}) corresponds to the ΔH_m value for 100% crystalline PLA.[17]

The effect of ChNCs on the crystallization of PLA was investigated using an XRD PANalytical Empyrean diffractometer (Almelo, The Netherlands) with Cu Kα radiation (λ = 1.5405 Å). Prior to the XRD measurements, the materials were isothermally crystallized in a manner similar to that in the previous experiments (at 125 °C for 30 min). The measurements were performed at an acceleration voltage and current of 45 kV and 40 mA, respectively, for 1 h over a 2θ range of 5–60° (step size: 0.026°). Further investigation of the crystal size of the materials was performed using the Scherrer equation[26]:

$$L = \frac{K\lambda}{B\text{Cos}\,(\theta)} \quad (2)$$

where L is the crystal size (crystalline lamella thickness); K is the dimensional shape factor (its value is 0.9 as reported by Sullivan *et al.*[20]), also known as the Scherrer constant; λ is the radiation wavelength; B is the full-width at half-maximum value of different peaks; and θ is the Bragg angle.

Fourier transform infrared (FTIR) spectroscopy was performed to further analyze the effect of addition of ChNCs to PLA–TEC and to observe the interactions of the PLA matrix with TEC and the ChNCs in the PLA–TEC–ChNC nanocomposites. A VERTEX 80 (Bruker, Billerica, MA) FTIR spectrophotometer with a range of 400–4000 cm^{-1} and a 128-scan resolution was used for the analysis. All samples were characterized by the KBr pellet method. A total of 0.03 mg of materials was mixed and ground with powdered KBr to make pellets, and the obtained pellets were used for further studies.

RESULTS AND DISCUSSION

Effect of TEC Plasticizer on Crystallinity

Figure 3 shows the results of POM studies of the effect of the TEC plasticizer on the crystallization of PLA at the three crystallization temperatures of 135, 130, and 125 °C. As the first step, the material was cooled from melt state to 135 °C and kept at this temperature for 5, 10, and 15 min. As seen in Figure 3, the

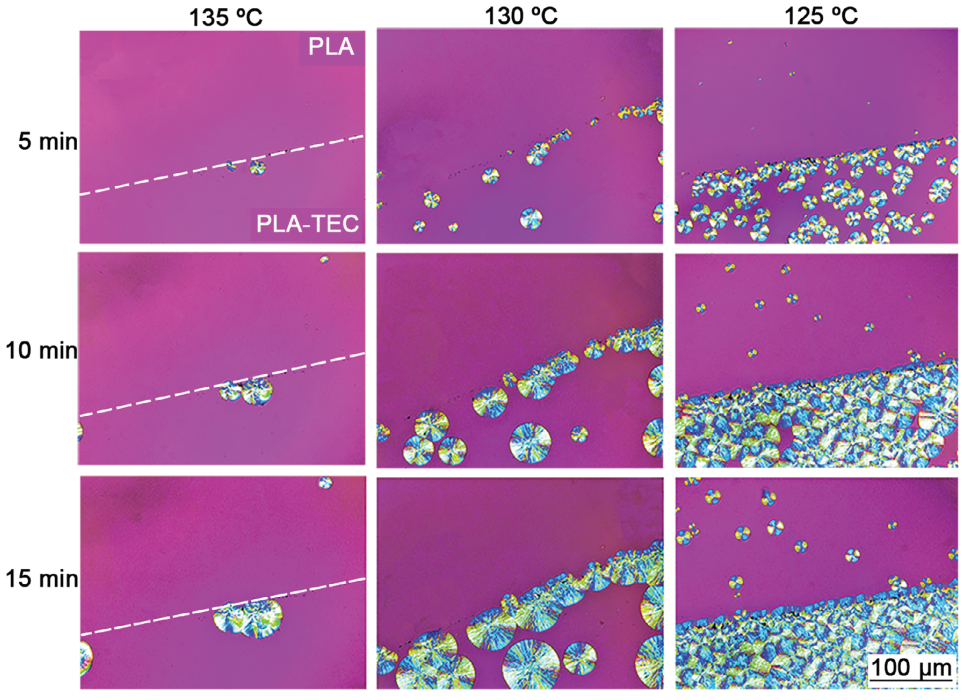

Figure 3. Comparison of isothermal crystallizations of neat PLA and PLA–TEC at different temperatures (135, 130, and 125 °C) with 5, 10, and 15 min holding times. Dashed line shows the interface between the PLA and PLA–TEC and the magnification is same for all the micrographs. [Color figure can be viewed at wileyonlinelibrary.com]

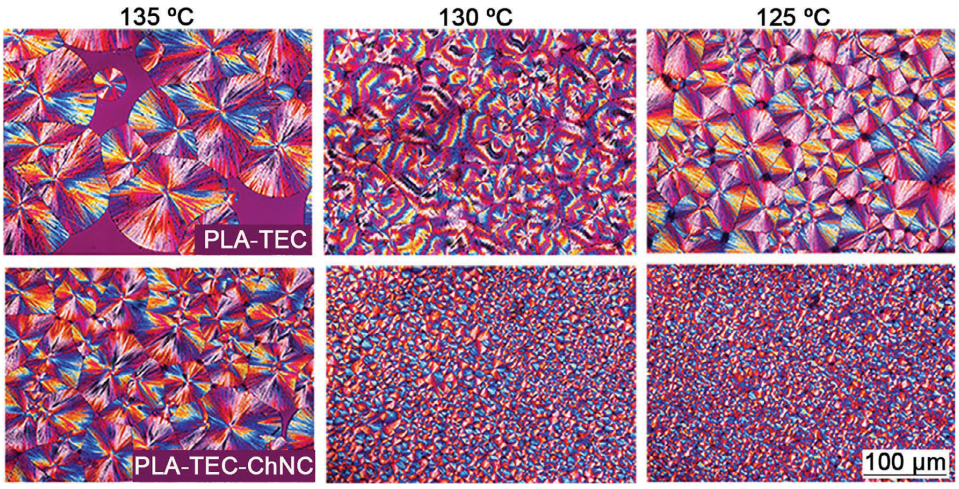

Figure 4. Comparison of isothermal crystallizations of PLA–TEC and PLA–TEC–ChNC nanocomposite at 135, 130, and 125 °C after 30 min. Scale bar (100 μm) is same for all the micrographs. PLA–TEC–ChNC showed faster nucleation at 125 °C and crystal size was also reduced compared to PLA–TEC. [Color figure can be viewed at wileyonlinelibrary.com]

crystallization rate was very slow at 135 °C, and only a few spherulites were visible and they located on the interface between PLA and PLA–TEC. When the crystallization temperature was decreased to 130 °C, nucleation was more noticeably already after 5 min, and after 15 min, a TCL was formed and also some large spherulites were visible in the plasticized PLA. However, no spherulites were seen in the PLA film. At the lowest temperature, that is, 125 °C, both bulk and heterogeneous nucleation occurred rapidly at this temperature, and consequently, the nucleation and growth rate was increased, the apparent nucleation effect of TEC was also confirmed the spherulites that were observed to have a typical Maltese-cross pattern spherulites[27] with negative birefringence[28] at this temperature.

Isothermal Crystallizations of PLA–TEC and PLA–TEC–ChNC Nanocomposite

Figure 4 shows comparison of isothermal crystallizations of PLA–TEC and the PLA–TEC–ChNC nanocomposite at 135, 130, and 125 °C after 30 min. Comparison of the isothermal crystallization of PLA–TEC with that of the PLA–TEC–ChNC nanocomposite clearly reveals that the addition of ChNC increased both crystallization rate and nucleation density of PLA–TEC. At 130 °C, multiring-banded spherulites were formed in the plasticized PLA–TEC whereas only negative spherulites were seen in PLA–TEC–ChNC. At 125 °C, nucleation occurred very rapidly in the PLA–TEC–ChNC nanocomposite and the spherulite size was smaller than the those in the plasticized PLA–TEC.

Further crystallization of PLA–TEC was performed in the presence of a thin film of the PLA–TEC–ChNC nanocomposite to see the TCL as shown in Figure 5. Initially, the crystallization was performed at 135 °C, and TCL was seen after 15 min. Then, the crystallization was performed at 130 °C, and at this temperature, TCL was visible even at 10 min. As mentioned before, multiring-banded spherulites were observed at 130 °C in both "phases" or film. Finally, crystallization was performed at 125 °C. At this temperature, bulk nucleation occurred at an extremely rapid rate, even at 5 min. The formed TCL was clearer after 5 min, and at 15 min, the surface of the PLA–TEC–ChNC film was almost fully covered with the spherulites. Some neutral type of spherulites along with negative types was also observed at this temperature.

Banding is usually observed in chiral polymers such as PLA, which consist of an asymmetric carbon atom in the backbone. In the case of PLA, banding can be observed at temperatures above 110 °C, usually over a range of ±5–10 °C.[27] Thermal history of PLA has an influence on the formations of banded spherulites of PLA. This banding of PLA is linked to polymorphism.[27] PLA generally forms three crystal phases, namely, α-form, α′-form, and β-form. The reason for the formation of ring-banded spherulites only in PLA–TEC film at 130 °C could be because of the transitions between the regime. Wang and Mano[29] studied banded spherulites of PLA and observed the banding-to-nonbanding morphological transition. They reported that the morphological transition in PLA occurred from Regime II to Regime III in temperature range of 125–145 °C. Figure 6 shows detailed views of multiring-banded spherulites, appeared at 130 °C. The number of rings inside a spherulite increased with increase in time from 5 to 30 min. At 5 min, the rings were not clear, but at 10 min, the rings were visible; further layering of rings was observed at 15 min. The number of rings increased up to 25 min, after which their growth was restricted by the formation of smaller spherulites on the surface of the larger ones. The rate of spherulite growth with temperature was evaluated and presented in Figure 6. It can be seen from Figure 6(a) that spherulite radius increases with time. Bai *et al.*[30] reported observation of similar behavior; they observed that the radius of spherulites

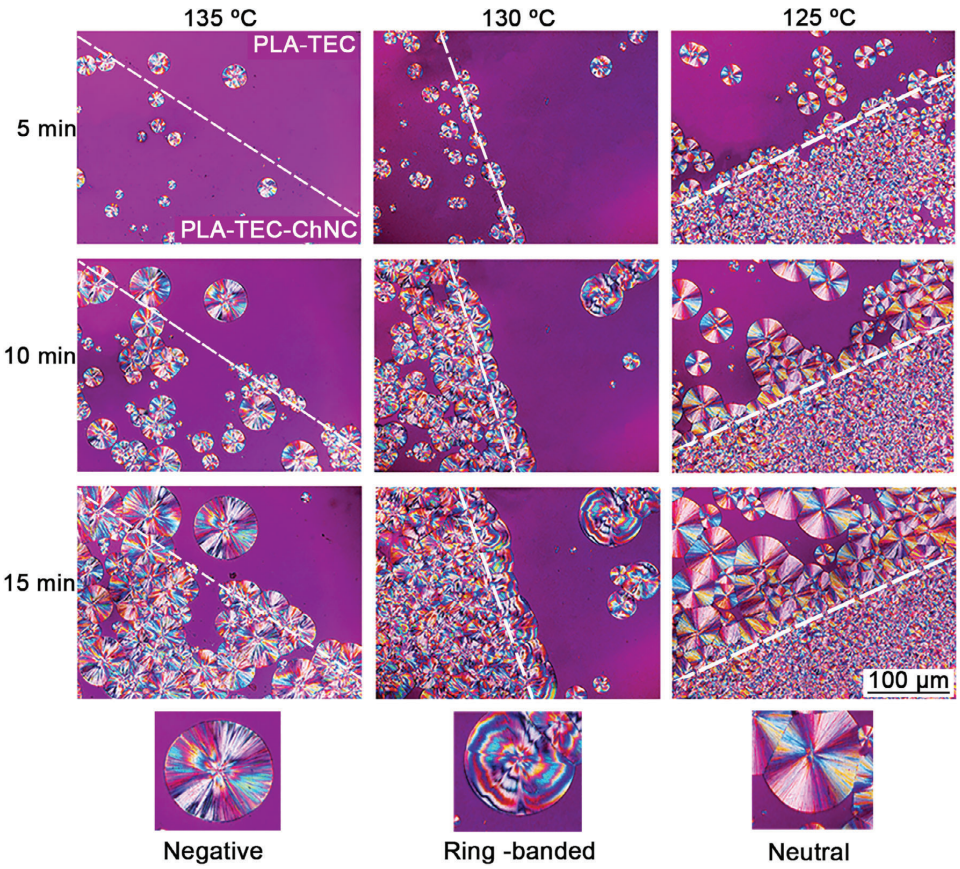

Figure 5. Comparison of isothermal crystallizations of PLA–TEC and PLA–TEC–ChNC nanocomposite at 135, 130, and 125 °C with 5, 10, and 15 min holding times. Dashed line shows the interface between the materials. [Color figure can be viewed at wileyonlinelibrary.com]

increased linearly with the crystallization time. Figure 6(b) shows a plot of the position of the spherulite bands versus their height; this plot reveals an almost regular pattern.

Effect of Pure ChNC Film on Crystallization of PLA–TEC

In order to see how pure ChNC film can increase the rate of crystallization of PLA–TEC, isothermal crystallization of PLA–TEC was performed at 135, 130, and 125 °C (see Figure 7). At 135 °C, nucleation occurred mainly at the interface between the ChNCs and the PLA–TEC film, which indicates good nucleation ability of the ChNCs. The number and size of the spherulites increased after 10 min, and a very prominent TCL was observed after 15 min. When the crystallization temperature was decreased to 130 °C, both bulk nucleation and heterogeneous nucleation increased and spherulites were observed in the vicinity of the ChNC film. Notably, ring-banded spherulites were also observed at 130 °C, and the TCL was thicker than that observed at 135 °C. When further crystallization was performed at 125 °C, the bulk nucleation improved greatly and numerous spherulites were observed inside the PLA–TEC film.

Crystallization Kinetics of PLA–TEC and PLA–TEC–ChNC Nanocomposite

The Lauritzen–Hoffman nucleation theory[31] was used to understand the effect of ChNCs on the crystallization of plasticized PLA and to study the crystallization kinetics. It was found that ChNCs decreased the nucleation constant (K_g) and the surface free energy (σ_e) of PLA–TEC, showed the good nucleation ability of ChNCs. The detailed description of crystallization kinetics is given in Appendix S1.

Evaluation of Lamellar Arrangements of PLA–TEC in Presence of ChNC

SEM studies were conducted to better understand the lamellar arrangements of spherulites formed during the isothermal crystallization of PLA–TEC film. Figure 8 shows the SEM images of the isothermal crystallization of the PLA–TEC film presence of pure ChNC and PLA–TEC–ChNC film and spherulites formed. As mentioned before, in the cases of the pure ChNC film and PLA–TEC–ChNC film, the ChNCs acted as a nucleating agent and TEC improved the growth of crystals. As shown in Figure 8

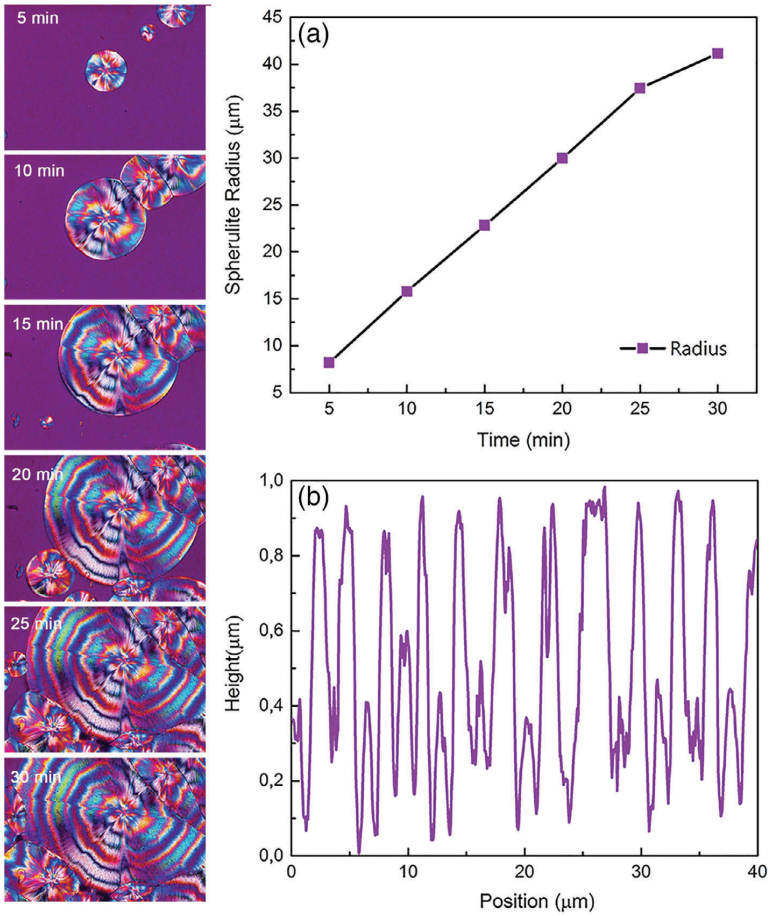

Figure 6. Multiring-banded spherulites formed at 130 °C. The figure depicts how the number of rings of spherulites increases with time 5–30 min. (a) Spherulite radius (ring-banded spherulite) as a function of time during isothermal crystallization at 130 °C. (b) Plot of position of spherulite bands versus their height. [Color figure can be viewed at wileyonlinelibrary.com]

(a,b), an interesting TCL is observed at the edge of the PLA–TEC–ChNC film, wherein the lamellae grow radially near the PLA–TEC–ChNC film and are organized in such a manner that they form a fan-shaped hemispherical structure. Further examination revealed the different types of spherulites shown in Figure 8(c–e). It can be seen from Figure 8(c) that the lamellae in the spherulites are oriented such that they form a ring inside the spherulites. Specifically, the circular fibrous texture of the lamellae leads to the formation of a circular ring within the periphery of the spherulites. However, the type of lamellar pattern of the spherulites as observed in Figure 8(d) is slightly different from that observed in Figure 8(a); the lamellae are observed to grow radially in Figure 8(d). A completely different type of lamellar pattern of the spherulite, a scattered lamellar pattern, is observed in Figure 8(e). Ni'mah *et al.*[32] reported a similar type of lamellar pattern for the spherulites of PLA. Both the POM and the SEM observations revealed that these different types of spherulites have different lamellar arrangements.

Thermal Analysis

DSC measurements were performed to estimate the glass-transition temperature (T_g), melt temperature (T_m), and cold crystallization temperature (T_{cc}); the measurement results are listed in Table II and the DSC scans are shown in Figure 9. The DSC curve of PLA showed T_g, T_{cc}, and T_m at 62, 101, and 174 °C, respectively, which are typical of semicrystalline polymers and similar to values reported in the literature.[33] The addition of TEC to PLA lowered the T_g, T_{cc}, and T_m values of PLA to 34, 68, and 163, respectively. This lowering of T_g, T_{cc}, and T_m of PLA is attributed to the plasticizing effect of the plasticizer, that is, TEC.[9] Maiza *et al.*[4] reported the same trend in their study of the plasticizing effect of TEC on the properties of PLA; they observed that T_g decreased with an increase in the TEC content. The reduction in the T_g, T_{cc}, and T_m of PLA with the addition of TEC was due to the higher flexibility of the polymer chains in the presence of plasticizers.[34] However, the incorporation of 1 wt % ChNCs into PLA–TEC did not lower the T_g, T_{cc}, and T_m of PLA

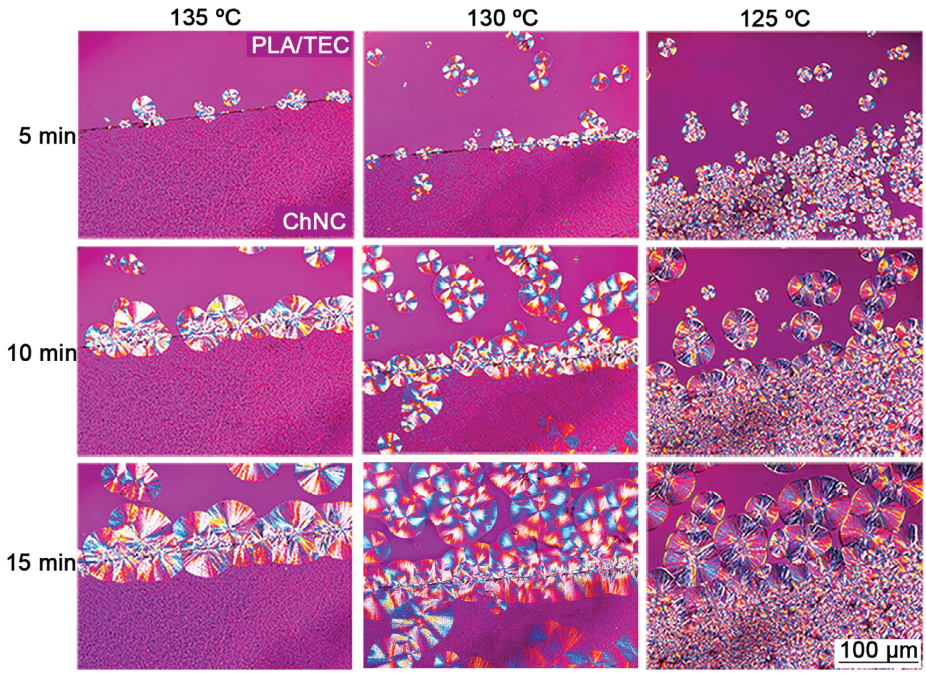

Figure 7. Isothermal crystallization of PLA–TEC in the presence of pure ChNC film at (a) 135, (b) 130, and (c) 125 °C with 5, 10, and 15 min holding times. Scale bar (100 µm) is same in all micrographs. It can be seen that ChNC has increased the crystallization of PLA–TEC and faster crystallization is seen at 125 °C. [Color figure can be viewed at wileyonlinelibrary.com]

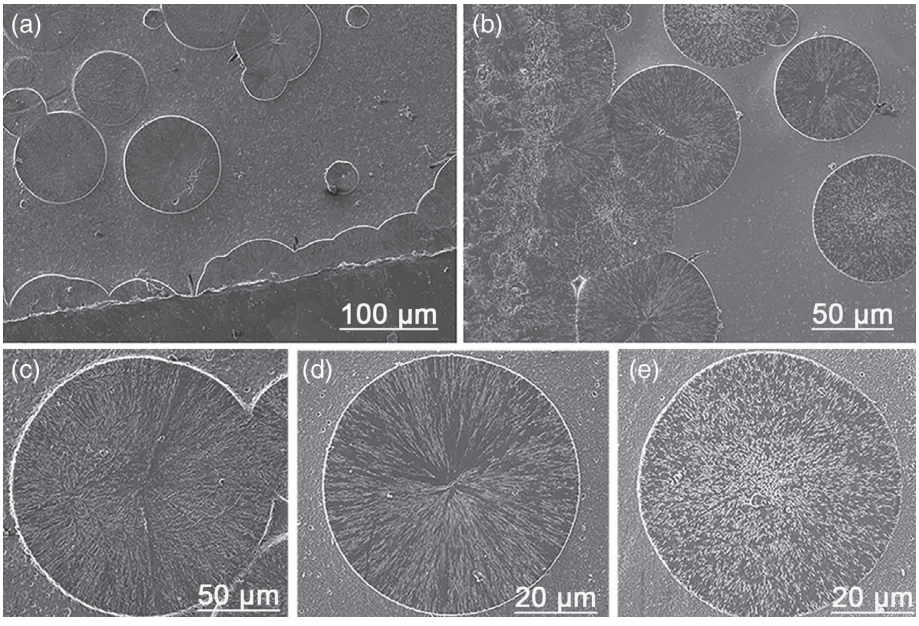

Figure 8. SEM images of isothermal crystallization of PLA–TEC in the presence of (a) pure ChNC and (b) PLA–TEC–ChNC film at 125 °C. It shows the lamellar arrangement of spherulites at the interface of the materials. Different types of spherulites formed during the isothermal crystallization of PLA–TEC (c) circular fibrous spherulites, (d) banded spherulites, and (e) spherulites with scattered lamellar pattern.

Table II. Glass-Transition Temperature (T_g), Melt Temperature (T_m), Cold Crystallization Temperature (T_{cc}), Heat of Melting (H_m), and Percentage Crystallinity Calculated By DSC and XRD

					Crystallinity (%)	
Materials	T_g (°C)	T_{cc} (°C)	T_m (°C)	δH_m (J g^{-1})	DSC	XRD
PLA	62	101	174	34.9	14.4	59.3
PLA–TEC	34	68	163	39.3	24.6	69.6
PLA–TEC–ChNC	37	73	166	42.3	32.0	79.6

as much as the addition of TEC did; these temperatures were 37, 73, and 166 °C, respectively, after the incorporation of ChNCs. The reason of the reduction in the T_g, T_{cc}, and T_m of the PLA–TEC–ChNC nanocomposite in this study (shown in Table II) is because of the plasticizing effect of TEC.[9] Figure 9 (b) shows the DSC traces of the second melting peaks of PLA, PLA–TEC, and the PLA–TEC–ChNC nanocomposite obtained after their isothermal crystallization for 30 min. An almost negligible double melting peak was observed for PLA. However, rather broad second melting peaks were observed for PLA–TEC and the PLA–TEC–ChNC nanocomposite. The melting peaks of PLA–TEC and the PLA–TEC–ChNC nanocomposite were shifted toward lower temperatures in comparison to that of PLA. The spikes in the second melting peak of the PLA–TEC–ChNC nanocomposite were extremely prominent. These prominent peaks can be because of the annealing process of the crystals populations, prematurely formed due to the nucleation effect that increases the T_m. Moreover, formation of the double melting peak indicated different crystal morphologies of PLA.[15] This shift in the melting peaks of PLA with the addition of TEC and ChNCs indicated the occurrence of some interaction of TEC and the ChNCs within the PLA chain. Muller *et al.*[35] studied the influence of poly(ethylene glycol) (PEG) on the crystallization and thermal behavior of PLA and found that PEG interacted with the PLA lattice and lowered the melting peak by about 5 °C.

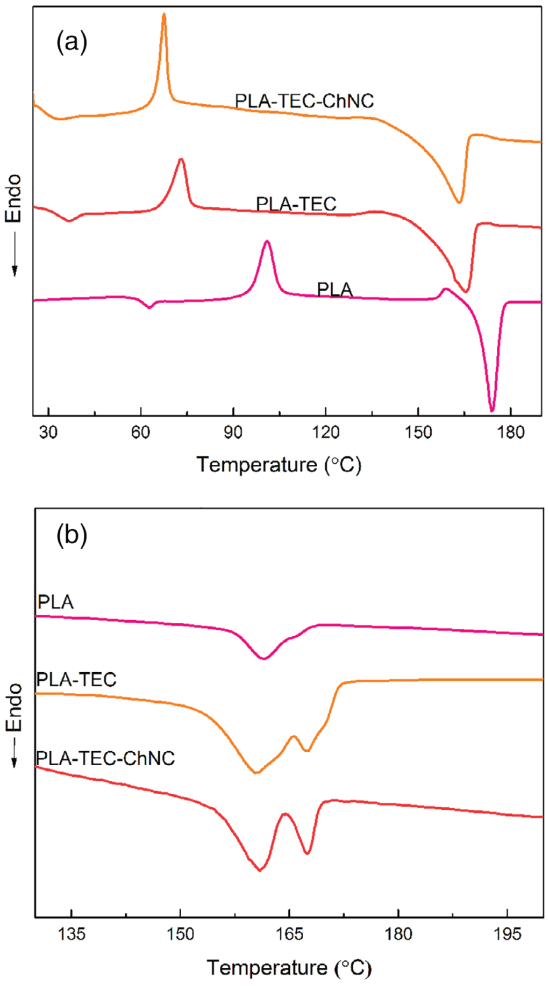

Figure 9. (a) 1st DSC heating scans of PLA, PLA–TEC, PLA–TEC–ChNC nanocomposite after isothermal crystallization at 125 °C for 30 min, (b) 2nd DSC heating scans of PLA, PLA–TEC, PLA–TEC–ChNC nanocomposite after isothermal crystallization at 125 °C for 30 min. [Color figure can be viewed at wileyonlinelibrary.com]

Crystalline Structure

XRD measurements were performed to investigate the influence of ChNCs on the crystallization of PLA. Figure 10 shows comparative XRD graphs of PLA, PLA–TEC, and the PLA–TEC–ChNC nanocomposite. Strong diffraction rings appeared at 2θ = 12.3, 14.7, 16.7, 19.0, and 22.3°, which correspond to the (004)/(103), (010), (200)/(110), (203), and (015) crystallographic planes, respectively.[36] Among them, the strongest peak, observed at 16.7°, was assigned to the α-form of PLA.[37] In addition, some weak diffraction peaks were observed at 20.7, 24.0, 24.9, 27.3, 29.3, and 31.1°. The peaks at 24.0 and 24.9° were ascribed to the α′-form of PLA.[38] Furthermore, the diffraction peak at 29.3° may have originated from the β-form of PLA, which is consistent with a previous finding[39] (2θ = 29.7° for the β-form of crystals). The peaks at 12.3 and 20.7° could be assigned to the D-form of PLA, since similar peaks at 2θ = 12.0 and 20.8° were reported by Han *et al.*[40] The XRD profile of PLA–TEC shows intense diffraction peaks, and it reveals that the intensity of the α-form of PLA was higher than that of its α′-form. The intensity of the peaks of PLA–TEC increased slightly with the incorporation of the ChNCs, and the positions of the peaks shifted to the left. The shift in the peak position suggests that PLA–TEC has a unit cell structure different from that of PLA; this, in turn, indicated that the incorporation of the ChNCs altered the crystal structure of

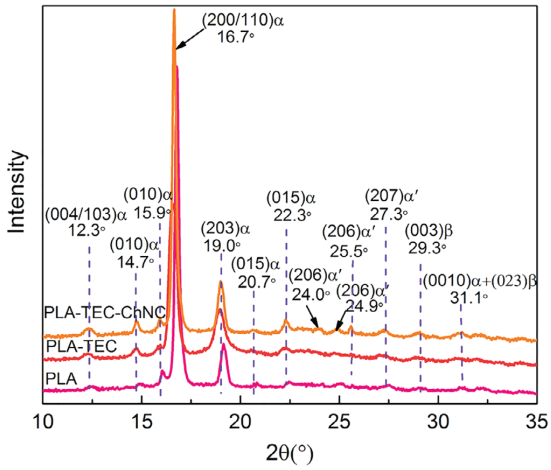

Figure 10. Comparative XRD graphs of isothermally crystallized PLA, PLA–TEC, and PLA–TEC–ChNC nanocomposite. [Color figure can be viewed at wileyonlinelibrary.com]

PLA. The overall intensity of the peaks of the PLA–TEC–ChNC nanocomposite was higher than that of PLA–TEC. A total of three forms of PLA, the α-form, α′-form, and β-form, were observed. Percentage crystallinity of the materials was calculated and data are listed in Table II. It was found that crystallinity of PLA increased in the presence of TEC and ChNC and it was 70 and 80%, respectively, and the ChNC resulted in decreased crystal size (see Table S2).

Mechanism of Improved Crystallization by Addition of ChNCs

We propose that the mechanism of the improved crystallization of plasticized PLA could be the H-bond interactions between PLA–TEC and the ChNCs, as shown in Figure 11. TEC has two types of functional groups: the acetyl functional group (—$OCOCH_3$) and the hydroxyl group (—OH). However, the acetamide group (—NH_2—CO—CH_3) and the hydroxyl group (—OH) on ChNCs have a better scope for interacting with the PLA chain. These functional groups on ChNCs can easily interact with the —C═O bond of PLA to achieve two types of H-bond interactions (—CO—OH and —CO—NH). These interactions are expected to be the cause of the improved crystallization of PLA–TEC in the presence of ChNCs; this belief is supported by the POM and DSC results.

The FTIR spectra of PLA, PLA–TEC, and the PLA–TEC–ChNC nanocomposite are shown in Figure 11(b); the peaks at 2997 and 2945 cm^{-1} in these spectra are ascribed to the asymmetric and symmetric stretching,[41] respectively, of CH_3. The peak at 2881 cm^{-1} is ascribed to the —C—H stretching of CH_3. The peaks originate from 1759 and 1188 cm^{-1}, respectively, the characteristic carbonyl (—C═O) and —C—O—C stretching of PLA.[41] The intensities of the C—O and C═O peaks increase with the addition of TEC and the ChNCs, and these peaks shift toward lower wavenumbers. Furthermore, weak peaks observed at 1658 and 1619 cm^{-1} correspond to the Amide I band of the acetamide

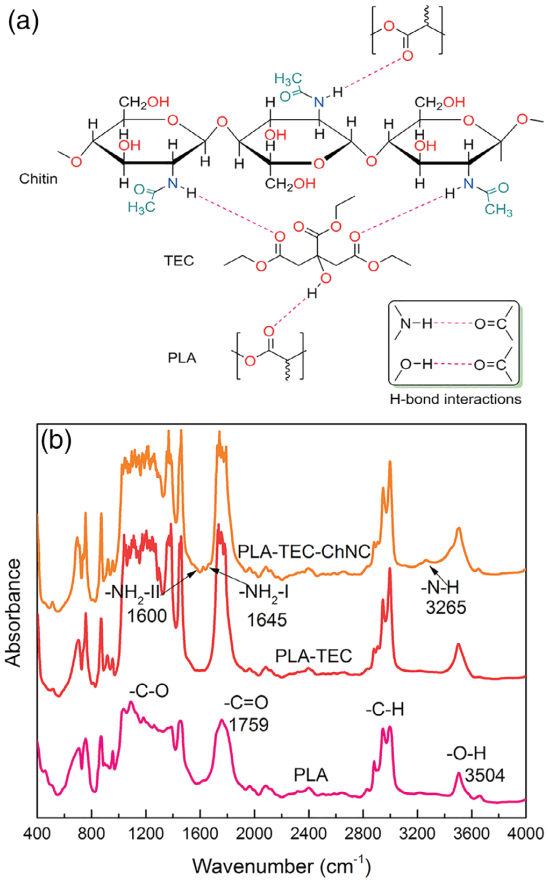

Figure 11. (a) Schematic of mechanism of the crystallization of PLA in the presence of ChNCs, showing two types of H-bond interactions, (b) FTIR graphs of PLA, PLA–TEC, and PLA–TEC–ChNC nanocomposite, showing characteristic peaks of PLA and ChNCs. The graphs also depict the shifting of the O—H stretching peaks of PLA toward lower wave numbers with the addition of ChNCs. [Color figure can be viewed at wileyonlinelibrary.com]

group (—NH_2—CO—CH_3) of the chitins in the PLA–TEC–ChNC nanocomposites and the weak peak at 1558 cm^{-1} correspond to Amide II band (i.e., N—H bending) of this acetamide group.[42] The peaks at 3265 and 3110 cm^{-1} correspond to the —N—H stretching.[43] The peak at 3504 cm^{-1} in PLA and that at 3504 cm^{-1} in PLA–TEC shift toward a lower wavenumber (3498 cm^{-1}) with the addition of ChNCs to PLA–TEC. This result indicated the occurrence of H-bond interactions between PLA–TEC and ChNCs.

CONCLUSIONS

A detailed study on the isothermal crystallization of plasticized PLA in the presence of ChNCs was conducted. The role of ChNCs in the crystallization was evaluated by POM, SEM, DSC, and XRD analysis. Additionally, FTIR spectroscopy was used to

study the interaction between the components of PLA–TEC–ChNC nanocomposites, that is, PLA, TEC, and ChNCs.

It was found that ChNCs are good nucleating agents as the crystallization of PLA–TEC was improved greatly by the addition of ChNCs. Microscopy observations showed that the addition of ChNCs improved the crystallization rate of PLA–TEC by reducing the crystallization time and size of the crystals. Ring-banded spherulites were formed at 130 °C, and rarely found neutral-type spherulites were observed at 125 °C. The Lauritzen–Hoffman nucleation theory revealed a decrease in the nucleation constant (K_g) and the surface free energy (σ_e) of PLA–TEC with the addition of ChNCs, indicating good nucleation ability of the ChNCs. The SEM study revealed an interesting nucleation effect of the ChNC nanoparticles on PLA–TEC, which resulted in different lamellar structures of spherulites. The DSC results showed that the T_g of PLA reduced upon addition of TEC, whereas it was comparatively higher after the addition of ChNC. Additionally, the percentage crystallinity was also increased with ChNC. The XRD results also confirmed the importance of the ChNCs, as higher crystallinity observed with ChNCs. Furthermore, knowledge of specific crystallization temperature [e.g., 125 °C, where we can get fast (5 min) and homogenous crystallization] gained from this study can be utilized during the processing of PLA-based nanocomposites to achieve films with better gas barrier and improved mechanical properties in our future work.

ACKNOWLEDGMENTS

The authors are grateful for the financial support provided by the Joint European Doctoral Programme in Advanced Material Science and Engineering (DocMASE) to S. Singh. The authors would also like to thank Natalia Herrera and Shokat Sarmad for their technical assistance with the AFM and FTIR spectroscopy studies.

REFERENCES

1. Rasal, R. M.; Janorkar, A. V.; Hirt, D. E. *Prog. Polym. Sci.* **2010**, *35*, 338.
2. Barrau, S.; Vanmansart, C.; Moreau, M.; Addad, A.; Stoclet, G.; Lefebvre, J.-M.; Seguela, R. *Macromolecules*. **2011**, *44*(16), 6496.
3. Tang, H.; Chen, J. B.; Wang, Y.; Xu, J. Z.; Hsiao, B. S.; Zhong, G. J.; Li, Z. M. *Biomacromolecules*. **2012**, *13*(11), 3858.
4. Maiza, M.; Benaniba, M. T.; Quintard, G.; Massardier-Nageotte, V. *Polimeros*. **2015**, *25*(6), 581.
5. Kulinski, Z.; Piorkowska, E. *Polymer*. **2005**, *46*(23), 10290.
6. Oksman, K.; Mathew, A. P.; Bondeson, D.; Kvien, I. *Compos. Sci. Technol.* **2006**, *66*(15), 2776.
7. Herrera, N.; Mathew, A. P.; Oksman, K. *Compos. Sci. Technol.* **2015**, *106*, 149.
8. Ljungberg, N.; Wesslén, B. *Biomacromolecules*. **2005**, *6*(3), 1789.
9. Maiza, M.; Benaniba, M. T.; Massardier-Nageotte, V. *J. Polym. Eng.* **2016**, *36*(4), 371.
10. Labrecque, L. V.; Kumar, R. a.; Dave, V.; Gross, R. a.; McCarthy, S. P. *J. Appl. Polym. Sci.* **1997**, *66*(8), 1507.
11. Pei, A.; Zhou, Q.; Berglund, L. A. *Compos. Sci. Technol.* **2010**, *70*(5), 815.
12. Zaldua, N.; Mugica, A.; Zubitur, M.; Iturrospe, A.; Arbe, A.; Re, G. L.; Raquez, J.-M.; Dubois, P.; Muller, A. J. *CrstEngComm*. **2016**, *18*(48), 9334.
13. Mustapa, I. R.; Chandran, S.; Shanks, R. A.; Kong, I. In Proceedings of the 37th Annual Condensed Matter and Materials Meeting, 5–8 February, **2013**. Wagga, NSW: Australia.
14. Dong, W.; Ren, J.; Shi, D.; Ma, P.; Li, X.; Duan, F.; Ni, Z.; Chen, M. *Polym. Degrad. Stab.* **2013**, *98*(9), 1790.
15. Su, Z.; Li, Q.; Liu, Y.; Hu, G. H.; Wu, C. *J. Polym. Sci. Part B: Polym. Phys.* **2009**, *47*(20), 1971.
16. Scaffaro, R.; Botta, L.; Lopresti, F.; Maio, A.; Sutera, F. *Cellulose*. **2017**, *24*(2), 447.
17. Mathew, A. P.; Oksman, K.; Sain, M. *J. Appl. Polym. Sci.* **2006**, *101*(1), 300.
18. Le Corre, D.; Bras, J.; Dufresne, A. *Biomacromolecules*. **2010**, *11*(5), 1139.
19. Gray, D. G. *Cellulose*. **2008**, *15*(2), 297.
20. Sullivan, E. M.; Moon, R. J.; Kalaitzidou, K. *Materials*. **2015**, *8*(12), 8106.
21. Trifol, J.; Plackett, D.; Sillard, C.; Hassager, O.; Daugaard, A. E.; Bras, J.; Szabo, P. *J. Appl. Polym. Sci.* **2016**, *133*, 43257.
22. Oksman, K.; Mathew, A. P.; Bismark, A.; Rojas, O.; Sain, M. Handbook of Green Materials: Processing Technologies, Properties and Applications. Vol. *1*; Word Scientific Publishing: Singapore, **2014**.
23. Herrera, N.; Salaberria, A. M.; Mathew, A. P.; Oksman, K. *Compos. Part A: Appl. Sci. Manuf.* **2016**, *83*, 89.
24. Herrera, N.; Roch, H.; Salaberria, A. M.; Pino-Orellana, M. A.; Labidi, J.; Fernandes, S. C. M.; Radic, D.; Leiva, A.; Oksman, K. *Mater. Des.* **2016**, *92*, 846.
25. Xu, H.; Xie, L.; Jiang, X.; Li, X. J.; Li, Y.; Zhang, Z. J.; Zhong, G. J.; Li, Z. M. *J. Phys. Chem. B*. **2014**, *118*(3), 812.
26. Langford, J. I.; Wilson, A. J. C. *J. Appl. Crystallogr*. **1978**, *11*(2), 102.
27. Crist, B.; Schultz, J. M. *Prog. Polym. Sci.* **2016**, *56*, 1.
28. Kalb, B.; Pennings, A. J. *Polymer*. **1980**, *21*(6), 607.
29. Wang, Y.; Mano, J. F. *J. Appl. Polym. Sci.* **2007**, *105*, 3500.
30. Bai, J.; Fang, H.; Zhang, Y.; Wang, Z. *CrstEngComm*. **2014**, *16*(12), 2452.
31. Lauritzen, J. I.; Hoffman, J. D. *J. Appl. Phys.* **1973**, *44*(10), 4340.
32. Ni'mah, H.; Woo, E. M.; Chang, S.-M. *RSC Adv.* **2014**, *4*(99), 56294.
33. Lim, L. T.; Auras, R.; Rubino, M. *Prog. Polym. Sci.* **2008**, *33*(8), 820.
34. Li, H.; Huneault, M. A. *Polymer*. **2007**, *48*(23), 6855.
35. Muller, J.; Jiménez, A.; González-Martínez, C.; Chiralt, A. *Polym. Int.* **2016**, *65*(8), 970.

36. Xu, J.-Z.; Chen, T.; Yang, C.-L.; Li, Z.-M.; Mao, Y.-M.; Zeng, B.-Q.; Hsiao, B. S. *Macromolecules*. **2010**, *43*(11), 5000.
37. Pluta, M.; Galeski, A. *J. Appl. Polym. Sci.* **2002**, *86*(6), 1386.
38. Chen, X.; Kalish, J.; Hsu, S. L. *J. Polym. Sci. Part B: Polym. Phys.* **2011**, *49*(20), 1446.
39. Sawai, D.; Takahashi, K.; Sasashige, A.; Kanamoto, T.; Hyon, S.-H. *Macromolecules*. **2003**, *36*(10), 3601.
40. Han, L.; Pan, P.; Shan, G.; Bao, Y. *Polymer*. **2015**, *63*, 144.
41. Krikorian, V.; Pochan, D. J. *Macromolecules*. **2005**, *38*(15), 6520.
42. Chen, C.; Li, D.; Hu, Q.; Wang, R. *Mater. Des.* **2014**, *56*, 1049.
43. Mathew, A. P.; Laborie, M. P. G.; Oksman, K. *Biomacromolecules*. **2009**, *10*(6), 1627.

Supporting information

Crystallization of triethyl citrate-plasticized poly(lactic acid) induced by chitin nanocrystals

Shikha Singh,[a,b] Maria Lluisa Maspoch[b] and Kristiina Oksman[a,c,d]*

[a]Division of Materials Science, Luleå University of Technology, SE-97 187 Luleå, Sweden

[b]Centre Català del Plàstic (CCP), Universitat Politècnica de Catalunya Barcelona Tech (EEBE-UPC), C/Colom, 114, Terrassa 08222, Spain

[c]Fibre and Particle Engineering, University of Oulu, FI-90014 Oulu, Finland

[d]Mechanical & Industrial Engineering (MIE), University of Toronto, Toronto, ON, Canada M5S 3G8

Correspondence to: Kristiina Oksman (E-mail: Kristiina.oksman@ltu.se)

Crystallization kinetics of PLA-TEC and PLA-TEC-ChNC nanocomposite. The Lauritzen–Hoffman nucleation theory[1] was used to understand the effect of ChNCs on the crystallization of plasticized PLA and to study the crystallization kinetics. The crystal growth rate (*G*) at a specific crystallization temperature can be expressed using the Lauritzen–Hoffman equation as follows:

$$G = G_0 \exp\left(\frac{-U*}{R(T_c - T_\infty)}\right) exp\left(-\frac{K_g}{T_c\,\Delta T_f}\right) \quad (1)$$

After simplification, equation 1 can be rewritten as

$$\ln \mathrm{G} + \frac{U^*}{R(T_c - T_\infty)} = \ln G_0 - \frac{K_g}{T_c\, \Delta T_f} \qquad (2)$$

where G_0 is a pre-exponential factor and U^* is the activation energy required for the transportation of the polymer segments across the interfacial boundary between the melt and the crystals, and its value is 6280 J/mol for PLA. R is the gas constant; T_c is the isothermal crystallization temperature; and T_∞ is the temperature below which diffusion stops, and it usually equals to T_g - 30 K. Further, K_g is the nucleation constant; ΔT is the degree of supercooling, which is expressed as $\Delta T = T_m^o - Tc$; and f is a correction factor that denotes the change in the heat of fusion and is close to unity at high temperatures. $f = 2Tc/T_m^o + Tc$, where T_m^o is the equilibrium melting temperature and is the most important parameter for studying the crystallization kinetics. T_m^o values can be determined by extrapolating the experimentally observed melting temperatures by means of the Hoffmann–Weeks equation[2]. The values of T_m^o for PLA, PLA-TEC, and the PLA-TEC-ChNC nanocomposite were calculated by the Hoffmann–Weeks extrapolation[2]; the corresponding plots are shown in Figure S1 and the observed values are listed in Table S1.

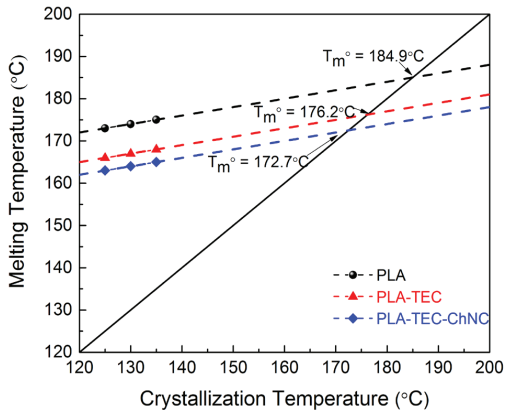

FIGURE S1. Determination of equilibrium melting temperature (T_m^o) of PLA, PLA-TEC, and PLA-TEC-ChNC nanocomposite by Hoffman–Weeks extrapolation.

The value of nucleation constant for heterogonous or secondary nucleation can be calculated as follows[3]:

$$K_g = \frac{nb\sigma\sigma_e}{\Delta H_f k} T_m^0 \qquad (3)$$

where *n* is a constant whose value depends on the crystallization regime (the value of 4 for the regime I and III, and 2 for the regime II); *b* is the layer thickness, which is equal to 5.17×10^{-10} for PLA; σ and σ_e are the lateral and folding surface free energies, respectively; and *k* is the Boltzmann constant.

Here, the growth rate (*G*) of all the materials was calculated by considering the spherulite growth as a function of time (S2–S7). The plots of G + U*/[R(Tc - T∞)] versus 10^5/(Tc·ΔTf) for PLA, PLA-TEC, and the PLA-TEC-ChNC nanocomposite are shown in S8; the K_g values were calculated from

the slopes of the fitted lines and are listed in Table S1. It can be seen from S8 that almost linear lines are obtained for all the materials. R^2 values for PLA, PLA-TEC, and the PLA-TEC-ChNC nanocomposite were 0.9489, 0.9959, and 0.9961, respectively. Bai et al.[3] also observed linear lines for PLA samples. Results of the Lauritzen–Hoffman analysis are presented in Table S1. It can be seen that the values of the nucleation constant (K_g) and surface free energy (σ_e) of PLA-TEC and the PLA-TEC-ChNC nanocomposite were decreased compared to those of PLA. These decreased values indicate that TEC and the ChNCs act as good heterogeneous nucleating agents.

TABLE S1. Lauritzen–Hoffman parameters for isothermal crystallization of PLA, PLA-TEC, and PLA-TEC-ChNC nanocomposite.

Materials	T_m^o/°C	$K_g/k^2(10^5)$	σ_e /J $m^{-2}(10^{-2})$
PLA	184.9	8.7	1.8
PLA-TEC	176.3	2.1	0.5
PLA-TEC-ChNC	172.7	1.6	0.3

POM was performed at three different crystallization temperatures (125, 130 and 135°C) and the spherulitic growth rate (G) of the materials (PLA, PLA-TEC and PLA-TEC-ChNC) was calculated by taking the slop of the spherulite radius versus time. Figure S2-S7 showing the POM image and graphs for measuring the G.

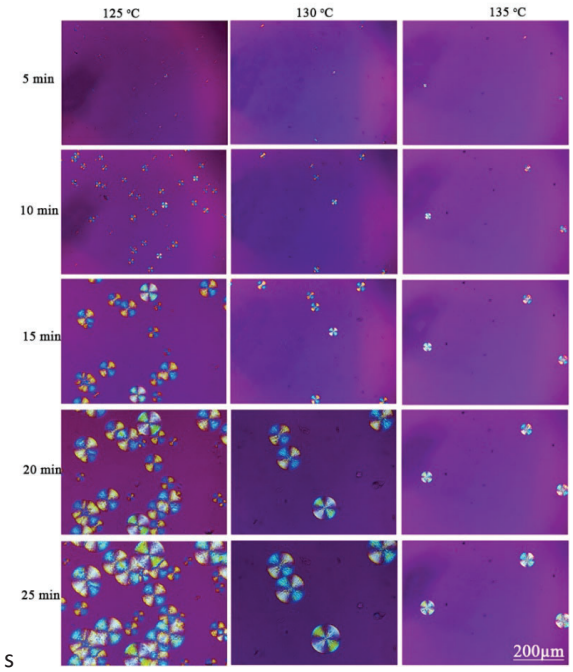

S

FIGURE S2. POM image of isothermal crystallization of PLA at different crystallization temperatures (125, 130 and 135 °C)

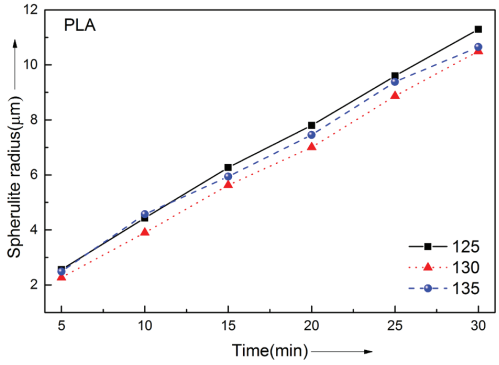

FIGURE S3. Change of spherulite radius of PLA crystallized at different temperature (125, 130 and 135 °C) as a function of time.

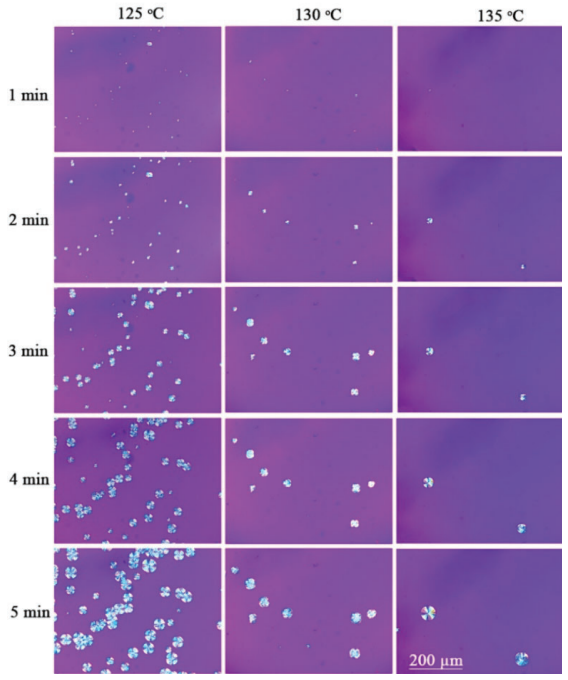

FIGURE S4. POM image of isothermal crystallization of PLA-TEC at different crystallization temperatures (125, 130 and 135 °C)

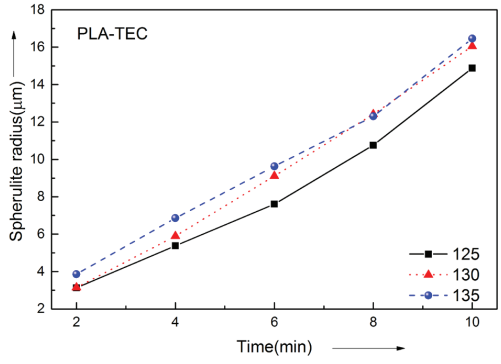

FIGURE S5. Graph plotted between the spherulite radius as a function of time for PLA-TEC during isothermal crystallization at 125, 130 and 135 °C.

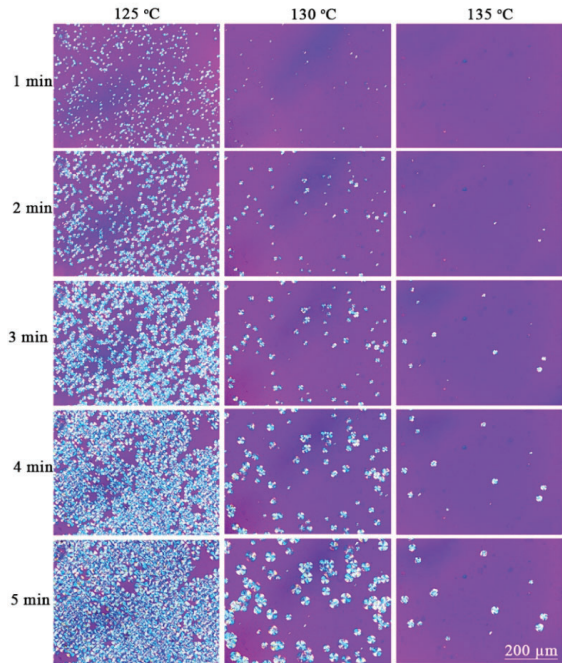

FIGURE S6. POM image of isothermal crystallization of PLA-TEC-ChNC at different crystallization temperatures (125, 130 and 135 °C)

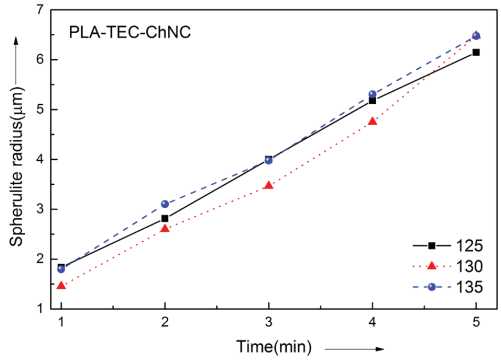

FIGURE S7. Change of spherulite radius of PLA-TEC-ChNC crystallized at different temperature (125, 130 and 135 °C) as a function of time.

The growth rate of spherulites can also be measured by observing the surface area covered with spherulites over a certain time duration (Figure S8). The spherulite radius increased linearly with time, and *G* was calculated from the slopes of the fitted lines. The dependence of the spherulite growth rate on the isothermal crystallization temperature (Tc) given in Figure S9.

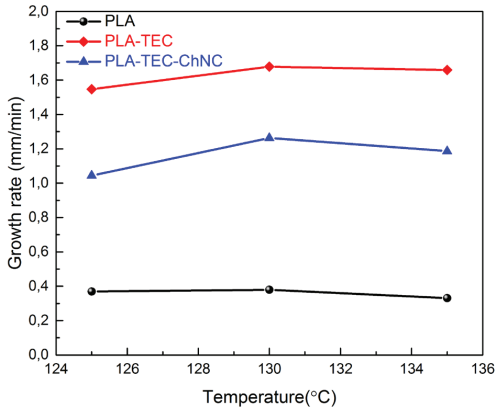

FIGURE S8. Estimation of spherulite growth rate (*G*) as a function of isothermal crystallization temperature (T_c) (125 °C, 130 °C, and 135 °C) for PLA, PLA-TEC, and PLA-TEC-ChNC nanocomposite.

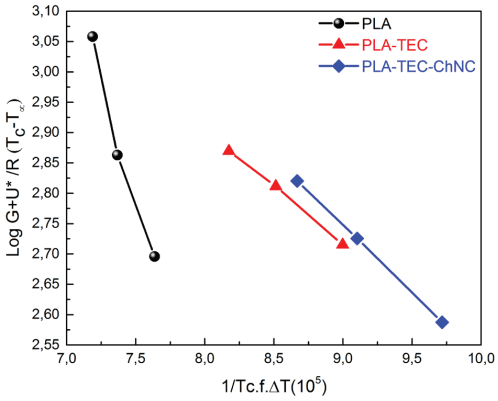

FIGURE S9. Lauritzen–Hoffman plots for PLA, PLA-TEC, and PLA-TEC-ChNC nanocomposite isothermally crystallized at designated temperatures.

The crystal size of the materials was calculated using the Scherrer equation[3] and data is given in Table S2. The data revealed that the crystal size of PLA decreased in the presence of TEC and the ChNCs. The crystal size decreased from 47 nm (PLA) to 41 nm (PLA-TEC). However, the crystal size reduced further with the incorporation of the ChNCs, to 33 nm. This reduction in the crystal size of PLA with the addition of ChNCs could have been caused by the good nucleation ability of the ChNCs. This hypothesis is consistent with the POM results, which revealed that the addition of ChNCs increased the nucleation density of PLA through a reduction in its crystal size.

TABLE S2. Comparison of crystal sizes of isothermally crystallized PLA, PLA-TEC, and PLA-TEC-ChNC nanocomposite at 125 °C with two intense peaks at 16.7°, 19.0°.

Materials	Crystal size (nm)	
	16.7° (peak 1)	19.0° (peak 2)
PLA	46.9	27.4
PLA-TEC	41.0	23.5
PLA-TEC-ChNC	32.5	20.6

REFERENCES.

1. Lauritzen, J. I.; Hoffman, J. D. Extension of Theory of Growth of Chain-Folded Polymer Crystals to Large Undercoolings. *J. Appl. Phys.* **1973**, 44 (10), 4340–4352.

2. Marand, H.; Xu, J.; Srinivas, S. Determination of the Equilibrium Melting Temperature of Polymer Crystals: Linear and Nonlinear Hoffman-Weeks Extrapolations. *Macromolecules* **1998,** 31 (23), 8219–8229.

3. Bai, J.; Fang, H.; Zhang, Y.; Wang, Z. Studies on Crystallization Kinetics of Bimodal Long Chain Branched Polylactides. *CrystEngComm* **2014**, 16 (12), 2452

4. Scherrer, P. "Bestimmung der Grösse und der inneren Struktur von Kolloidteilchen mittels Röntgenstrahlen," Nachr. Ges. Wiss. Göttingen **1918**, (26) 98-100

PAPER II

Effect of chitin nanocrystals on crystallization and properties of poly(lactic)-based nanocomposites

Shikha Singh, Mitul Patel, Daniel Schwendemann, Marta Zaccone, Shiyu Geng, Maria Lluïsa Maspoch, Kristiina Oksman

Polymers, ***2020,*** 12 (3), 726

DOI: 10.3390/polym1230726

polymers

MDPI

Article

Effect of Chitin Nanocrystals on Crystallization and Properties of Poly(lactic acid)-Based Nanocomposites

Shikha Singh [1,2], Mitul Patel [1], Daniel Schwendemann [1,3], Marta Zaccone [4], Shiyu Geng [1], Maria Lluisa Maspoch [2] and Kristiina Oksman [1,5,*]

1 Division of Materials Science, Luleå University of Technology, SE-97 187 Luleå, Sweden; shikha.singh@ltu.se (S.S.); mitul.patel@ltu.se (M.P.); daniel.schwendemann@hsr.ch (D.S.); shiyu.geng@ltu.se (S.G.)
2 Centre Català del Plàstic (CCP), Universitat Politècnica de Catalunya Barcelona Tech (EEBE-UPC), C/Colom 114, Terrassa 08222, Spain; maria.lluisa.maspoch@upc.edu
3 IWK Institut für Werkstofftechnik und Kunststoffverarbeitung, CH-8640 Rapperswil, Switzerland
4 Proplast, Via Roberto di Ferro 86, 15122 Alessandria, Italy; marta.zaccone@proplast.it
5 Mechanical & Industrial Engineering, University of Toronto, Toronto, ON M5S 3BS, Canada
* Correspondence: Kristiina.oksman@ltu.se; Tel.: +46-920-493-371

Received: 2 March 2020; Accepted: 16 March 2020; Published: 24 March 2020

Abstract: The crystalline phase of poly(lactic acid) (PLA) has crucial effects on its own properties and nanocomposites. In this study, the isothermal crystallization of PLA, triethyl citrate-plasticized PLA (PLA–TEC), and its nanocomposite with chitin nanocrystals (PLA–TEC–ChNC) at different temperatures and times was investigated, and the resulting properties of the materials were characterized. Both PLA and PLA–TEC showed extremely low crystallinity at isothermal temperatures of 135, 130, 125 °C and times of 5 or 15 min. In contrast, the addition of 1 wt % of ChNCs significantly improved the crystallinity of PLA under the same conditions owing to the nucleation effect of the ChNCs. The samples were also crystallized at 110 °C to reach their maximal crystallinity, and PLA–TEC–ChNC achieved 48% crystallinity within 5 min, while PLA and PLA–TEC required 40 min to reach a similar level. Moreover, X-ray diffraction analysis showed that the addition of ChNCs resulted in smaller crystallite sizes, which further influenced the barrier properties and hydrolytic degradation of the PLA. The nanocomposites had considerably lower barrier properties and underwent faster degradation compared to PLA–TEC110. These results confirm that the addition of ChNCs in PLA leads to promising properties for packaging applications.

Keywords: poly(lactic acid); chitin nanocrystals; nanocomposites; liquid-assisted extrusion; crystallinity; barrier properties; hydrolytic degradation

1. Introduction

Poly(lactic acid) (PLA)-based nanocomposites have been widely researched owing to their potential applications. The mechanical properties of PLA are comparable to those of polystyrene (PS) and polyethylene terephthalate (PET), that are commercial polymers used for packaging applications. PLA has good optical properties. However, PLA has slow crystallization rate, moderate gas permeability, and low elongation at break that limits its use in the packaging industry [1,2].

Crystallinity plays a vital role in the improvement of mechanical, thermal, optical, and barrier properties of polymers. Usually, nucleating agents are added to the polymers to increase their crystallinity [3]. Chitin whiskers (ChNWs), also known as chitin nanocrystals (ChNCs), were first isolated from a crab shell by Marchessault et al. [4] in 1959 via acid hydrolysis. ChNCs have attracted significant attention as nucleating agents because of their natural origin, low toxicity, low density,

large surface area, and biodegradability [5]. ChNCs exhibit a rod-like shape, have a length of 50–300 nm, a diameter of 10–30 nm, an aspect ratio of approximately 15, and a modulus of 150 GPa [6]. Furthermore, ChNCs have acid amide functional groups on the surface that provide better scope of interactions with the polymers [7]. Additionally, they possess antibacterial [8] and antifungal properties [9] that further expand their usage for packaging applications.

Polymer nanocomposites containing ChNCs were first prepared by Paillet and Dufresne, in 2001 [6]. Initially, ChNCs were incorporated into poly(styrene-co-butyl acrylate) nanocomposites [6]. Subsequently, ChNCs were successfully added into several other polymers [10–12]. Morin and Dufresne prepared a nanocomposite adding ChNC in poly(caprolactone) (PCL) and observed that ChNC increased the relaxed modulus of PCL/ChNC composites from 0.6 MPa to 6.8 MPa [10]. Lu et al. [11] added ChNCs in a soy protein isolate (SPI) matrix and reported that ChNC (20 wt %) increased the mechanical properties of the SPI/ChNC nanocomposites. The tensile strength increased from 4 MPa to 8 MPa and Young's modulus increased from 26 MPa to 158 MPa. Wang et al. [13] reported that on adding 0.5 wt % of surface-modified ChNCs into poly(3-hydroxybutyrate-co-3-hydroxyvalerate) (PHBV), the ChNCs improved both the Young's modulus and strength of the PHBV composites by 44% and 67%, respectively.

The development of PLA nanocomposites with ChNCs [9,14–16] has attracted considerable interest. Generally, PLA nanocomposites have been prepared by solvent casting technique because solvent casting is easy and the dispersion of ChNC into dissolved polymer is convenient as well, but it is difficult to upscale and also organic solvents are used if non-water-soluble polymer is used as matrix. The main challenge in the preparation of PLA nanocomposites with ChNCs is to develop up-scalable processing methods where ChNCs are homogenously dispersed into PLA [14]. Poor compatibility between the hydrophobic PLA and hydrophilic ChNC resulted to the poor dispersion which eventually forms a weak polymer-nanoreinforcement interactions and thus, formation of agglomeration of the ChNCs are found. Oksman et al. [17], used liquid-assisted extrusion to overcome this problem of dispersion of hydrophilic nano-reinforcements into a hydrophobic polymer matrix and successfully prepared well-dispersed cellulose nanocrystal (CNC) PLA nanocomposites. Later, they used the same technique to prepare PLA nanocomposites using ChNCs and CNCs [18]. The compositions of PLA, triethyl citrate (TEC), and ChNC in the nanocomposites were in the proportions of 79:20:1(wt %) [18]. Microscopy revealed a number of small aggregates in the nanocomposites. However, it was observed that the ChNC and CNC nanocomposite films prepared with slow and fast cooling rates affected the final properties of the PLA, and the addition of ChNC resulted in better properties than the addition of CNC [18]. In another study, the process was upscaled with film blowing and PLA/ChNC nanocomposite films were successfully produced using 6 wt % of TEC and 1 wt % of ChNC [19]. They reported that ChNCs acted as a multifunctional additive that increased the viscosity, melt strength, thermal stability, and the crystallinity. In addition, an increase in tear strength and puncture strength (175% and 300%, respectively) in PLA/ChNC nanocomposites was reported [19].

We previously conducted a detailed investigation on the effect of ChNCs on the crystallization behavior (crystallization rate, kinetics, crystal types) of TEC-plasticized PLA [20]. It was observed that a very low amount of ChNC (1 wt %) increased the crystallization rate by acting as an excellent nucleating agent, and therefore reduced the overall crystallization time of the plasticized PLA.

The aim of the present study is to further explore the knowledge of crystallization and investigate how ChNC affects the crystallinity and the thermal, optical, barrier, and hydrolytic degradation properties of nanocomposites. Isothermal crystallization was carried out at different temperatures (135, 130, 125, and 110 °C) and holding times (5, 15, and 40 min) using compression molding. The morphology and dimensions of the ChNCs were analyzed by atomic force microscopy (AFM). Scanning electron microscopy (SEM) was used to analyze the dispersion and morphology of the materials. Fourier transform infrared (FTIR) spectroscopy was used to investigate the interaction between ChNC and PLA during the isothermal crystallization of materials. The thermal properties and degree of crystallinity were investigated using differential scanning calorimetry (DSC). X-ray diffraction (XRD) was used

to investigate the crystal structure and polarized optical microscopy (POM) was used to determine the spherulite size. The barrier properties of the materials were tested with water vapor transmission rate (WVTR) and oxygen permeability (OP) tests. The effect of crystallinity induced by ChNCs on the hydrolytic degradation was further examined. Finally, the influence of hydrolytic degradation on the thermal stability of the materials was investigated by thermogravimetric analysis (TGA).

2. Materials and Methods

2.1. Materials

Polylactic acid (PLA) in pellet form (Ingeo 4043D) from NatureWorks, (Minnetonka, MN, USA) was used as the matrix. Chitin powder from shrimp shell was purchased from Sigma-Aldrich (grade C7170 (Stockholm, Sweden) and used as a starting material for the isolation of ChNCs. HCl (ACS reagent, 37%) for acid hydrolysis was purchased from Merck (Darmstadt, Germany). TEC (M_w: 276.3 g/mol) in liquid form was purchased from VWR (Stockholm, Sweden), and ethanol (99.5%) was purchased from Solveco (Stockholm, Sweden).

2.2. Preparation of ChNCs

ChNCs were isolated via hydrochloride acid hydrolysis treatment according to the procedure described by Herrera et al. [21]. Briefly, the chitin powder was hydrolyzed using 3 M HCl at 90 ± 5 °C under vigorous stirring for 90 min. The ratio of acid to chitin solids was 30 mL per gram of chitin. After acid hydrolysis, the suspension was diluted with distilled water and subjected to centrifugation at 8000 rpm for 10 min. The supernatant after centrifugation was decanted and the precipitate was diluted again with distilled water. This centrifugation process was repeated three times. Afterwards, the suspension was transferred to dialyze for 5 days. For the disintegration of the remaining large particles, the suspension was subjected to ultrasonication treatment for 20 min. The final suspension was then evaporated to obtain a ChNC gel with a solid content of 18 wt % and was subsequently stored at 4 °C for later use.

2.3. Preparation of Nanocomposite Pellets via Liquid-Assisted Extrusion

PLA nanocomposites were prepared by melt compounding via liquid-assisted extrusion as reported by Oksman and co-workers [17,19,21]. In this method, ChNCs were fed in liquid form and the suspension was prepared as follows: ChNC gel in water (18 wt %) was pre-dispersed in a water/ethanol solvent mixture with a weight ratio of 1:5 for 2 h via magnetic stirring and then mixed with TEC (2.61 wt % solid content was added to achieve 10 wt % of TEC). To feed the suspension into the extrusion a peristaltic pump PD 5001 Heidolph (Schwalbach, Germany) was used. The specific feeding rates of the PLA and the suspension as well as the final composition of materials are displayed in Table 1.

Table 1. Sample codes and compositions of prepared materials.

Materials	Feeding Rate (kg/h)		Composition of Materials (wt %)		
	PLA	Suspension	PLA	TEC	ChNCs
PLA	2.00	0.00	100	0	0
PLA-TEC	1.80	0.75 *	90	10	0
PLA-TEC-ChNC	1.78	0.77 *	89	10	1

* Fed into extruder out of which 0.09 kg/h of water and 0.46 kg/h ethanol were removed as vapor during extrusion.

A co-rotating twin-screw extruder ZSK-18 MEGALab, Coperion W&P (Stuttgart, Germany) length to diameter screw ratio (L/D) 40 and screw diameter 18 mm, equipped with K-tron gravimetric feeder (Niederlenz, Switzerland) was used for the production of nanocomposites. a schematic representation of

the nanocomposite pellet preparation process is shown in Figure 1a. Finally, pellets of PLA–TEC–ChNC with 1 wt % of ChNCs and neat PLA and PLA–TEC as references were prepared for later processing.

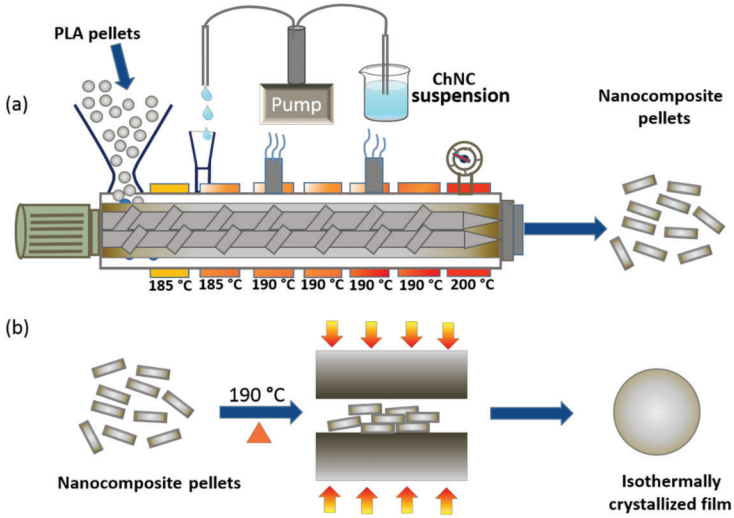

Figure 1. Schematics of (**a**) preparation of nanocomposites pellets (PLA–TEC–ChNC) via liquid-assisted extrusion process, and (**b**) preparation of isothermally crystallized nanocomposite films.

2.4. Preparation of Isothermal-Crystallized Films

PLA, PLA–TEC, PLA–TEC–ChNC films were prepared by compression molding using a laboratory press LPC-300 Fontijne Grotnes (Vlaardingen, Netherlands). For this, 4 g of each material was placed between two metallic sheets to mold the films. First, the material was preheated at 190 °C and was then compression-molded using a pressure of 8.2 MPa for 1 min. Thereafter, the film was cooled to the isothermal crystallization temperature (135 °C, 130 °C, 125 °C, or 110 °C) and kept for 5, 15, or 40 min, and was subsequently cooled to room temperature using a water cooling system equipped with the laboratory press (Figure 1b). The prepared samples were coded according to their corresponding isothermal crystallization temperature (IC_{TEMP}) and time (IC_{TIME}), as shown in Table 2.

Table 2. Temperature and time used for preparation of different isothermally crystallized films of PLA, PLA–TEC, and PLA–TEC–ChNC.

Sample Codes	IC_{TEMP} (°C)	IC_{TIME} (min)
PLA	N/A	0
PLA–TEC	N/A	0
PLA–TEC–ChNC	N/A	0
PLA135–5	135	5 *
PLA–TEC135–5	135	5 *
PLA–TEC–ChNC135–5	135	5 *
PLA135–15	135	15 *
PLA–TEC135–15	135	15 *
PLA–TEC–ChNC135–15	135	15 *
PLA130–5	130	5 *
PLA–TEC130–5	130	5 *
PLA–TEC–ChNC130–5	130	5 *
PLA130–15	130	15 *
PLA–TEC130–15	130	15 *
PLA–TEC–ChNC130–15	130	15 *
PLA125	125	5 *
PLA–TEC125	125	5 *
PLA–TEC–ChNC125	125	5 *
PLA125	125	15 *
PLA–TEC125	125	15 *
PLA–TEC–ChNC125	125	15 *
PLA110	110	40 **
PLA–TEC110	110	40 **
PLA–TEC–ChNC110	110	5 **

Note: * At 5 and 15 min, all the materials exhibited incomplete crystallization. ** For further experiments, complete and homogenous crystallization has been considered (which was achieved at 110 °C), PLA110 and PLA–TEC110 took 40 min while PLA–TEC–ChNC110 was completely crystallized within 5 min.

2.5. Characterizations

Atomic force microscopy (AFM) was used to characterize the morphology and dimensions of the ChNCs using a Veeco Multimode Nanoscope (Santa Barbara, CA, USA) in the tapping mode. The length and diameter of the ChNCs were analyzed using the Gwyddion software version 2.55 (Czech Metrology Institute, Brno, Czech) [22].

Differential scanning calorimetry (DSC) Mettler Toledo 822e (Schwerzenbach, Switzerland) was used to study the crystallinity of the isothermally crystallized films. Additionally, the crystallinity of hydrolytic degraded films was investigated. Samples were placed in an aluminum crucible, and then analyzed under a nitrogen atmosphere from −20 to 200 °C at a heating rate of 10 °C/min. The crystallinity of the samples was calculated using following Equation [23]:

$$Crystallinity(\%) = \frac{\Delta H_m - \Delta H_{cc}}{93.1} \times \frac{100}{w} \quad (1)$$

where ΔH_m is the melting enthalpy, ΔH_{cc} is the cold crystallization enthalpy, the constant 93.1 (unit: J/g) corresponds to the ΔH_m for 100% crystalline PLA [23], and w is the weight fraction of PLA in the samples [23].

The thermal stability of the isothermally crystallized films was investigated using thermo-gravimetric analysis (TGA), TA Instrument Q500 (New Castle, DE, USA) under nitrogen atmosphere. Approximately 9 mg of material was subjected for testing at a heating rate of 10° C/min in a temperature range of 0–600 °C.

X-ray diffraction using a PANalytical Empyrean diffractometer (Almo, Malvern, UK)) was performed to investigate the crystallite size of the PLA. The measurements were performed with Cu–Kα radiation (λ = 1.5405 Å). An acceleration voltage of 45 kV and current of 40 mA were used

over a range of 5°–45° with a step size of 0.026°. The crystallite size was investigated using the Scherrer Equation:

$$Crystallite\ size = \frac{k\lambda}{\beta Cos\theta} \quad (2)$$

where k is the dimensional shape factor, and is 0.9 [24], λ is the wavelength, β is the full-width at half maximum for different peaks, and θ is the Bragg angle.

The light transmittance of the materials was measured using a UV–Vis spectrophotometer (GENESYS, 10 UV, Thermo-Scientific, Dreieich, Germany) at a constant wavelength of 550 nm, and three specimens from each sample were tested to calculate the average values.

Polarized microscopy (POM) Nikon Eclipse LV 100 Pol (Kanagawa, Japan), was used to study the spherulite morphology and size developed during isothermal crystallization.

Fractured surfaces of the PLA110, PLA–TEC110, and PLA–TEC–ChNC110 were studied by scanning electron microscopy (SEM) JEOL, JSM-IT300 (Tokyo, Japan). Prior to the study, the surfaces of the samples were sputter-coated (Leica EM ACE220, Wetzlar, Germany) with platinum to avoid the charging effect. The acceleration voltage was 15 kV, and secondary electron images were collected.

Fourier infrared spectroscopy with the attenuated total reflectance mode (ATR-FTIR) VERTEX 80, Bruker, (Ettlingen, Germany) was carried out to investigate the interaction between PLA, TEC, and ChNCs, induced during the isothermal crystallization of PLA110, PLA–TEC110, and PLA–TEC–ChNC110. The spectra were recorded in the wavenumber range of 400–4000 cm^{-1}.

Water vapor transmission rate (WVTR) was measured using a modified method according to ASTM E96. Films were cut into circular discs with diameters of 0.04 m. The test samples were placed on a cup filled with silica gel and then placed in a chamber with controlled temperatures of 23 °C and 50% relative humidity (RH). The cups were weighed after specific time intervals and WVTR (g/m^2 day) was determined using the following equation [25]:

$$WVTR = \frac{G/t}{A} \quad (3)$$

where G/t is the slope of the curve with increased weight gain (g) as a function of time (h) and A is the exposed area (m^2).

The oxygen permeability (OP) tests were performed on the PLA–TEC and PLA–TEC–ChNC films using a Multiperm 037 equipment (ExtraSolution, Pieve Fosciana, Italy), according to the ASTM F2622–08. The surface area of the formed square films was 2 cm^2 and the thickness was approximately 120 μm; the films were previously conditioned for 12 h under a continuous flux of electronically controlled anhydrous nitrogen. This preliminary step is necessary to stabilize the specimens and to remove the oxygen already present inside the sample before the beginning of the test. The duration of this phase is strongly related to both the barrier properties and the thickness of the material under testing. The thicker the specimen, the longer will be the conditioning phase. Typically, the following empirical equation is used to calculate this duration:

$$Conditioning\ time[h] = \frac{thickness\ [\mu m]}{10} \quad (4)$$

At the end of the conditioning phase, the oxygen flux was determined for the surfaces of the specimens. a carrier collected and a sensor detected the amount of oxygen that permeated through the films. The test was performed at 23 °C and 50% RH. The oxygen flux of the film surfaces was maintained at 13.5 mL/min on an average. Two specimens were tested for each formulation. The reported data were referred to mediated values. The oxygen transmission rate (OTR) from the test corresponds to the oxygen permeability of the material and is calculated using following Equation:

$$\frac{OTR_f}{A_{ts}} = OTR \quad (5)$$

where OTR is the oxygen transmission rate [cc/m^2 24h], A_{ts} is the surface area of the test sample [m^2], and OTR_f [cm^3/day] is the final measured permeation concentration. This parameter is also calculated as:

$$OTR_f = OTR_m - OTR_b \quad (6)$$

where OTR_m is the measured oxygen transmission rate and OTR_b corresponds to the background oxygen transmission rate.

Hydrolytic degradation of the materials was performed according to the ASTM F163 on 30 mm × 30 mm × 0.1 mm films. The samples were dipped into distilled water kept inside in an oven set at 58 °C. Intermittently, the samples were taken out and gently wiped with tissue paper to remove the water droplets present on the surface, and the weights of the samples were recorded. The degradation process was monitored up to 18 days. Water uptake studies were also performed to investigate the diffusion kinetics of PLA110, PLA–TEC110, and PLA–TEC–ChNC110. Furthermore, the effect of hydrolytic degradation on thermal properties was studied.

3. Results

Inspired by our previous studies on liquid-assisted extrusion [18,19,21], we have successfully produced PLA/ChNCs nanocomposites by using a co-rotating twin-screw extruder. The liquid feeding of ChNCs along with TEC plasticizer lead to PLA–TEC–ChNCs nanocomposites with improved dispersion and distribution of ChNCs. Furthermore, it is very important to have a controlled and effective atmospheric venting, as well as a vacuum system to evacuate the vapor (550 g/hr) of liquid (water: ethanol) during the extrusion process. Therefore, a co-rotating twin-screw extruder is the best choice of equipment due to its excellent degassing properties.

3.1. Morphology of ChNCs and Visual Appearance of Neat Films

The size and shape of the nanoreinforcement play an important role in the nanocomposites. Therefore, the morphology of the ChNCs were examined using AFM and image displays rod-shaped ChNCs (Figure 2a). The length and diameter of the ChNCs were in the range of 273 nm and 11 nm, respectively, and the corresponding histograms are shown in Figure 2b–c. The very small diameter and high aspect ratio of the ChNCs ensure that they can present excellent functionalities, e.g., serving as reinforcements and improving barrier properties, when they are well-dispersed in the PLA–TEC matrix. Photographs and optical micrographs of the prepared neat PLA, PLA–TEC, and PLA–TEC–ChNC films (without isothermal crystallization) are presented in Figure 2d–f,d′–f′.

All films are clear and transparent, which is attributed to the fast cooling process during the compression molding resulting in very low crystallinity in all three samples (Table 3). This also confirms that the ChNCs were well-dispersed and distributed in the PLA–TEC matrix and no large agglomerates were visible under an optical microscope, as shown in Figure 2f′.

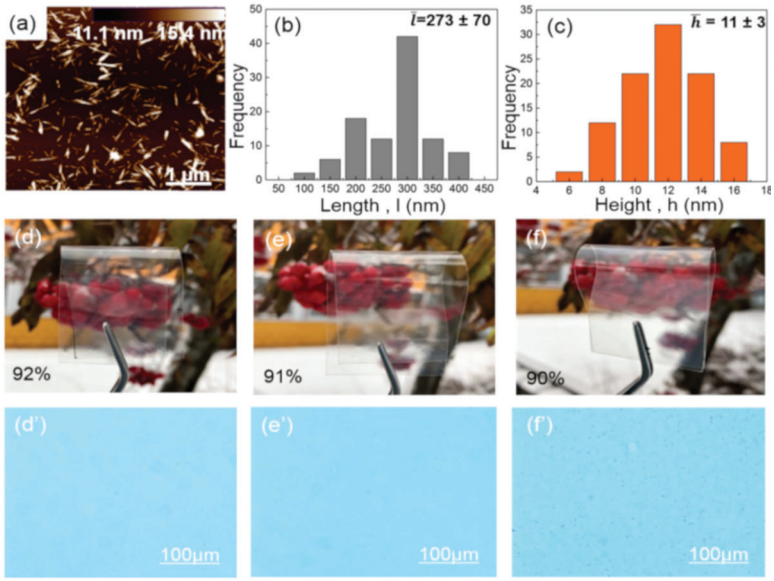

Figure 2. ChNCs characteristics including (**a**) height AFM image showing shape of ChNCs, (**b**) length and (**c**) diameter (height) distributions indicating average length ($\bar{l}$) and width ($\bar{h}$). Photographs and optical micrographs of neat (**d**–**d′**) PLA, (**e**–**e′**) PLA–TEC, and (**f**–**f′**) PLA–TEC–ChNC films showing high transparency and well-dispersed ChNCs in PLA–TEC.

Table 3. Thermal properties of neat PLA, PLA–TEC, and PLA–TEC–ChNC, and isothermally crystallized PLA110, PLA–TEC110, and PLA–TEC–ChNC110 films.

Materials	T_g (°C)	T_{cc} (°C)	T_m (°C)	Crystallinity (%)
PLA	61.7	110.4	170.4	4.0
PLA–TEC	48.8	98.0	164.8	6.6
PLA–TEC–ChNC	48.1	95.4	164.4	6.7
PLA135-5	58.9	108.6	169.6	7.5
PLA–TEC135–5	46.0	97.4	164.6	7.8
PLA–TEC–ChNC135–5	46.3	94.7	163.2	8.6
PLA135–15	60.6	110.6	170.0	1.3
PLA–TEC135–15	47.5	97.4	164.4	4.5
PLA–TEC–ChNC135–15	44.8	93.4	163.4	14.2
PLA130–5	59.4	108.4	169.4	2.6
PLA–TEC130–5	46.8	96.2	164.5	7.5
PLA–TEC–ChNC130–5	46.3	94.5	163.6	8.2
PLA130–15	58.6	108.5	168.6	7.0
PLA–TEC130–15	45.7	96.0	163.3	7.2
PLA–TEC–ChNC130–15	39.1	87.1	163.3	34.5
PLA125–5	59.5	109.7	169.5	6.0
PLA–TEC125–5	46.9	97.0	164.8	7.2
PLA–TEC–ChNC125–5	46.5	95.8	164.7	7.3
PLA125–15	59.8	110.4	169.6	5.8
PLA–TEC125–15	47.3	96.9	163.7	6.0
PLA–TEC–ChNC125–15	37.7	86.9	162.7	36.5
PLA110–40	59.4	111.8	164.9	45.5
PLA–TEC110–40	44.7	113.7	164.8	49.9
PLA–TEC–ChNC110–5	36.8	-	164.6	47.5

3.1.1. Surface Morphology

The morphologies of the surface and cross-section of the fractured samples IC_{TEMP} at 110 °C were studied by SEM as shown in Figure 3. The fractured surface of the PLA110 film was relatively coarse, as evidenced by the surface view as well as the cross-sectional view. In contrast to PLA,

the incorporation of TEC into PLA (i.e., PLA–TEC110) exhibited a homogenous behavior. In the surface view of PLA–TEC–ChNC110, a highly ordered pattern of spherulites was seen which may be due to the well-dispersed ChNCs resulting in the formation of homogenous spherulites. In the cross-sectional view of PLA–TEC–ChNC110, no agglomerates were found which is attributed to the homogenous dispersion and distribution of the ChNCs in the nanocomposite.

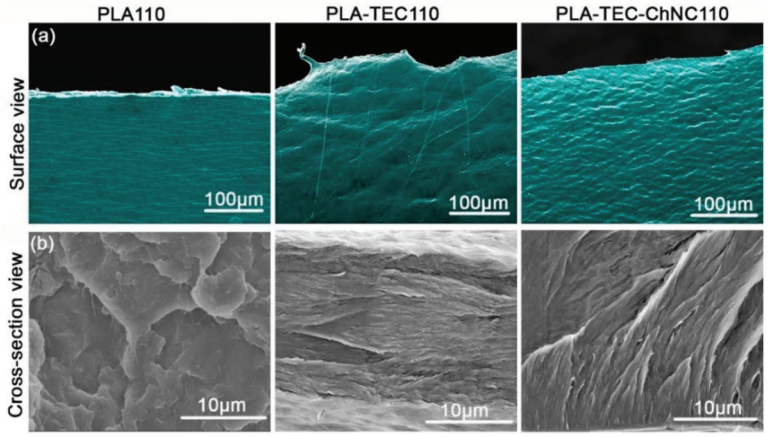

Figure 3. SEM images of fractured samples of isothermally crystallized PLA110, PLA–TEC110, and PLA–TEC–ChNC110 films (**a**) surface view and (**b**) cross-sectional view.

3.1.2. Surface Interaction between PLA, TEC, and ChNC

Isothermal crystallization (especially at 110 °C) induced some interactions between the PLA, TEC, and ChNC which further investigated with ATR-FTIR and spectra of PLA110, PLA–TEC110, and PLA–TEC–ChNC110 are presented in Figure 4. All samples show a sharp peak at 1751 cm^{-1} that corresponds to the characteristic carbonyl peak of the PLA. The –C=O peak intensity of the nanocomposite was slightly reduced compared to PLA110 and PLA–TEC110. Peaks at 2997, 2954, 1453, 1386, 1358, 1266, 1128, 923, and 869 cm^{-1} are attributed to the asymmetric and symmetric –CH stretching, methyl bending, asymmetric and symmetric –CH bending, –C=O bending, –C–O– stretching, and –C–C– stretching (backbone) of PLA, respectively [26]. In PLA–TEC110, peaks observed at 3658 and 3506 cm^{-1} are attributed to –OH stretching [27]. The FTIR spectra of PLA–TEC110 showed certain molecular changes in the 2992–3509 cm^{-1} range that corresponds to –CH aliphatic stretching [27]. One new broad band appeared at 2925 cm^{-1}. PLA–TEC–ChNC110 did not show significant differences but the overall intensity of the nanocomposites decreased and some overlapping bands were found in the fingerprint region. This may be due to certain molecular interactions that may have occurred between the components of the nanocomposites.

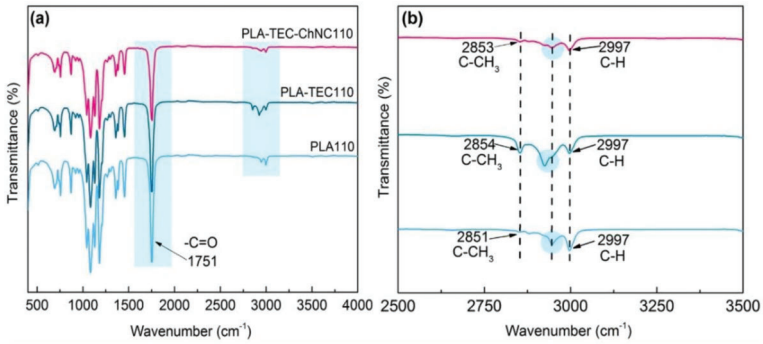

Figure 4. ATR-FT-IR spectra of (**a**) PLA110, PLA–TEC110, and PLA–TEC–ChNC110 (**b**) zoomed view of PLA, PLA–TEC110, and PLA–TEC–ChNC110 showing the –C–CH_3 and –C–H peaks.

3.2. Thermal Properties, Crystallinity and Crystal Strucutre

The thermal properties of all samples with various IC_{TEMPs} and IC_{TIMEs}, including the glass transition temperature (T_g), cold crystallization temperature (T_{cc}), melt temperature (T_m), and crystallinity were determined from the first DSC heating scan, and the obtained data are summarized in Table 3. The crystallinity of the nanocomposites crystallized at 135, 130, or 125 °C for 15 min was much higher than that of neat PLA and PLA–TEC. At 110 °C, the nanocomposites achieved 47.5% crystallinity within 5 min of crystallization, while for PLA and PLA–TEC, 40 min was required to reach similar crystallinity. These indicate that the well-dispersed ChNCs can act as very effective nucleation agents for PLA crystallization. PLA had a constant T_g (approximately 59 °C) under all isothermal conditions, which is much higher than that of PLA–TEC (approximately 46 °C) owing to the presence of the plasticizer in PLA–TEC. PLA–TEC–ChNC showed a similar T_g as compared to PLA–TEC within 5 min of crystallization (at 135, 130, or 125 °C). However, the T_g of nanocomposites was relatively lower than that of PLA–TEC for 15 min of crystallization. This could be owing to the excellent nucleation ability of ChNCs resulting in higher crystallinity (increasing from 14.2% to 36.5%) under this condition. Interestingly, at the lowest temperature, i.e., 110 °C, PLA–TEC–ChNC exhibited the lowest T_g (37 °C). In addition, the T_{cc} of PLA–TEC was lower than that of neat PLA because of more flexible polymer chains, and the PLA–TEC–ChNC samples with higher crystallinity possessed lower T_{cc} owing to their more plasticized amorphous phase. PLA showed a T_m of approximately 169 °C at all isothermal conditions; on the other hand, there were no significant differences in the T_m of PLA–TEC and PLA–TEC–ChNC (approximately 164 °C), as observed under all isothermal conditions.

As similar crystallinity (45.5%–49.9%) was achieved at IC_{TEMP} of 110 °C for all three types of materials, i.e., PLA, PLA–TEC, and PLA–TEC–ChNC, the following characterizations focused on these three samples was to avoid further influence from different crystallinities. XRD analyses were carried out to investigate the crystal structure of the samples. Figure 5a shows the XRD patterns of PLA110, PLA–TEC110, and PLA–TEC–ChNC110. All materials exhibited peaks at 14.8°, 16.6°, 18.9°, and 22.2°, corresponding to the (200), (110), (203), and (015) planes of the PLA crystals, respectively. The crystallite sizes of the materials were calculated from the XRD patterns according to the Scherrer Equation (Equation (2)). The crystallite size of PLA–TEC was 14 nm, which was slightly larger than that of neat PLA (12 nm). PLA–TEC–ChNC showed the smallest crystallite size (8 nm), which is attributed to the nucleation effect of the ChNCs. The spherulite structures of these three samples were also studied by POM as shown in Figure 5c–e. Spherulites sizes of the PLA110, PLA–TEC110, and PLA–TEC–ChNC110 were measured to be 49, 56, and 23 μm, respectively, which are consistent with the XRD results.

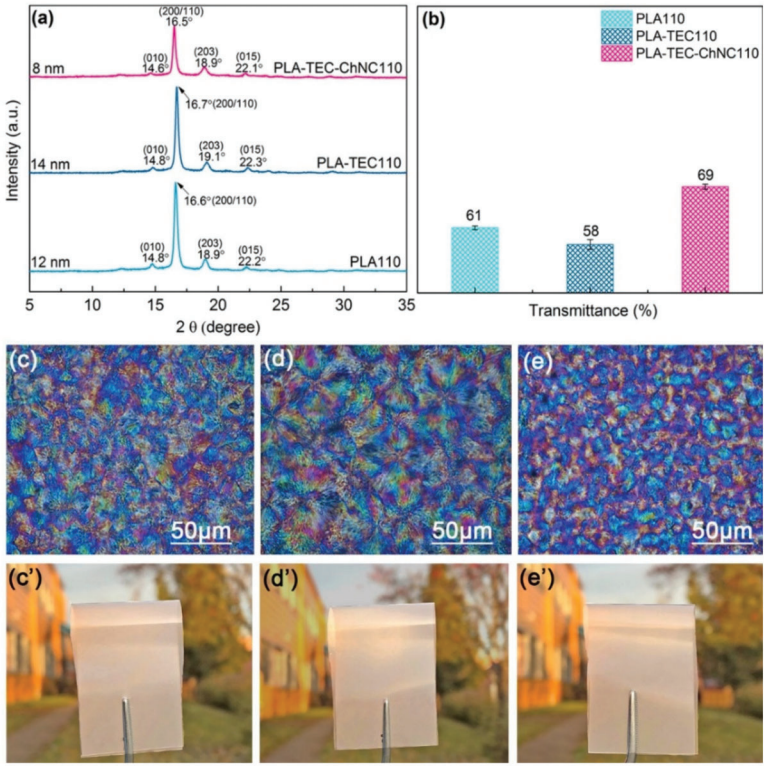

Figure 5. (**a**) XRD and (**b**) UV spectra at 550 nm, optical micrographs and photographs of isothermally crystallized (**c**–**c'**) PLA110, (**d**–**d'**) PLA–TEC110, and (**e**–**e'**) PLA–TEC–ChNC110.

3.3. Optical Properties

The optical transparency of the materials was investigated, and the light transmittance data are presented in Figure 5b and in Table S1 (see Supplementary Materials). In general, samples with higher crystallinity exhibited lower transparency owing to the light scattering of the crystalline region in the materials. For the samples with 110 °C of IC_{TEMP} that showed similar crystallinity, the transparency was influenced by the crystallite size. As shown in Figure 4b, PLA110 exhibited a transmittance of 61% that was higher than that of PLA–TEC110 (58%), while PLA–TEC–ChNC110 showed the highest value of 69%. This is because of the well dispersed ChNC which resulted into the formation of homogenous crystallites. In addition, the photographs of samples with IC_{TEMP} of 110 °C shown in Figure 5c'–e' illustrate that they were significantly opaquer compared to the films without isothermal crystallization (Figure 2d–f).

3.4. Barrier Properties

The barrier properties of the PLA–TEC110 and PLA–TEC–ChNC110 were investigated and the values of WVTR, OTR, and OP are summarized in Table 4. Compared to the WVTR and OTR values of amorphous PLA reported in the literature (200 g/m^2 day and 746 cc/m^2 24h, respectively) [25] PLA–TEC110 and PLA–TEC–ChNC110 presented significantly better barrier properties. Both WVTR and OTR of PLA–TEC110 were 78% lower than those values reported in literature, owing to its very high crystallinity (49.9%, Table 4). Moreover, with only 1 wt % ChNCs in PLA–TEC–ChNC110, its WVTR and OTR were reduced to 28 g/m^2.day and 113 cc/m^2.24h, respectively, which are 36% and 32% lower than those of PLA–TEC110. It is well known that the gas transport properties of polymer composites

are greatly affected by a tortuous path and this tortuosity depends on factors such as the shape and aspect ratio of the reinforcement, degree of orientation, and loading of the reinforcement, interface, and crystallinity [28–30]. Trifol et al. [31] investigated the effect of nanocellulose and nanoclays on the barrier properties of the PLA. They reported that nanocellulose showed better barrier properties than nanoclays. They attributed this to the increased crystallinity and different shapes of the nanocellulose. In the present study, the improvement of the barrier properties of PLA–TEC–ChNC110 can be attributed to both the good dispersion and distribution of ChNCs and smaller spherulite size that inhibits the permeation of the gas molecules within the polymer matrix. Martinez-Sanz et al. [32] reported that PLA nanocomposites with well-dispersed bacterial cellulose nanowhiskers significantly lowered the water permeability of the PLA nanocomposites.

Table 4. Comparison of WVTR, OTR, and OP of PLA, PLA110, and PLA–TEC–ChNC110. (PLA data is from references [25,33])

Materials	WVTR [g/m^2 day]		OTR [ml/(m^2 24h)]		OP [(ml μm)/(m^2 24h kPa)]	
	Ave	std	Ave	std	Ave	std
PLA	200 [25]	-	746 [33]	-	-	-
PLA–TEC110	44	(3)	165	(21)	19,425	(3076)
PLA–TEC–ChNC110	28	(2)	113	(18)	11,563	(2210)

3.5. Hydrolytic Degradation

Hydrolytic degradation tests for PLA110, PLA–TEC110, and PLA–TEC–ChNC110 were performed and the results are presented in Figure 6. As shown in Figure 6a, all three films were degraded and disintegrated after 18 days. With the increase in degradation time, the pH of the aqueous medium of the samples decreased considerably owing to the extraction of lactic acid originating from the PLA. The calculated weight losses of the materials during the tests are presented in Figure 6b. In the initial three days, the degradation of all samples was quite slow, but after one week, the degradation rate increased significantly. Both PLA–TEC110 and PLA–TEC–ChNC110 demonstrated considerably higher degradation rates compared to PLA110, owing to the presence of the TEC plasticizer that increases the free volume of the PLA. It is interesting to note that the nanocomposite degraded slightly faster than PLA–TEC110. The possible reason for this is that the smaller crystallites in the nanocomposite were more easily accessed by water molecules compared to the larger ones in the PLA–TEC110. Similar phenomena have been reported by Paul et al. [34]. They studied the effect of different types of montmorillonites (MMTs) on the hydrolytic degradation of PLA and observed that MMT accelerated the degradation of PLA. The authors concluded that both the composite structure and relative hydrophilicity played vital roles in the hydrolytic degradation of PLA.

The degradation of the polymers in aqueous media proceeds through water uptake followed by chain scission of the ester bond [35]. During degradation, first, the high-molecular-weight PLA chains break down into lower molecular weight chains by the cleavage of the ester bonds of the polymer followed by further disintegration into lactic acid and finally into water and carbon dioxide (see in Figure 7) [36]. Chain scission of the ester bonds is controlled by different parameters such as the amount of water absorbed, the diffusion coefficient of the polymer chain fragment within the polymer, and solubility of the degradation product [37]. The rate of hydrolysis depends on the molecular weight of the oligomers, environmental factors (e.g., temperature), pH of the medium, hydrophilicity, and crystallinity of the given polymer [37,38]. Generally, the hydrolytic degradation of PLA can take place via two different mechanisms: (i) acid hydrolysis (ii) base hydrolysis [39]. Here, hydrolytic degradation is understood to have occurred through acid hydrolysis because the pH substantially decreased from 7 to 3. Acid hydrolysis reactions follow fast chain end sessions and occur by nucleophilic substitution (SN_2) reactions. The schematic for the acid hydrolyzed degradation of PLA is presented in Figure 7.

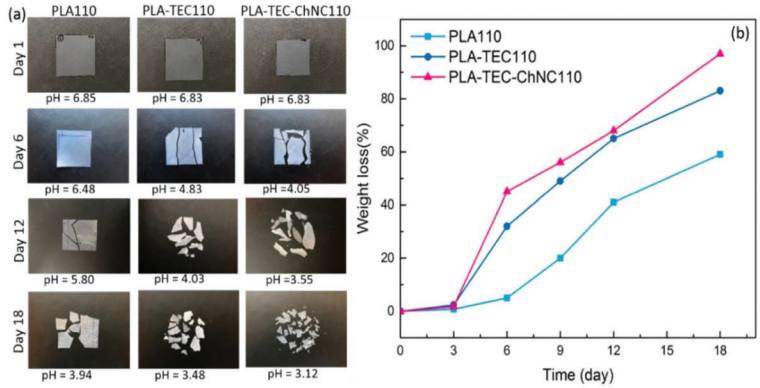

Figure 6. Visual changes in PLA110, PLA–TEC110, and PLA–TEC–ChNC110 after 18 days of hydrolytic degradation (performed at 58 °C). (**a**) Degradation greatly affected the pH and (**b**) chart showing the degradation of PLA110, PLA–TEC110, and PLA–TEC–ChNC110.

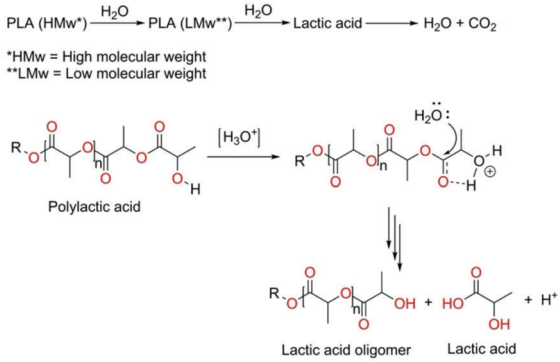

Figure 7. Mechanism of hydrolysis of PLA showing how chain secession of PLA occurs in the acidic medium; here, R=CH_3.

Effect of Hydrolytic Degradation on Thermal Properties

Hydrolytic degradation affects the thermal properties of PLA110, PLA–TEC110, and PLA–TEC–ChNC110. DSC and TGA curves were recorded before and after hydrolytic degradation and the data are provided in Figure S1 (see Supplementary Materials). DSC results show an increase in the degree of crystallinity of the materials after hydrolytic degradation, following the order, PLA110 (61%), PLA–TEC110 (69%), and PLA–TEC–ChNC110 (64%). This was desirable to obtain higher crystallinity after the hydrolytic degradation.

It was observed from the TGA curves that before hydrolytic degradation materials were very stable up to 285 °C. However, after hydrolytic degradation, water has immensely influenced the rate of degradation due to this the materials began degrading much earlier (at 220 °C). DTG curves of all the materials before degradation showed only one peak, whereas those after degradation showed two peaks. These results indicate that water molecules influence the thermal stability of the materials, further confirming the hydrolytic degradation of materials.

3.6. Water Uptake Study

In order to investigate the diffusion of water molecules into PLA110, PLA–TEC110, and PLA–TEC–ChNC110 films, the water uptake was recorded at two temperatures; room temperature

and at 58 °C. Plots of water uptake vs. time are shown in Figure 8. The water uptake of all the materials was rapid, and the materials were saturated within 1 h. This faster saturation of the materials may be caused by the high crystallinity of the isothermally crystallized films. Generally, an increase in the crystalline domains decreases permeation because high crystallinity reduces the chain mobility and free volume that eventually hinders the attack of water molecules [40]. The water uptake of PLA–TEC–ChNC110 was lower compared to that of PLA110 and PLA–TEC110. This can be attributed to the smaller spherulite size of the ChNC and strong filler-matrix interfacial interaction that may have restricted the water molecules.

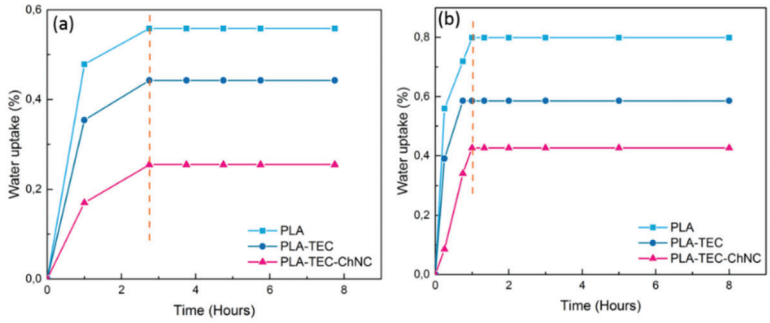

Figure 8. Water uptake as a function of time showing the effect of isothermal crystallization on PLA, PLA–TEC, and PLA–TEC–ChNC films (**a**) at room temperature and (**b**) at 58 °C.

The effect of crystallinity on diffusion kinetics of PLA was studied and the data was accumulated in the Table 5. Diffusion behavior is differentiated into three categories *viz.* Case I known as Fickian diffusion, Case II also called as Super Case II, and Case III which is Non-Fickian or anomalous diffusion [41]. The addition of TEC decreases the diffusion coefficient, however, the addition of ChNCs increase the diffusion coefficient. This differentiation is based on the diffusional exponent (n) value. If the value of n is 0.5, it will be Fickian diffusion. For Super Case II, $n > 1$ and for Non-Fickian n value varies as $1/2 < n < 1$.

Table 5. Kinetics of water uptake of the PLA110, PLA–TEC110, and PLA–TEC–ChNC110.

Materials	Diffusional Exponent (n)	Kinetic Constant (K)	Diffusion Coefficient (D) (m^2 s^{-1})
PLA110	0.248	0.909	1.62×10^{-6}
PLA–TEC110	0.315	1.095	1.09×10^{-6}
PLA–TEC–ChNC110	1.230	0.979	0.10×10^{-6}

Table 5 shows that the diffusion exponent for PLA110 and PLA–TEC110 is lower than 0.5, whereas it is greater than 1 for the nanocomposites. This implies that PLA110 and PLA–TEC110 follow the Fickian model, whereas the nanocomposites follow the Super Case II. Higher diffusion exponent (n) value in PLA–TEC–ChNC110 was obviously because of the presence of ChNCs in the nanocomposites. The addition of ChNCs decreases both the water uptake and diffusion coefficient as the spherulites of nanocomposites must have hindered the entry of the water molecules into the nanocomposite films. The mechanism of entry of water molecules into the nanocomposite film is illustrated in Figure 9. Chow et al. [41], studied the effect of organo-montmorillonite (OMMT) and nano-precipitated calcium carbonate (NPCC) on the water absorption of PLAs, and found that the n values for PLA, OMMT, and NPCC were in the range of 0.25–0.38 i.e., below 0.5, indicating that the Fickian diffusion model (i.e., Case I) was followed.

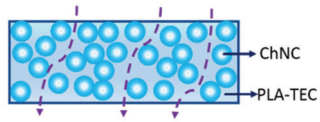

Figure 9. Schematics showing how water enters in PLA–TEC–ChNC110; spherulites developed in the nanocomposites are hindering the water molecules and forming a tortuous path.

4. Conclusions

In this study, neat PLA, plasticized PLA–TEC, and plasticized PLA nanocomposites with 1 wt % of ChNC (PLA–TEC–ChNC) were prepared with liquid-assisted extrusion. Compression molding was performed at varying temperatures and holding times to prepare films with different crystallinities. The effect of well dispersed and distributed ChNC on the crystallinity and properties of PLA nanocomposites was investigated.

Dispersion of ChNC into PLA-TEC was examined by SEM and it was observed that nanocomposites exhibited homogenous dispersion and distribution of ChNC. It is noticeable that PLA–TEC–ChNC110 exhibited very high crystallinity (48%) within 5 min of crystallization as confirmed by DSC which is ascribed due to the good dispersion of the ChNC. On the other hand, PLA110 and PLA–TEC110 required 40 min to achieve similar crystallinity of 45% and 49%, respectively.

Addition of properly dispersed ChNCs increased the nucleation ability which further affected the crystallite size of PLA as examined by XRD analysis. The crystallite size of nanocomposites was smaller (8 nm) than that of the neat PLA (12 nm) and PLA–TEC (14 nm). In addition, the spherulites sizes of the PLA110, PLA–TEC110, and PLA–TEC–ChNC110 were determined by POM as 49, 56, and 23 μm, respectively. The spherulites size affected the optical properties of the films; consequently, the light transmittance of PLA110, PLA–TEC110, and PLA–TEC–ChNC110 was determined to be 61%, 58% and 69%, respectively. Owing to smaller spherulites of PLA–TEC–ChNC110, light can pass through the films; therefore, the transmittance of nanocomposites is higher than PLA110 and PLA–TEC110.

It was found that ChNCs significantly reduced the water and oxygen barrier properties of PLA–TEC110. WVTR and OTR of PLA–TEC110 were, respectively, 36% and 32%, lower in comparison to PLA–TEC–ChNC110. The positive effect of ChNCs on the barrier properties is attributed to be due to the good dispersion, better nucleation ability and smaller spherulite size. Crystallinity caused a decrease in water diffusion. Increased crystallinity and ChNC strongly affected the hydrolytic degradation of the PLA.

This study provides a prominent enhancement in the properties of plasticized PLA when 1 wt % ChNCs are homogenously mixed in PLA–TEC. The knowledge gained from this study is expected to be helpful for the preparation of materials for packaging applications.

Supplementary Materials: The following are available online at http://www.mdpi.com/2073-4360/12/3/726/s1, Optical properties (Table S1) and effect of hydrolytic degradation on thermal properties (Figure S1).

Author Contributions: S.S., S.G. and K.O. designed the experiments and mainly contributed to writing. S.S. performed most of the experiments and analyzed the data. M.P. and D.S. contributed with preparation of the PLA and their chitin nanocomposites and wrote the materials section (preparation of ChNCs and PLA nanocomposites). M.Z. contributed with barrier testing (OP) and has written the barrier testing (OP) part. S.G., K.O. and M.L.M. contributed with paper reviewing. All authors have read and agreed to the published version of the manuscript.

Funding: Bio4Energy strategic research program and NewPack BBI Horizon 2020 EU project (Grant number: 792261).

Acknowledgments: Authors are grateful for the financial support from Bio4Energy and Horizon 2020 BBI project NewPack (Grant number: 792261). Authors are also thankful to the Kempe foundation for financial support for AFM. First author would like to thank Joint European Doctoral Programme in Advanced Material Science and Engineering European (DocMASE) for providing her Ph.D. scholarship.

Conflicts of Interest: The authors declare no conflict of interest.

References

1. Lim, L.T.; Auras, R.; Rubino, M. Processing technologies for poly(lactic acid). *Prog. Polym. Sci.* **2008**, *33*, 820–852. [CrossRef]
2. Cailloux, J.; Hakim, R.N.; Santana, O.O.; Bou, J.; Abt, T.; Carrasco, F.; Maspoch, M.L. Reactive extrusion: a useful process to manufacture structurally modified PLA/o-MMT composites. *Compos. Part A* **2016**, *88*, 106–115. [CrossRef]
3. Gamez-Perez, J.; Nascimento, L.; Bou, J.J.; Franco-Urquiza, E.; Santana, O.O.; Carrasco, F.; Maspoch, M.L. Influence of crystallinity on the fracture toughness of poly(lactic acid)/montmorillonite nanocomposites prepared by twin-screw extrusion. *J. Appl. Polym. Sci.* **2011**, *120*, 896–905. [CrossRef]
4. Marchessault, R.H.; Morehead, F.F.; Walter, N.M. Liquid crystal systems from fibrillar polysaccharides. *Nature* **1959**, *184*, 632–633. [CrossRef]
5. Ravi Kumar, M.N.V. a review of chitin and chitosan applications. *React. Funct. Polym.* **2000**, *46*, 1–27. [CrossRef]
6. Paillet, M.; Dufresne, A. Chitin whisker reinforced thermoplastic nanocomposites. *Macromolecules* **2001**, *34*, 6527–6530. [CrossRef]
7. Zeng, J.-B.; He, Y.-S.; Li, S.-L.; Wang, Y.-Z. Chitin whiskers: An overview. *Biomacromolecules* **2012**, *13*, 1–11. [CrossRef] [PubMed]
8. Wei, J.; Liu, J.; Qiang, J.; Yang, L.; Wan, Y.; Wang, H.; Gao, W.; Ko, F. Antibacterial performance of chitin nanowhisker reinforced Poly(lactic acid) composite nanofiber membrane. *Adv. Sci. Lett.* **2012**, *10*, 649–651. [CrossRef]
9. Salaberria, A.; Diaz, R.H.; Andrés, M.; Fernandes, S.; Labidi, J. The antifungal activity of functionalized chitin nanocrystals in poly (Lactid Acid) films. *Materials* **2017**, *10*, 546. [CrossRef]
10. Morin, A.; Dufresne, A. Nanocomposites of chitin whiskers from riftia tubes and poly(caprolactone). *Macromolecules* **2002**, *35*, 2190–2199. [CrossRef]
11. Lu, Y.; Weng, L.; Zhang, L. Morphology and properties of soy protein isolate thermoplastics reinforced with chitin whiskers. *Biomacromolecules* **2004**, *5*, 1046–1051. [CrossRef] [PubMed]
12. Uddin, A.J.; Fujie, M.; Sembo, S.; Gotoh, Y. Outstanding reinforcing effect of highly oriented chitin whiskers in PVA nanocomposites. *Carbohydr. Polym.* **2012**, *87*, 799–805. [CrossRef]
13. Wang, B.; Li, J.; Zhang, J.; Li, H.; Chen, P.; Gu, Q.; Wang, Z. Thermo-mechanical properties of the composite made of poly (3-hydroxybutyrate-co-3-hydroxyvalerate) and acetylated chitin nanocrystals. *Carbohydr. Polym.* **2013**, *95*, 100–106. [CrossRef] [PubMed]
14. Scaffaro, R.; Botta, L.; Lopresti, F.; Maio, A.; Sutera, F. Polysaccharide nanocrystals as fillers for PLA based nanocomposites. *Cellulose* **2017**, *24*, 447–478. [CrossRef]
15. Coltelli, M.B.; Cinelli, P.; Gigante, V.; Aliotta, L.; Morganti, P.; Panariello, L.; Lazzeri, A. Chitin nanofibrils in poly(Lactic acid) (PLA) nanocomposites: Dispersion and thermo-mechanical properties. *Int. J. Mol. Sci.* **2019**, *20*, 504. [CrossRef] [PubMed]
16. Nakagaito, A.; Kanzawa, S.; Takagi, H. Polylactic Acid Reinforced with Mixed Cellulose and Chitin Nanofibers—Effect of Mixture Ratio on the Mechanical Properties of Composites. *J. Compos. Sci.* **2018**, *2*, 36. [CrossRef]
17. Oksman, K.; Mathew, A.P.; Bondeson, D.; Kvien, I. Manufacturing process of cellulose whiskers/polylactic acid nanocomposites. *Compos. Sci. Technol.* **2006**, *66*, 2776–2784. [CrossRef]
18. Herrera, N.; Salaberria, A.M.; Mathew, A.P.; Oksman, K. Plasticized polylactic acid nanocomposite films with cellulose and chitin nanocrystals prepared using extrusion and compression molding with two cooling rates: Effects on mechanical, thermal and optical properties. *Compos. Part a Appl. Sci. Manuf.* **2016**, *83*, 89–97. [CrossRef]
19. Herrera, N.; Roch, H.; Salaberria, A.M.; Pino-Orellana, M.A.; Labidi, J.; Fernandes, S.C.M.; Radic, D.; Leiva, A.; Oksman, K. Functionalized blown films of plasticized polylactic acid/chitin nanocomposite: Preparation and characterization. *Mater. Des.* **2016**, *92*, 846–852. [CrossRef]
20. Singh, S.; Maspoch, M.L.; Oksman, K. Crystallization of triethyl-citrate-plasticized poly(lactic acid) induced by chitin nanocrystals. *J. Appl. Polym. Sci.* **2019**, *136*, 47936. [CrossRef]
21. Herrera, N.; Singh, A.A.; Salaberria, A.M.; Labidi, J.; Mathew, A.P.; Oksman, K. Triethyl citrate (TEC) as a dispersing aid in polylactic acid/chitin nanocomposites prepared via liquid-assisted extrusion. *Polymers* **2017**, *9*, 406. [CrossRef] [PubMed]

22. Nečas, D.; Klapetek, P. Gwyddion: An open-source software for SPM data analysis. *Cent. Eur. J. Phys.* **2012**, *10*, 181–188. [CrossRef]
23. Mathew, A.P.; Oksman, K.; Sain, M. The effect of morphology and chemical characteristics of cellulose reinforcements on the crystallinity of polylactic acid. *J. Appl. Polym. Sci.* **2006**, *101*, 300–310. [CrossRef]
24. Sullivan, E.M.; Moon, R.J.; Kalaitzidou, K. Processing and characterization of cellulose nanocrystals/polylactic acid nanocomposite films. *Materials* **2015**, *8*, 8106–8116. [CrossRef]
25. Somord, K.; Somord, K.; Suwantong, O.; Thanomsilp, C.; Peijs, T.; Soykeabkaew, N. Self-reinforced poly(lactic acid) nanocomposites with integrated bacterial cellulose and its surface modification. *Nanocomposites* **2018**, *4*, 102–111. [CrossRef]
26. Garlotta, D. a literature review of poly(lactic acid). *J. Polym. Environ.* **2001**, *9*, 63–84. [CrossRef]
27. Maiza, M.; Benaniba, M.T.; Massardier-Nageotte, V. Plasticizing effects of citrate esters on properties of poly(lactic acid). *J. Polym. Eng.* **2016**, *36*, 371–380. [CrossRef]
28. Fortunati, E.; Peltzer, M.; Armentano, I.; Torre, L.; Jiménez, A.; Kenny, J.M. Effects of modified cellulose nanocrystals on the barrier and migration properties of PLA nano-biocomposites. *Carbohydr. Polym.* **2012**, *90*, 948–956. [CrossRef]
29. Sanchez-Garcia, M.D.; Gimenez, E.; Lagaron, J.M. Morphology and barrier properties of solvent cast composites of thermoplastic biopolymers and purified cellulose fibers. *Carbohydr. Polym.* **2008**, *71*, 235–244. [CrossRef]
30. Martino, V.P.; Ruseckaite, R.A.; Jiménez, A.; Averous, L. Correlation between composition, structure and properties of poly(lactic acid)/polyadipate-based nano-biocomposites. *Macromol. Mater. Eng.* **2010**, *295*, 551–558. [CrossRef]
31. Trifol, J.; Plackett, D.; Sillard, C.; Hassager, O.; Daugaard, A.E.; Bras, J.; Szabo, P. a comparison of partially acetylated nanocellulose, nanocrystalline cellulose, and nanoclay as fillers for high-performance polylactide nanocomposites. *J. Appl. Polym. Sci.* **2016**, *133*, 43257. [CrossRef]
32. Martínez-Sanz, M.; Lopez-Rubio, A.; Lagaron, J.M. Optimization of the dispersion of unmodified bacterial cellulose nanowhiskers into polylactide via melt compounding to significantly enhance barrier and mechanical properties. *Biomacromolecules* **2012**, *13*, 3887–3899. [CrossRef] [PubMed]
33. Fukuzumi, H.; Saito, T.; Iwata, T.; Kumamoto, Y.; Isogai, A. Transparent and high gas barrier films of cellulose nanofibers prepared by TEMPO-mediated oxidation. *Biomacromolecules* **2009**, *10*, 162–165. [CrossRef] [PubMed]
34. Paul, M.A.; Delcourt, C.; Alexandre, M.; Degée, P.; Monteverde, F.; Dubois, P. Polylactide/montmorillonite nanocomposites: Study of the hydrolytic degradation. *Polym. Degrad. Stab.* **2005**, *87*, 535–542. [CrossRef]
35. De Jong, S.J.; Arias, E.R.; Rijkers, D.T.S.; Van Nostrum, C.F.; Kettenes-Van Den Bosch, J.J.; Hennink, W.E. New insights into the hydrolytic degradation of poly(lactic acid): Participation of the alcohol terminus. *Polymer* **2001**, *42*, 2795–2802. [CrossRef]
36. Maharana, T.; Mohanty, B.; Negi, Y.S. Melt-solid polycondensation of lactic acid and its biodegradability. *Prog. Polym. Sci.* **2009**, *34*, 99–124. [CrossRef]
37. Schliecker, G.; Schmidt, C.; Fuchs, S.; Kissel, T. Characterization of a homologous series of D,L-lactic acid oligomers; a mechanistic study on the degradation kinetics in vitro. *Biomaterials* **2003**, *24*, 3835–3844. [CrossRef]
38. Proikakis, C.S.; Mamouzelos, N.J.; Tarantili, P.A.; Andreopoulos, A.G. Swelling and hydrolytic degradation of poly(d,l-lactic acid) in aqueous solutions. *Polym. Degrad. Stab.* **2006**, *91*, 614–619. [CrossRef]
39. Elsawy, M.A.; Kim, K.H.; Park, J.W.; Deep, A. Hydrolytic degradation of polylactic acid (PLA) and its composites. *Renew. Sustain. Energy Rev.* **2017**, *79*, 1346–1352. [CrossRef]
40. Zhou, Q.; Xanthos, M. Nanoclay and crystallinity effects on the hydrolytic degradation of polylactides. *Polym. Degrad. Stab.* **2008**, *93*, 1450–1459. [CrossRef]
41. Chow, W.S.; Leu, Y.Y.; Mohd Ishak, Z.A. Water Absorption of Poly(lactic acid) Nanocomposites: Effects of Nanofillers and Maleated Rubbers. *Polym. Plast. Technol. Eng.* **2014**, *53*, 858–863. [CrossRef]

polymers

MDPI

Supplementary Materials:

Effect of chitin nanocrystals on crystallization and properties of poly(lactic acid)-based nanocomposites

Shikha Singh[1, 2], Mitul Patel[1], Daniel Schwendemann[1], Marta Zaccone[3], Shiyu Geng[1], Maria Lluisa Maspoch[2], and Kristiina Oksman[1, 4*]

[1] Division of Materials Science, Luleå University of Technology, SE-97 187 Luleå, Sweden
[2] Centre Català del Plàstic (CCP), Universitat Politècnica de Catalunya Barcelona Tech (EEBE-UPC), C/Colom, 114, Terrassa 08222, Spain
[3]Proplast, Via Roberto di Ferro 86, 15122 Alessandria (AL), Italy
[4]Mechanical & Industrial Engineering, University of Toronto, Toronto, M5S 3BS, Canada
*Correspondence: Kristiina.oksman@ltu.se; Tel: +46-920-493-371

Table S1. Optical properties of neat and isothermally crystallized PLA, PLA–TEC, and PLA–TEC–ChNC films at different temperatures and time periods

Materials	Transmittance (%)
PLA	92 (±0.25)
PLA-TEC	91 (±0.23)
PLA-TEC-ChNC	90 (±0.24)
PLA135-5	92 (±0.29)
PLA-TEC135-5	92 (±0.28)
PLA-TEC-ChNC135-5	90 (±0.29)
PLA135-15	91 (±0.26)
PLA-TEC135-15	91 (±0.47)
PLA-TEC-ChNC135-15	86 (±0.21)
PLA130-5	92 (±0.21)
PLA-TEC130-5	91 (±0.21)
PLA-TEC-ChNC130-5	89 (±0.29)
PLA130-15	93 (±0.61)
PLA-TEC130-15	92 (±0.58)
PLA-TEC-ChNC130-15	65 (±0.57)
PLA125-5	93 (±0.12)
PLA-TEC125-5	91 (±0.16)
PLA-TEC-ChNC125-5	85 (±0.18)
PLA125-15	91 (±0.20)
PLA-TEC125-15	90 (±0.46)
PLA-TEC-ChNC125-15	64 (±0.32)
PLA110	61 (±0.32)
PLA-TEC110	58 (±0.45)
PLA-TEC-ChNC110	69 (±0.44)

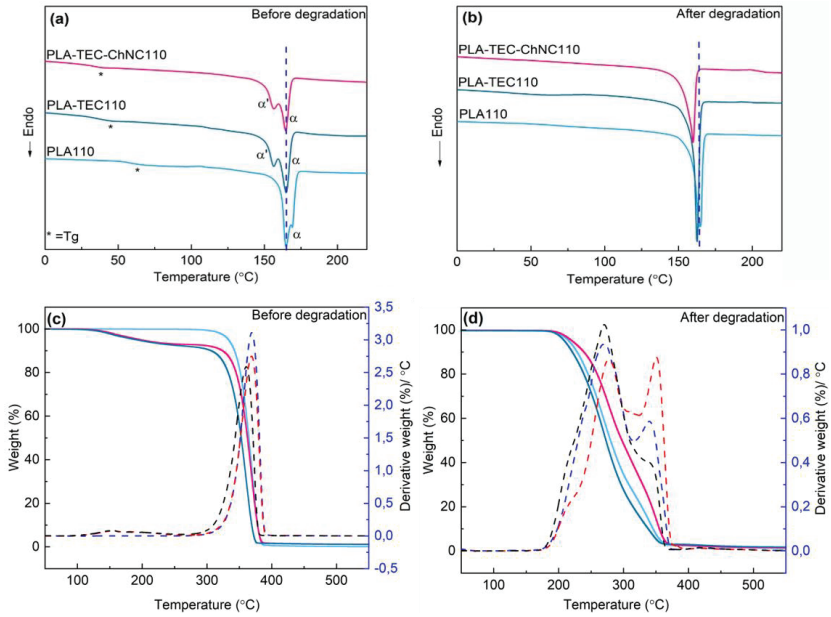

Figure S1. DSC thermograms of isothermally crystallized PLA110, PLA–TEC110, and PLA–TEC–ChNC110 films (a) before and (b) after hydrolytic degradation taken from first heating scans. TGA and DTG curves (dotted lines) of isothermally crystallized films (c) before and (d) after hydrolytic degradation

PAPER III

Effect of orientation on PLA/chitin nanocomposite films with a combination of melt and solid-state drawing

Shikha Singh, Mitul Patel, Daniel Schwendemann, Shiyu Geng, Natalia Herrera, Maria Lluïsa Maspoch, Kristiina Oksman

(Manuscript to be submitted in polymers)

Effects of orientation on PLA/chitin nanocomposite films achieved via combination of melt and solid-state drawing

Shikha Singh [1,2], Mitul Patel [1], Daniel Schwendemann [1,3], Shiyu Geng [1], Natalia Herrera [1], Maria Lluisa Maspoch [2], and Kristiina Oksman [1,4,*]

[1] Division of Materials Science, Luleå University of Technology, SE-97 187 Luleå, Sweden; shikha.singh@ltu.se (S.S.); mitul.patel@ltu.se (M.P.); daniel.schwendemann@hsr.ch (D.S.); shiyu.geng@ltu.se (S.G.)
[2] Centre Català del Plàstic (CCP)-Universitat Politècnica de Catalunya Barcelona Tech (EEBE-UPC)-ePLASCOM. Avda. Eduard Maristany, 14, 08019 Barcelona, Spain
Spain; maria.lluisa.maspoch@upc.edu
[3] IWK Institut für Werkstofftechnik und Kunststoffverarbeitung, CH-8640 Rapperswil, Switzerland
[4] Mechanical & Industrial Engineering, University of Toronto, Toronto, M5S 3BS, Canada
* Correspondence: Kristiina.oksman@ltu.se; Tel: +46 920 493371

Abstract: The orientation of polymers plays an important role in many applications including packaging, biomedical, and electronics. However, the orientation behaviors of polymer-based nanocomposites have not been extensively investigated yet. The objective of this study was to evaluate the effects of orientation on the structure and properties of chitin nanocrystal (ChNC) poly (lactic acid) (PLA) nanocomposites prepared via liquid assisted extrusion. Two different methods were employed to obtain the orientation of PLA nanocomposite films, *viz.* (1) melt-state drawing and (2) solid-state drawing. The results showed that the orientation achieved by a two-step process has increased the overall mechanical properties of the nanocomposites especially the strength and toughness. For example, the strength improved from 37 MPa to 170 MPa and the toughness increased from 1 to 96 MJ/m^3 compared to undrawn samples. Further, the degree of crystallinity of oriented films increased from 8 to 53%. Polarized optical microscopy results exhibited strain-induced birefringence behavior due to the orientation of the molecular chains. Moreover, orientation resulted in reduced crystallite size. Mechanism revealed that some tie molecules developed during orientation led to high strength and toughness. This study demonstrates that the orientation achieved by two-step process has potential for packaging applications.

Keywords: poly(lactic acid); chitin nanocrystals; nanocomposite; oriented structure; film calendaring; solid-state drawing; mechanical properties; crystallinity

1. Introduction

There is a growing interest to develop bio-based materials for sustainable development worldwide, to mitigate the waste disposal problems created by petroleum-based polymeric materials. In this context, poly(lactic acid) (PLA), which is derived from natural resources such as corn, sugar, is gaining much attention due to its potential properties that are comparable to some of the petroleum-based polymers (e.g., poly(styrene) and poly(ethylene terephthalate) used for the packaging applications[1]. PLA is superior compared to many petroleum-based polymers due to its bio-compostability (decomposes to H_2O, CO_2, and organic materials), low energy consumption, and lower CO_2 emission. Easy production of PLA at a large scale with reasonable price has expanded its applications in many areas such as packaging, medical, electronic, fiber materials etc.[2]. However, PLA has some limitations, for instance, inherent brittleness, poor elongation at break (2-5%), and very low toughness (1 MJ/m^3) make it difficult to practically use in the packaging industry[3]. The reasons for the brittle nature of the PLA is (1) glass transition temperature T_g (around 55°C), which makes polymer chain rigid and inflexible and (2) low nucleation ability, therefore it has slow crystallization rates, which led to the formation of large spherulites size[4]. To overcome the brittle nature of the

PLA, researchers have used plasticizers[5], copolymers[6], and nucleating agents[7]. However, it is challenging to fine-tune both the tensile strength and toughness at the same time. For example, by adding plasticizers into the PLA matrix, elongation at break increases but the strength and stiffness compromise[8].

The orientation of the polymer can significantly improve its tensile strength and toughness[9]. This orientation can be achieved by two methods: 1) melt drawing [9] and/or 2) solid-state drawing [10]. The orientation is affected by processing factors *viz*. draw speed, draw temperature, and draw ratio. Several investigations on orientation effects produced by drawing on the final PLA properties have been published [11][12][13][14][15]. For example, Mai et al.[10], made oriented PLA tapes, and showed that the orientation leads to significant improvement in the elongation at break (3 times) and toughness (13 times) of the PLA as compared to reference PLA. Velazquez-Infante et al.[16], investigated the effect of the unidirectional drawing on the thermal and mechanical properties of PLA films. Orientation increased the tensile strength, from 58.4 to 71.3 MPa, respectively when drawn at 22°C with a speed of 100 mm/min and draw ratio 4. Gao et al.[17] confirmed that the strain-induced orientation of PLA increased the yield strength from 45.3 to 135.5 MPa, and the elongation at break 17 to 295%, respectively. They concluded that the mechanical properties of the PLA film could be controlled by precisely controlling the structures that developed during the orientation.

In previous studies from our research group, the uniaxial orientation of PLA nanocomposites with nanocellulose was performed using solid-state drawing[18,19]. Singh et al.[18] studied the effect of drawing conditions including draw temperature, draw speed, and draw ratio of the PLA nanocomposites with 1 wt% cellulose nanofibers (CNFs) and 10 wt.% plasticizer. The effect of the orientation on the thermal, mechanical and microstructures were investigated. Noticeably, the mechanical properties of the drawn samples were improved; especially the toughness increased 60 times as compared to the undrawn samples. This improvement in the mechanical properties of the nanocomposites was due to the synergistic effect of the nano-reinforcement and polymer orientation achieved by solid-state drawing. Additionally, orientation also improved the thermal properties such as glass transition temperature and degree of crystallinity of the oriented samples. Geng et al.[19] reported that the orientation of PLA nanocomposite reinforced with only 0.1 wt.% cellulose nanofibers, showed superior mechanical properties; the tensile strength increased from 64 to 343 MPa and the toughness from 2 to 83 MJ/m^3 at a draw ratio of 8, as compared to the un-oriented PLA nanocomposites[19].

In another study by Singh et al.[20] PLA nanocomposites with 1 wt.% and 5 wt.% chitin nanocrystals (ChNC) were oriented and it was observed that the most drawn sample (DR3) with 5 wt.% ChNC improved the mechanical properties particularly, ultimate tensile strength and Young's modulus of the PLA/ChNC nanocomposites. Ultimate tensile strength increased from 56 MPa to 71 MPa and Young's modulus increased from 0.76 GPa to 1.72 GPa, respectively, as compared to the plasticized PLA. However, the percentage elongation at break and toughness reached to 60% and 43 $MJ/m^{3,}$ respectively.

Inspired from previous research work on the orientation of the PLA-based nanocomposites with solid-state drawing (SSD) we decided to further study the effect of the orientation process. In this study, a melt-state drawing (MSD) was also applied with SSD to pre-orient the nanocomposites. The objective of this study was to achieve highly oriented PLA-GTA-ChNC nanocomposite films by combining MSD using film calendaring followed by SSD in uniaxial testing equipment with the temperature-controlled chamber. The hypothesis is that a pre-orientation achieved by MSD may allow a higher degree of orientation in the SSD. The oriented nanocomposite films were compared to the undrawn compression molded composite films. The effect of the orientation induced by the presence of ChNC and increased degree of orientation on properties and structure of the nanocomposites were studied.

2. Materials and Methods

2.1 Materials

PLA pellets were kindly provided by FUTERRO (Escanaffles, Belgium), used as a polymer matrix, had an MFI of 8 g/10 min (measured at 190°C and 2.16 kg). Glycerol triacetate (GTA) was supplied by Sigma-Aldrich (Stockholm, Sweden), used as a plasticizer for the PLA matrix. Antarctic Seafood S.A. (Coquimbo, Chile) supplied chitin powder from yellow squat lobster (*Cervimunida johni*) waste. Acid hydrolysis was done to isolate chitin nanocrystals (ChNCs) from chitin powder, which was used as a reinforcing agent. Solvents used for this acid hydrolysis including hydrochloric acid (HCl) (ACS reagent 37%), sodium hydroxide (NaOH), and sodium hypochlorite (NaClO) were purchased from Merck (Chile, SA). Ethanol (99.5%) was purchased from Solveco (Stockholm, Sweden).

2.2 Methods

PLA/ChNC nanocomposites with GTA plasticizer were prepared using liquid-assisted extrusion as explained in an earlier study[21]. An attempt was taken to prepare nanocomposites with a higher concentration of ChNCs (5 wt.%). The compositions of the polymer, plasticizer, and nanomaterial were in the following order: 80 wt.%: 20 wt.%: 5 wt.%. Briefly, the nanocomposites were extruded using a co-rotating twin-screw extruder (ZSK-18 Coperion W&P, Stuttgart, Germany) with a length to diameter screw ratio (L/D) of 40 and the screw diameter of 18 mm. The temperature profile was range from 170 to 190°C from feeding to die zone and materials were processed at a screw speed of 250 rpm with a throughput of 1.5 kg/h. A vacuum venting was equipped with the extruder to remove the moisture from the materials during the processing.

To achieve oriented nanocomposites films two types of pretreatments performed *viz.*, (1) compressions molding and (2) film calendaring using a single screw extruder. Both compression molded and calendared films were further oriented using SSD to reach a higher draw ratio. The goal was to gain an understanding of how pre-oriented films achieved by film calendaring could affect the orientation and resulting nanocomposite properties. Schematics of the pre-orientation process (MSD) and SSD of the PLA-GTA-ChNC nanocomposites are shown in Figure 1.

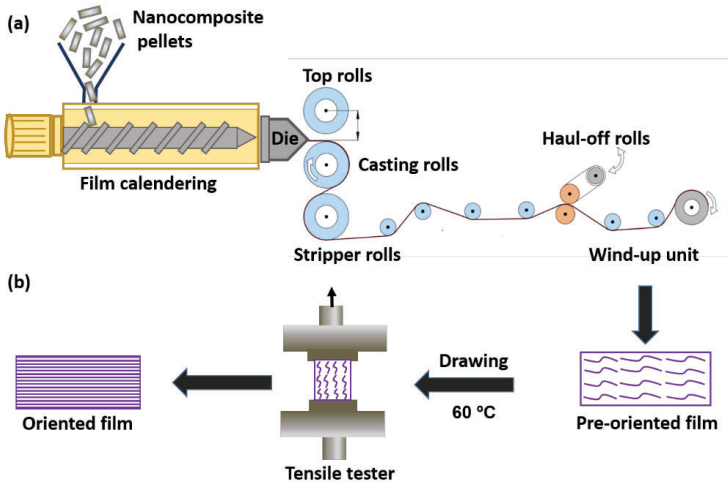

Figure 1. Schematic representation of (a) melt-state drawing and (b) solid-state drawing of PLA nanocomposite films carried out on film calendaring and uniaxial tensile testing machine in a temperature chamber respectively

To prepare un-oriented nanocomposite films, extruded pellets of PLA-GTA-ChNC nanocomposites were compression-molded; LPC-300 Fontijne Grotnes press (Vlaardingen, Netherlands). Approximately 5 g material was placed between two metallic sheets. Materials were heated to 190°C, where it kept for 2 min using contact mode and then compression molded for

another 1 min under a pressure of 10 MPa. Finally, rapidly cooled to room temperature using the water cooling system to make undrawn nanocomposite film.

Pre-orientated PLA-GTA-ChNC nanocomposites prepared by a single screw extruder with an L/D screw ratio of 30:1 (Lab Tech Engineering Company Ltd., Samutprakan, Thailand). Photographs of the different steps of the MSD process is illustrated in the Figure 2. Molten polymer extruded through a 100 mm slit die at a screw speed of 65 rpm. The process settings for film calendaring of the nanocomposite films are shown in Table 1. The extruded films were quenched on a casting roll, accompanied by post drawing on heated rollers at 60°C (Lab Tech Engineering Company Ltd., Thailand, type LUMCR -50) to produce the oriented films. The nanocomposite film was drawn by applying the tension between stripper roll and haul-off rolls by increasing the speed of the windup unit. The draw ratio (DR) is defined as the ratio of increased film length to the original film length produced in a specified period.

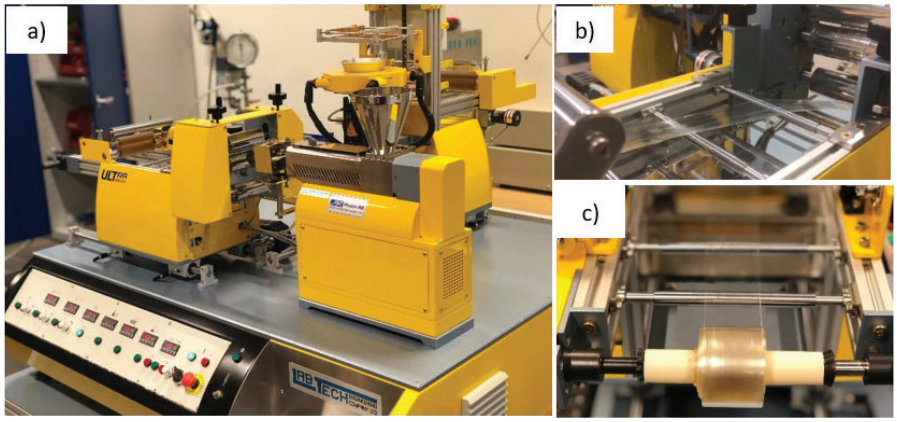

Figure 2. Melt-state drawing process (a) film calendaring set-up (b) pressing, stretching and calendaring (c) film winding process

Table 1. Processing parameters used for the film calendaring to produce pre-oriented nanocomposite films

Materials	Extruder (°C)	Die (°C)	Stack rolls (°C)	Draw ratio (DR)
FC*	190	200	60	--
FC-2**	190	200	60	2

*FC means film calendering and **FC-2 means film calendered samples drawn at DR 2

Nanocomposite films produced by compression molding and film calendaring were further, uniaxially drawn to achieve high orientation. Schematic of the processes shown in Figure 1b. SSD was done in a Shimadzu Autograph AG-X (Kyoto, Japan) universal testing machine equipped with a temperature chamber using a load cell of 5 kN. Research articles on the orientation of PLA films revealed that to get good orientation, it is important that polymer must be drawn between its glass transition and melting temperature[22]. Therefore, in this work, the orientation of both un-oriented and pre-oriented nanocomposite films was carried out at 60°C and with a speed of 100 mm/min, respectively to reach a draw ratio (DR) of 5. A gauge length of 10 mm and a sample size of 40 × 6 × 0.1 mm^3 was used for the SSD. Before the drawing, the samples were marked to be able to calculate the draw ratio (DR) using the equation (1).

$$Draw\ ratio\ (DR) = \frac{Final\ length\ of\ the\ ink\ mark\ (l)}{Original\ lenght\ of\ the\ ink\ mark\ (lo)} \qquad \text{(eq 1)}$$

For CM and FC nanocomposite films, a maximum DR of 4 was reached. However, the solid-state drawing of the pre-oriented nanocomposites (i.e. FC-2) a slightly higher DR 5 was achieved. Finally, depending on the process used for the orientation and draw ratio gained, samples were coded, and data are accumulated in Table 2. Nanocomposites that processed with compression molding and film calendaring named as CM and FC, respectively.

Table 2. Coding of the nanocomposites based on the techniques used for the orientation and draw ratio (DR) obtained

Codes	Process involved for orientation	DR	Samples
CM	Compression molding	N/A	Undrawn sample
FC	Film calendaring	N/A	----
FC-2	Film calendaring	2	Pre-drawn sample
CM-SSD-4	Compression molding / solid state drawing	4	Drawn sample
FC-SSD-4	Melt state drawing /solid state drawing	4	Drawn sample
FC-2-SSD-5	melt state drawing/solid state drawing	5	Drawn sample

2.3 Characterization

The effect of orientation on the thermal stability of the undrawn (CM) and partially drawn samples (FC, FC/DR2) was investigated using a thermo-gravimetric analysis TGA-Q500 (New Castle, DE, USA). The isothermal test was carried out to quantify the amount of plasticizer lost during this process in an air atmosphere. First, nanocomposites were heated from 0 to 150°C, then hold at this temperature for 2 hr and then continue to 900°C at a rate of 10°C/min.

Differential scanning calorimetry (DSC) was used to investigate how the orientation of the nanocomposites affected the thermal properties. The films were subjected to Mettler Toledo DSC 822e (Schwerzenbach, Switzerland) analysis in the temperature range -20 to 200°C at a heating rate of 10 °C/min. The glass transition temperature (T_g), melt temperature (T_m), cold crystallization temperature (T_{cc}), and heat of melting (H_m) were determined before and after orientation. The degree of crystallinity (%) corresponding to each curve was calculated using equation (2) [23]:

$$Crystallinity(\%) = \frac{\Delta H_m - \Delta H_c}{\Delta H_m^0} \times \frac{100}{w} \qquad \text{(eq 2)}$$

where, ΔH_m and ΔH_{cc} is the melting and cold crystallization enthalpy, respectively. ΔHm^0 is the melting enthalpy for 100% crystalline PLA (93 J/g) [23,24] and w, is the weight fraction of the PLA in samples.

Mechanical properties of undrawn and drawn nanocomposite films were tested using Shimadzu AG-X universal tensile tester (Kyoto, Japan) with a 5 kN load cell, the distance between the grips was 20 mm and crosshead speed of 2 mm/min was used. Tensile strength, elongation at break, tensile modulus, and toughness of the materials were determined from the data and the toughness (work of fracture) was calculated as the area under the stress-strain curves. The results are the average of the 7 samples tested for each material.

Nikon Eclipse LV100NPOL (Kanagawa, Japan) polarized optical microscope (POM) was used to analyze the effect of orientation on the microstructure of the nanocomposites and observe the birefringence behavior. The nanocomposites films tested under cross-polarized conditions and polarized optical micrographs of the sample recorded using a charge-coupled device (CCD) camera.

Percentage transmittance of the un-oriented, pre-oriented, and oriented nanocomposites investigated by a UV-Vis spectrophotometer (GENESYS, 10UV, Thermo-Scientific, Dreieich, Germany) at a constant wavelength of 220 nm and total three specimens of each samples tested to calculate the average values.

The surface morphology was investigated by JEOL-IT 300 (Tokyo, Japan). Tensile fractured and etched surface of undrawn and drawn nanocomposite films were tested. Etching of the samples done by sodium hydroxide and water (1:2 by volume) for 12 hours. The surface of both fractured and etched samples coated (Leica EM ACE 220, Wetzlar, Germany) with platinum to avoid the charging effect.

The crystal structure of the undrawn and drawn nanocomposite films examined by a PANalytical Empyrean X-ray diffractometer (Almo, Malvern, UK) with CuKα radiation in a 2θ angular range of 5-40°. Scherrer equation employed to calculate the crystallite size as given below:

$$Crystallite\ \ size\ \ = \frac{k\lambda}{\beta Cos\ \ (\theta)} \qquad \text{(eq 3)}$$

where λ is the wavelength of CuKα radiation (1.5418 A°), β is the full-width at half-maximum (FWHM) value of peaks, θ is the Bragg angle, and K is the dimensional shape factor (0.9)[25].

The Fourier-transform infrared spectroscopy (FT-IR) was used to study if the orientation has any effect on the molecular interaction between the different components in the nanocomposites (PLA, GTA, and ChNC) VERTEX 80 (Ettlingen, Germany) was used. The scanning was performed in a spectral range of 400–4000 cm^{-1} with a resolution of 128 cm^{-1}.

3. Results and discussions

3.1 Effect of orientation on visual appearance

The dispersion of ChNC in the PLA matrix is crucial because it affects the final properties of the materials. In this study, well-dispersed PLA-GTA-ChNC nanocomposites pellets were prepared by a liquid assisted extrusion. The photographs of the undrawn, film calendared and solid-state drawn nanocomposite films are shown in Figure 3. The drawing has influenced the overall percentage transparency of the materials. It can be seen from the visual images of the sample (see Figure 3a-c) that before applying to the solid-state drawing, all the samples looked transparent and after the solid-state drawing, samples turned into opaque (see Figure 3a′-c′).

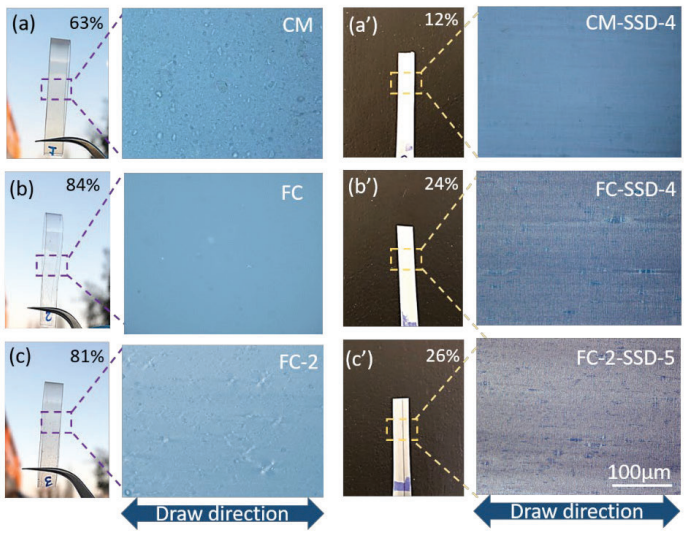

Figure 3. Visual appearance, optical micrographs and percentage transmittance of the nanocomposite films

Further, samples were observed under the optical microscopy and it was seen that the undrawn sample (CM) exhibited some aggregates that led to relatively lower percentage transmittance

compared to the per-drawn samples (FC and FC-2). After SSD of the undrawn and pre-drawn samples, the percentage transmittance was further reduced. This reduction in the transparency of the samples is due to the spherulites developed during the further stretching of the materials, which prohibited the lights to pass through the samples.

3.2 Effect of orientation on thermal properties

The TGA was carried out to evaluate if the pre-orientation process of the nanocomposites has affected the plasticizer content present in the nanocomposites. Noticeably, processing techniques including compression molding and film calendaring had no significant effect on the plasticizer and only 7% of GTA was lost in both the processing (Table S1).

The DSC was performed to find out the effect of orientation on glass transition temperature (T*g*), cold crystallization temperature (T*cc*), melting temperature (T*m*), and crystallinity. Thermal properties of the nanocomposites corresponding to the first heating scans of the samples are shown in Table 3 and their DSC thermograms provided in Figure S1. The orientation of the nanocomposites has increased the overall degree of crystallinity of the materials. Thermal behavior showed that on increasing the DR, the T*g* and T*cc* of the materials were decreased. It has already been reported in the literature that plasticizer reduces the T*g* by facilitating the flexibility of the molecular chains of polymers[26,27]. Further, reduction in the *Tcc* attributed to the synergistic effect of the plasticizer, ChNC as well as the strain-induced crystallization. It is well known that both crystallization and orientation of the molecular chains will shift the T*cc* towards lower temperatures. In this study, the T*cc* of undrawn sample (CM) was 100°C, while the T*cc* of FC-2-SSD-5 shifted to 63°C. No significant change in T*m* of the nanocomposites was seen. As seen from Table 3, the undrawn CM was almost amorphous (only 8% crystallinity) compared to the CM-SSD-4, where crystallinity increased up to 46%. Furthermore, the pre-oriented film when subjected to SSD, the degree of crystallinity further increased and reached to 51% for the FC-SSD-4 nanocomposites. This further increase in the crystallinity of the FC-SSD-4 is due to the ordering of the molecular chains of the PLA resulted from strain-induced crystallization. On increasing the DR to five, the degree of crystallinity further increased and reached a maximum value of 53% in FC-2-SSD-5. In our recent study, we achieved a maximum crystallinity of 50% in triethyl citrate-plasticized PLA/ChNC nanocomposites after isothermal crystallization[29], which also supports these results of the highest degree of crystallinity.

Table 3. Thermal properties determined from the first heating scans of different nanocomposite films

Materials	T*g* (°C)	T*cc* (°C)	T*m* (°C)	Crystallinity (%)
CM	55	100	169	8
FC	54	94	170	13
FC-2	48	67	171	35
CM-SSD-4	---	65	170	46
FC-SSD-4	---	66	173	51
FC-2-SSD-5	---	63	171	53

3.3 Effect of orientation on mechanical properties

The effect of orientation on the mechanical properties of the nanocomposite films was investigated and the results are shown in Table 4. As expected, the orientation dramatically increased the mechanical properties of the oriented films after a two-step orientation. Consequently, highly drawn (FC-2-SSD-5) nanocomposites (i.e. drawn at DR5) showed the highest tensile modulus, strength, and elongation at break and toughness, these increased with 74%, 360%, and 2400%, 9500%, respectively as compared to the undrawn (CM) nanocomposites.

The pre-orientation of the nanocomposites affected the mechanical properties of the nanocomposites even if drawn at the same drawn ratio (DR4). Consequently, the tensile modulus, tensile strength, elongation at break of FC-SSD-4 was increased and were 50%, 4%, 63%, and 66% respectively, with respect to the CM-SSD-4. This increment in the tensile strength is due to the higher

crystallinity and orientation obtained with MSD. Further, improvement in the elongation at break contributed to the toughness of the aligned PLA nanocomposites. The pre-orientation has further significantly improved the drawing ability and hence the mechanical properties of the FC-2-SSD-5, where higher tensile strength and toughness obtained as compared to FC-SSD-4. However, tensile modulus and percentage elongation at break remain the same. This could be because of the crystallinity. As already mentioned in the DSC results that there is no significant difference in the degree of crystallinity of FC-SSD-4 and FC-2-SSD-5 observed (51% for FC-SSD-4 and 53% for FC-2-SSD-5). Moreover, the elastic modulus in general controlled by the alignment of the polymeric chains.

Table 4. Mechanical properties of the different nanocomposite films

Materials	Tensile modulus (GPa)	Tensile strength (MPa)	Elongation at break (%)	Toughness (MJ/m^3)
CM	2.3^{a} (±0.1)	36.8^{a} (±2.5)	3^{a} (±1)	0.6^{a} (±0.1)
FC	2.5^{c} (±0.2)	41.1^{c} (±2.3)	24^{c} (±6)	9.0^{c} (±1.2)
FC-2	2.9^{d} (±0.2)	57.7^{d} (±2.5)	143^{d} (±5)	59.3^{d} (±2.1)
CM-SSD-4	2.6^{b} (±0.1)	134.8^{b} (±3.0)	46^{b} (±2)	47.0^{b} (±2.7)
FC-SSD-4	3.9^{e} (±0.2)	139.8^{e} (±6.7)	75^{e} (±9)	78.0^{e} (±8.9)
FC-2 SSD-5	4.0^{f} (±0.2)	169.9^{f} (±10.3)	75^{f} (±9)	95.8^{f} (±12.0)

It was observed from the ANOVA test that F > Fcrit. Hence, the null hypothesis is rejected which means there is a difference between the samples. Different superscript in each column represent a significant difference in the materials.

3.4 Effect of orientation on fractured surface

As shown in the earlier sections, orientation influenced the mechanical properties of the nanocomposites. In order to gain better insight into the effect of orientation on the mechanical properties, fractured tensile samples of undrawn (CM) and highly drawn (FC-2-SSD-5) were examined. Representative stress-strain curves of CM, FC-2-SSD-5 and their visual images of tensile fracture are shown in Figure 4. As it can observe from the curves (Figure 4a, b) that CM showed a brittle fracture, contrary FC-2-SSD-5 exhibited a ductile fracture.

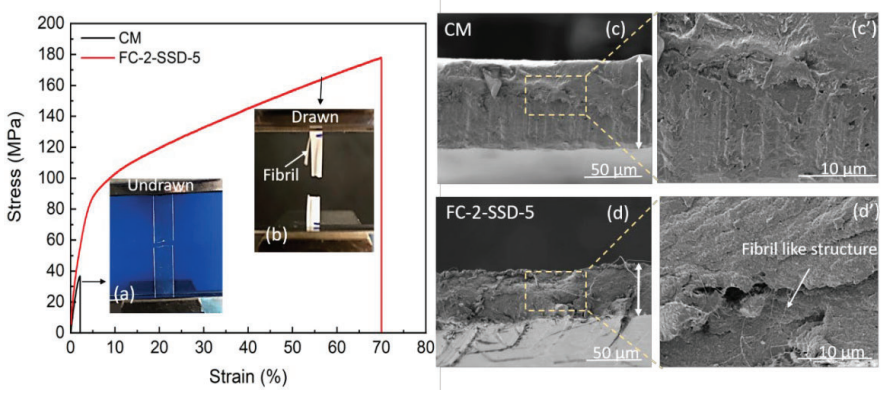

Figure 4. Representative stress-strain curves, visual appearance of tensile fracture samples of (a) CM exhibited brittle behavior and (b) FC-2-SSD-5 showing the ductile behavior and scanning electron micrographs of fractured surface of CM (c-c') and FC-2-SSD-5 (d-d')

A visual inspection of tensile fractured samples of CM revealed no crazes on the surface and the sample looked transparent (see Figure 4a) while the surface of the drawn sample turned white (see Figure 4b) due to the stress. The appearance of this stress whitening in the tensile samples of the FC-2-SSD-5 samples evident the crazing effect that resulted in the enhanced elongation at break and

toughness for these samples. Further, visual images of the undrawn sample after tensile test, fractured into two parts whereas, in undrawn samples, some fibril like structures developed as shown in Figure 4b. SEM micrographs of the tensile fractured samples of undrawn and drawn nanocomposites are shown in Figure 4c-d and high magnification images are shown in Figure 4c'-d'. It can be seen from the SEM images that drawn nanocomposite films showed narrower cross-section as compared to the undrawn film as shown by white arrows. This reduction in cross-section is because of the high orientation of the molecular chains in drawn samples. No significant difference in the SEM micrographs of the fractured samples was observed.

To better understand and visualize how different processing and draw ratio has induced the orientation in the nanocomposites; POM used and compared micrographs shown in Figure 5. Generally drawing of the PLA chains results in strain-induced birefringence. The color produced during the drawing depends on the degree of the orientation of the molecular chains of the polymers[35]. In this study, undrawn samples showed either no color or single color. Nanocomposite (CM-SSD-4) after drawing at DR4, exhibited grey shade. This was due to the strain hardening effect, resulted in bigger spherulites developed during the stretching that prohibits the lights to pass through the samples (also seen in the visual images in Figure 2a'). However, film calendered samples even at the same DR of 4, demonstrated very bright colors, induced by the synergistic effect of the ChNC and PLA orientation achieved by both film calendaring combined with SSD. Additionally, drawn samples (FC-2-SSD-5) exhibited a very homogenous orientation that attributed to the better dispersion and distribution of the ChNC into the GTA-plasticized matrix as compared to the undrawn samples.

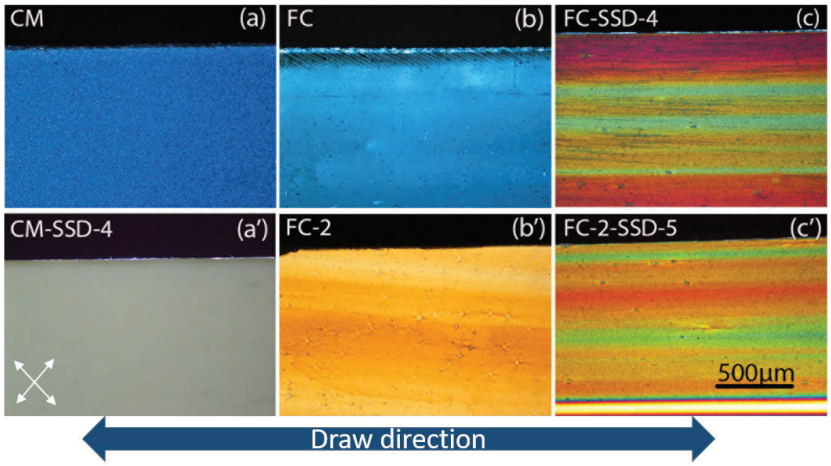

Figure 5. POM micrographs of the nanocomposite films; undrawn samples and its drawn (a, a'), partially drawn with film calendaring and its drawn (b, b') and finally drawn with SSD (c, c'). The oriented films show brightest and multicolor in FC-2-SSD-5 due to the orientation of the molecular chains of the PLA. Arrows at the left corner of the image indicate the directions of the crossed polarizers

Furthermore, to investigate the effects of two-step orientation on the surface morphology of the undrawn and highly drawn samples were evaluated using POM and SEM. Figure 6 illustrates the surface morphology of the un-etched and etched samples. The etching is commonly performed to remove the amorphous part of the PLA to examine the structures[36]. Figure 6 shows that after etching, undrawn samples showed that the surface of these samples randomly etched out whereas drawn samples exhibited aligned morphology that indicates the alignment. Figure 6d and 6d' illustrates that some cross- patterned developed in the drawn samples perpendicular to the direction

of the orientation after etching. It is worth mentioning that the development of this cross-patterned structure in the drawn nanocomposites results inthe popularly known shish kebab morphology [37].This Shish- kebab morphology formed due to the folding of the polymer chains[37].

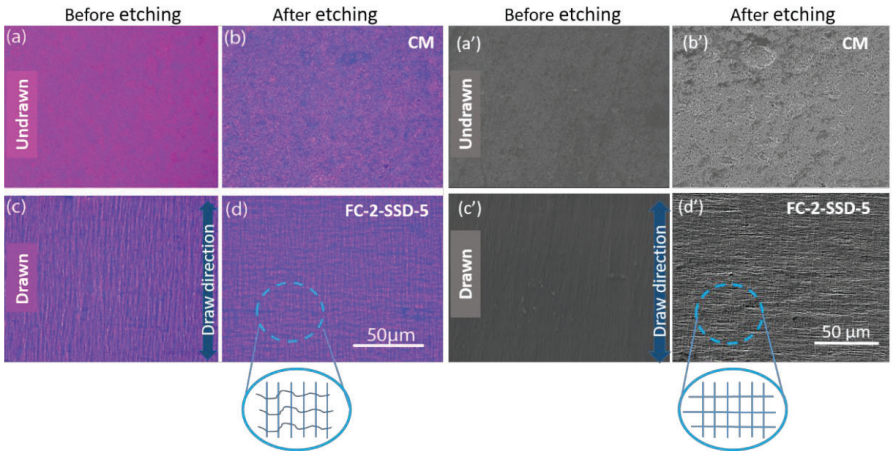

Figure 6. POM and SEM micrographs of the undrawn (CM) and drawn (FC-2-SSD-5) nanocomposite films (a-b) before and (c-d) after drawing. Highly drawn samples showed an oriented pattern after etching the surface of the nanocomposite films due to the formation of shish kebab morphology

3.5 Effect of orientation on structural properties

XRD spectra of undrawn PLA nanocomposites and pre-drawn nanocomposites after SSD are drawn one shown in Figure 7. The intensity of the peaks of FC-2-SSD-5 nanocomposites was reduced after the orientation as compared to the CM-SSD-4. This was attributed to the stress and/or strain developed during the orientation. Both CM-SSD-4 and FC-2-SSD-5 films exhibited a broad diffraction pattern with one very sharp peak at 16.3° assigned to the crystalline phase of the PLA. Some more weak diffraction peaks appeared at 6.0°, 9.3°, 9.9°, 12.3°, 16.4°, 19.3°, 23.3°, and 26.7°. This was due to α phase of the PLA. A newly peak appeared at 31.0° corresponding to the (003) plane attributed to the β phase of PLA. It can be formed due to the stress-induced crystallization of PLA. It further confirmed the orientation of the polymer chains of the PLA nanocomposites. The crystallite size of the sharpest peak i.e., 16.3° of CM-SSD-4 and FC-2-SSD-5 was 8 nm and 7 nm, respectively. However, the average crystallite size of all peak (including weak and strong peaks) of the FC-2-SSD-4 nanocomposites was reduced to 40 nm with respect to the CM-SSD-4 nanocomposites (47 nm). This structural change was the reason for the drastic increase in the toughness of the drawn nanocomposite films. In a study performed by Jariyasakoolroj et al.[38], oriented PLA films using bi-axial stretching and observed that very small crystallite lamellae of about 10 nm size. They also reported that the smaller crystallite size of the PLA resulted in the improvement in the toughness (3 times increased) of the PLA.

FTIR has also been carried out to understand the influence of orientation on the structure of the nanocomposites and spectra has been presented in Figure 7b. Drawn nanocomposites exhibited a reduced intensity compared to the undrawn nanocomposites. The main difference was noticed in the fingerprint region, especially in the range of 1200 -1000 cm^{-1}. Undrawn nanocomposites showed peaks at 1082 cm^{-1} and 1180 cm^{-1} that shifted to higher wavenumber in drawn nanocomposites (1089 cm^{-1}, 1184 cm^{-1}). This can be because of the intermolecular interactions developed between the PLA with ChNC and GTA.

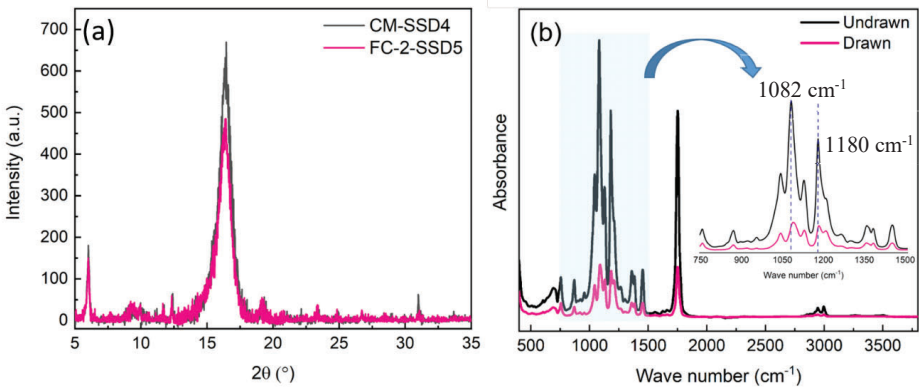

Figure 7. XRD spectra of (a) undrawn and pre-drawn samples after solid-sate drawing. (b) ATR-FTIR of undrawn and drawn nanocomposite films. Figure print region of the spectra showing that bands of drawn nanocomposite are shifting towards the higher wave number.

It was shown that the orientation of the structure has greatly influenced the properties of the PLA nanocomposites. The schematic of the ordering of the molecular chains during the orientation have shown in the Figure 8. Semicrystalline polymers exhibit two regions, one is the amorphous part and other one is a crystalline part. Generally, the amorphous part plays an important role at the time of stretching or stress. In this study, during melt state drawing, PLA chain must have folded together and formed some spherulites as depicted in Figure 8 (a-b). As mentioned before, the SSD employed after MSD in the present study. SSD was done at 60°C, therefore during the stretching, some tie molecules must have developed in the PLA nanocomposites, especially in the amorphous part. Due to the formation of tie-molecules in the amorphous region of the polymer, the mechanical properties of the drawn nanocomposites have increased especially the toughness and strength. These tie molecules can be attached to the crystalline lamellae and help in the flexibility of the nanocomposites. The reason for the formation of the tie molecules can be the presence of –NH_2-CO- group in the molecular structure of the nanochitin that can form some hydrogen bond interaction with the polymer (PLA) and plasticizer (GTA).

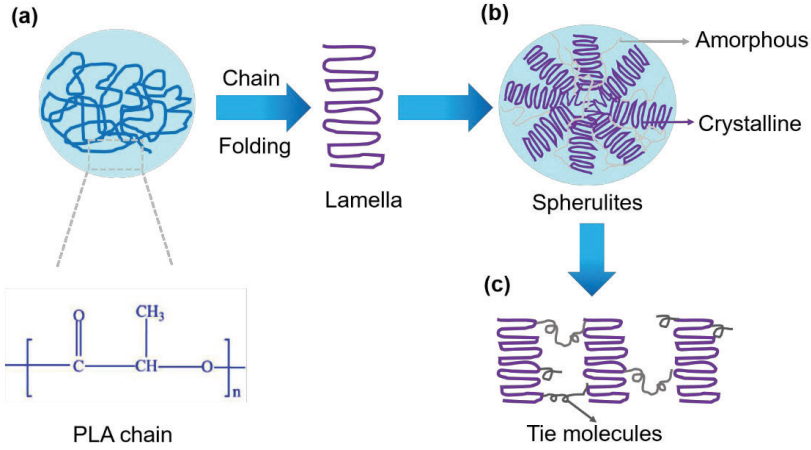

Figure 8. Schematics representing the ordering of the polymer chains during the orientation of the nanocomposites (a) arrangement of the polymer chains to form the ordered lamella (b) shows the amorphous and crystalline part of the PLA (c) formation of tie molecules in the amorphous part of PLA due to the orientation

5. Conclusions

Oriented PLA-GTA-ChNC nanocomposite films were produced by combining film melt- and solid-state drawing. A two-step orientation procedure has influenced the overall properties of the nanocomposites. Further, the pre-orientation of the polymer chains achieved by MSD had enhanced the flexibility of the polymeric chains and alignments of ChNCs, resulted in improved properties.

The effect of the orientation on nanocomposites thermal, mechanical, surface morphology, and structural behavior studied. The results confirmed that the orientation achieved by combining both MSD and SSD affected the degree of crystallinity of the nanocomposites. This was due to the orientation of the ChNC and molecular chains PLA as well as strain-induced crystallization led to an increase in the degree of crystallinity of highly oriented nanocomposite films made by two-step orientation. Therefore, the degree of crystallinity of FC-2-SSD-5 increased from 8% to 53% as compared to CM nanocomposite films. Noticeably, the mechanical properties of the nanocomposites also immensely influenced by the pre-orientation resulted in good mechanical properties. Multiple fold increment observed in the tensile modulus (2 fold), tensile strength (5 fold), elongation at break (25 fold), and toughness (96 fold) of the FC-2-SSD-5 nanocomposites compared to the undrawn nanocomposites. Furthermore, the surface of the un-oriented and oriented nanocomposite films observed with polarized microscopy. Oriented films exhibited more homogenous colors due to the strain-induced birefringence of the PLA developed by the drawing. It was obvious that highly drawn films showed more colors due to the alignments of the molecular chains. XRD study showed a reduction in the crystallite size due to the orientation of nanocomposite films. FT-IR further confirmed enhanced properties for drawn samples. The results obtained from the present study demonstrates the potential path for the development of sustainable materials for packaging applications.

Supplementary Materials: TGA and DSC curves of the materials are presented in the Table S1 and Figure S1, respectively.

Author Contributions: S.S, S.G., and K.O., planned the work. S.S., has performed most of the experiments, analyzed the data, written the original manuscript, edited and written the manuscript. N.H. prepared the PLA-GTA-ChNC nanocomposites. M.P., and D.S. performed MSD and written the film calendering process part in the material section. M.P, D.S., S.G. and M. Ll. reviewed and edited the manuscript. K.O., reviewed, edited written and funding acquisitions.

Funding: Bio4Energy strategic research program and NewPack BBI Horizon 2020 EU project (Grant number: 792261).

Acknowledgments: Authors are thankful to the Bio4Energy, Horizon 2020 BBI project NewPack (Grant number: 792261), and Kempe Foundation for financial support. S.S. would like to thanks Jiayuan Wei for helping in the XRD test. S.S. is grateful to the European Union for the Joint European Doctoral Programme in Advanced Material Science and Engineering (DocMASE).

Conflicts of Interest: The authors declare no conflict of interest.

References

1. Lim, L.T.; Auras, R.; Rubino, M. Processing technologies for poly(lactic acid). *Prog. Polym. Sci.* **2008**, *33*, 820–852.

2. Drumright, R.E.; Gruber, P.R.; Henton, D.E. Polylactic acid technology. *Adv. Mater.* **2000**, *12*, 1841–1846.

3. Auras, R.; Lim, L.T.; Selke, S.E.M.; Tsuji, H. *Poly(Lactic Acid): Synthesis, Structures, Properties, Processing, and Applications*; **2010**; ISBN 9780470293669.

4. El-Hadi, A.M. Increase the elongation at break of poly (lactic acid) composites for use in food

packaging films. *Sci. Rep.* **2017**, *7*, 46767.

5. Tanrattanakul, V.; Bunkaew, P. Effect of different plasticizers on the properties of bio-based thermoplastic elastomer containing poly(lactic acid) and natural rubber. *Express Polym. Lett.* **2014**, *8*, 387–396.

6. Ma, P.; Hristova-Bogaerds, D.G.; Goossens, J.G.P.; Spoelstra, A.B.; Zhang, Y.; Lemstra, P.J. Toughening of poly(lactic acid) by ethylene-co-vinyl acetate copolymer with different vinyl acetate contents. *Eur. Polym. J.* **2012**, *48*, 146–154.

7. Nagarajan, V.; Zhang, K.; Misra, M.; Mohanty, A.K. Overcoming the fundamental challenges in improving the impact strength and crystallinity of PLA biocomposites: Influence of nucleating agent and mold temperature. *ACS Appl. Mater. Interfaces* **2015**, *7*, 11203–11214.

8. Jacobsen, S.; Fritz, H.G. Plasticizing polylactide - the effect of different plasticizers on the mechanical properties. *Polym. Eng. Sci.* **1999**, *39*, 1303–1310.

9. Penning, J.P.; Grijpma, D.W.; Pennings, A.J. Hot-drawing of poly(lactide) networks. *J. Mater. Sci. Lett.* **1993**, *12*, 1048–1051.

10. Mai, F.; Tu, W.; Bilotti, E.; Peijs, T. The influence of solid-state drawing on mechanical properties and hydrolytic degradation of melt-spun poly(lactic acid) (PLA) tapes. *Fibers* **2015**, *3*, 523–538.

11. Smith, P.B.; Leugers, A.; Kang, S.; Yang, X.; Hsu, S.L. Raman characterization of orientation in poly(lactic acid) films. *Macromol. Symp.* **2001**, *175*, 81–94.

12. Ou, X.; Cakmak, M. Influence of biaxial stretching mode on the crystalline texture in polylactic acid films. *Polymer (Guildf).* **2008**, *49*, 5344–5352.

13. Xu, R.; Xie, J.; Lei, C. Influence of melt-draw ratio on the crystalline behaviour of a polylactic acid cast film with a chi structure. *RSC Adv.* **2017**, *7*, 39914–39921.

14. Iwasaki, H.; Nakamura, M.; Komatsubara, N.; Okano, M.; Nakasako, M.; Sato, H.; Watanabe, S. Controlled Terahertz Birefringence in Stretched Poly(lactic acid) Films Investigated by Terahertz Time-Domain Spectroscopy and Wide-Angle X-ray Scattering. *J. Phys. Chem. B* **2017**, *121*, 6951–6957.

15. Ou, X.; Cakmak, M. Comparative study on development of structural hierarchy in constrained annealed simultaneous and sequential biaxially stretched polylactic acid films. *Polymer (Guildf).* **2010**, *51*, 783–792.

16. Velazquez-Infante, J.C.; Gamez-Perez, J.; Franco-Urquiza, E.A.; Santana, O.O.; Carrasco, F.; Ll Maspoch, M. Effect of the unidirectional drawing on the thermal and mechanical properties of PLA films with different L -isomer content. *J. Appl. Polym. Sci.* **2013**, *127*, 2661–2669.

17. Gao, X.R.; Li, Y.; Huang, H.D.; Xu, J.Z.; Xu, L.; Ji, X.; Zhong, G.J.; Li, Z.M. Extensional Stress-

Induced Orientation and Crystallization can Regulate the Balance of Toughness and Stiffness of Polylactide Films: Interplay of Oriented Amorphous Chains and Crystallites. *Macromolecules* **2019**, *52*, 5278–5288.

18. Singh, A.A.; Geng, S.; Herrera, N.; Oksman, K. Aligned plasticized polylactic acid cellulose nanocomposite tapes: Effect of drawing conditions. *Compos. Part A Appl. Sci. Manuf.* **2018**, *104*, 101–107.

19. Geng, S.; Yao, K.; Zhou, Q.; Oksman, K. High-Strength, High-Toughness Aligned Polymer-Based Nanocomposite Reinforced with Ultralow Weight Fraction of Functionalized Nanocellulose. *Biomacromolecules* **2018**, *19*, 4075–4083.

20. Singh, A.A.; Wei, J.; Herrera, N.; Geng, S.; Oksman, K. Synergistic effect of chitin nanocrystals and orientations induced by solid-state drawing on PLA-based nanocomposite tapes. *Compos. Sci. Technol.* **2018**, *162*, 140–145.

21. Herrera, N.; Roch, H.; Salaberria, A.M.; Pino-Orellana, M.A.; Labidi, J.; Fernandes, S.C.M.; Radic, D.; Leiva, A.; Oksman, K. Functionalized blown films of plasticized polylactic acid/chitin nanocomposite: Preparation and characterization. *Mater. Des.* **2016**, *92*, 846–852.

22. Walker, J.; Melaj, M.; Giménez, R.; Pérez, E.; Bernal, C. Solid-State Drawing of Commercial Poly(Lactic Acid) (PLA) Based Filaments. *Front. Mater.* **2019**, *6*, 280 .

23. Mathew, A.P.; Oksman, K.; Sain, M. The effect of morphology and chemical characteristics of cellulose reinforcements on the crystallinity of polylactic acid. *J. Appl. Polym. Sci.* **2006**, *101*, 300–310.

24. Ljungberg, N.; Wesslén, B. Preparation and properties of plasticized poly(lactic acid) films. *Biomacromolecules* **2005**, *6*, 1789–1796.

25. Patterson, A.L. X-Ray Diffraction Procedures for Polycrystalline and Amorphous Materials. *J. Am. Chem. Soc.* **1955**, *77*, 2030–2031.

26. Maiza, M.; Benaniba, M.T.; Quintard, G.; Massardier-Nageotte, V. Biobased additive plasticizing Polylactic acid (PLA). *Polimeros* **2015**, *25*, 581–590.

27. Maiza, M.; Benaniba, M.T.; Massardier-Nageotte, V. Plasticizing effects of citrate esters on properties of poly(lactic acid). *J. Polym. Eng.* **2016**, *36*, 371–380.

28. Singh, S.; Maspoch, M.L.; Oksman, K. Crystallization of triethyl-citrate-plasticized poly(lactic acid) induced by chitin nanocrystals. *J. Appl. Polym. Sci.* **2019**, *136*, *36*, 47936.

29. Singh, S.; Patel, M.; Schwendemann, D.; Zaccone, M.; Geng, S.; Maspoch, M.L.; Oksman, K. Effect of chitin nanocrystals on crystallization and properties of poly(lactic acid)-based nanocomposites. *Polymers (Basel).* **2020**, *12*, 3, 726.

30. Mathew, A.P.; Oksman, K.; Sain, M. Mechanical properties of biodegradable composites from

poly lactic acid (PLA) and microcrystalline cellulose (MCC). *J. Appl. Polym. Sci.* **2005**, *97*, 2014–2025.

31. Dufresne, A.; Dupeyre, D.; Paillet, M. Lignocellulosic flour-reinforced poly(hydroxybutyrate-co-valerate) composites. *J. Appl. Polym. Sci.* **2002**, *87*, 1302–1315.

32. Perego, G.; Cella, G.; Bastioli, C. Effect of molecular weight and crystallinity on poly (lactic acid) mechanical properties. *J. Appl. Polym. Sci.* **1996**, *59*, 37–43.

33. Grijpma, D.W.; Altpeter, H.; Bevis, M.J.; Feijen, J. Improvement of the mechanical properties of poly(D,L-lactide) by orientation. *Polym. Int.* **2002**, *51*, 845–851.

34. Jonoobi, M.; Harun, J.; Mathew, A.P.; Oksman, K. Mechanical properties of cellulose nanofiber (CNF) reinforced polylactic acid (PLA) prepared by twin screw extrusion. *Compos. Sci. Technol.* **2010**, *70*, 1742–1747.

35. Luis Orellana, J.; Wichhart, D.; Kitchens, C.L. Mechanical and optical properties of polylactic acid films containing surfactant-modified cellulose nanocrystals. *J. Nanomater.* **2018**, *2018*, 1-12.

36. Sun, S.P.; Wei, M.; Olson, J.R.; Shaw, M.T. Alkali etching of a poly(lactide) fiber. *ACS Appl. Mater. Interfaces* **2009,** *1*, *7*, 1572-1578.

37. Somani, R.H.; Yang, L.; Zhu, L.; Hsiao, B.S. Flow-induced shish-kebab precursor structures in entangled polymer melts. *In Proceedings of the Polymer*. **2005**, *46*, 8587–8623.

38. Jariyasakoolroj, P.; Tashiro, K.; Wang, H.; Yamamoto, H.; Chinsirikul, W.; Kerddonfag, N.; Chirachanchai, S. Isotropically small crystalline lamellae induced by high biaxial-stretching rate as a key microstructure for super-tough polylactide film. *Polymer (Guildf).* **2015**, *68*, 234–245.

Supporting Information

Effects of orientation on PLA/chitin nanocomposite films achieved via combination of melt and solid-state drawing

Shikha Singh [1,2], Mitul Patel [1], Daniel Schwendemann [1,3], Shiyu Geng [1], Natalia Herrera [1], Maria Lluisa Maspoch [2], and Kristiina Oksman [1,4,*]

[1] Division of Materials Science, Luleå University of Technology, SE-97 187 Luleå, Sweden; shikha.singh@ltu.se (S.S.); mitul.patel@ltu.se (M.P.); daniel.schwendemann@hsr.ch (D.S.); shiyu.geng@ltu.se (S.G.)

[2] Centre Català del Plàstic (CCP)-Universitat Politècnica de Catalunya Barcelona Tech (EEBE-UPC)-ePLASCOM. Avda. Eduard Maristany, 14, 08019 Barcelona, Spain Spain; maria.lluisa.maspoch@upc.edu

[3] IWK Institut für Werkstofftechnik und Kunststoffverarbeitung, CH-8640 Rapperswil, Switzerland

[4] Mechanical & Industrial Engineering, University of Toronto, Toronto, M5S 3BS, Canada

* Correspondence: Kristiina.oksman@ltu.se; Tel: +46 920 493371

The amount of plasticizer lost during the compression molding, film-calendering process was measured by TGA, and data are summarized in Table S1.

Table S1. Thermal properties obtained from TGA curves of un-oriented and pre-oriented nanocomposite films

Materials	Initial Value	Final Value	Lost plasticizer (GTA) (%)
CM	100	93.3	6.7
FC	100	93.2	6.7
FC-2	100	93.4	6.6

DSC curves of all the materials before and after solid-state drawing are presented in Figure S1.

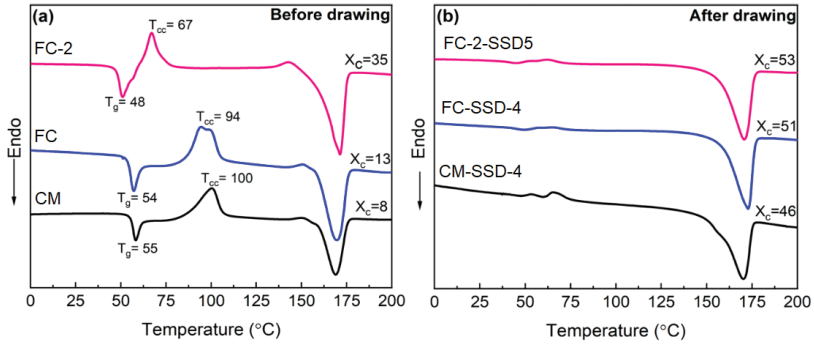

Figure S1. DSC thermograms of the reference, pre-drawn and drawn nanocomposite films taken from the first heating cycles

PAPER IV

Evaluation of Mechanical Properties of Poly (Lactic Acid)/Cellulose Nanocrystal Nanocomposites: A Comparative Study of Conventional Tensile Test and Small Punch Test

Shikha Singh, Christina Rodriguez, Orlando Santana Perez, Kristiina Oksman, Maria Lluïsa Maspoch

eXPRESS Polymer Letters, **2020** (accepted manuscript)

DOI: 10.3144/expresspolymlett.2020.92

eXPRESS Polymer Letters Vol.14, No.x (2020) x–x
Available online at www.expresspolymlett.com
https://doi.org/10.3144/expresspolymlett.2020.92

Mechanical behaviour of poly(lactic acid)/cellulose nanocrystal nanocomposites: A comparative study between conventional tensile test and small punch test

S. Singh[1,2], O. Santana-Pérez[1], C. Rodriguez[3], K. Oksman[2], M. Ll. Maspoch[1]*

[1]Centre Català del Plàstic (CCP)-Universitat Politècnica de Catalunya Barcelona Tech (EEBE-UPC)-ePLASCOM. Avda. Eduard Maristany, 14. 08019 Barcelona, Spain
[2]Luleå University of Technology (LTU), SE 97187 Luleå, Sweden
[3]IUTA, Universidad de Oviedo, Edificio Departamental Oeste, N-7, 33203 Gijón, Spain

Received 25 February 2020; accepted in revised form 25 May 2020

Abstract. The use of nanocomposites is increasingly frequent as a way to improve the mechanical behaviour of polymers. In the specific case of poly(lactic acid) (PLA), the use of cellulose nanocrystals (CNC) as a reinforcing material is an interesting option, once the tendency of CNCs to agglomerate has been solved. One of the possible solutions to this problem is a superficial modification of CNC's nanocrystals through a ring-opening polymerization (ROP) process. This work analyzes the use of CNC nanocrystals modified using ROP (mCNC) as a reinforcement of PLA. The mechanical properties of PLA/CNC nanocomposites are evaluated using tensile tests and small punch tests (SPT) on films prepared by extrusion calendering and post processed by compression molding. The addition of non-modified CNC promotes multiple crazing in PLA, increasing its ductility. mCNC leads to a more dispersed nanocomposite, a slight increase in the elastic modulus and a drastic decrease of crazing in tensile tests. The same tendency has been observed with SPT, and the applicability of this test in the prediction of the tensile modulus (E) of polymeric nanocomposites has been demonstrated. However, more work is needed to find the ideal SPT parameter to estimate the yield point.

Keywords: *biopolymers, biocomposites, material testing, poly(lactic acid) (PLA), cellulose nanocrystals (CNC), small punch test (SPT)*

1. Introduction

Poly(lactic acid) (PLA) is a bio-based polymer which has gained much attention from the research community due to its potential to substitute some oil-based polymers. It has been used in medical applications for many decades, but in recent years its application in packaging field is being explored. Its mechanical properties are similar to polystyrene (PS) and comparable to poly(ethylene terephthalate) (PET). However, it has some drawbacks such as a slow crystallization rate, low maximum temperature for use, poor barrier properties and brittleness which restrict its use in packaging applications [1, 2].

One way to reduce these drawbacks is by the addition of nanofillers. Naturally available reinforcing agents such as cellulose nanocrystals (CNC) are highly promising materials due to their availability, biodegradability, high aspect ratio and good mechanical properties [3]. CNC has been used as a reinforcing agent in polymers such as polypropylene (PP) [4] and polyvinyl alcohol (PVA) [5]. In the case of PLA, CNC has shown effectiveness as a second stage nucleating agent (during the cold crystallization process), increasing crystallinity and consequently the mechanical properties in the rubbery state (post-T_g), after undergoing a process of annealing at 80 °C

*Corresponding author, e-mail: maria.lluisa.maspoch@upc.edu

for 3 days [6]. Similar results could be inferred from the work of Yu *et al*. [7].

However, the dispersion and distribution of CNC in PLA is challenging during processing as it has a tendency to agglomerate due to its hydrophilic character as opposed to the hydrophobic nature of PLA [3]. To overcome this difficulty, efforts have been made to modify the surface of CNC using different methods [8]. One way is to graft reactive or compatible groups with PLA, on the CNC surface. In this work, the surface of CNC was modified by grafting PLA using ring-opening polymerization (ROP) [9]. This modification has a double function: it improves the dispersion and distribution of CNC, while increasing its compatibility with PLA.

One way to evaluate this compatibility is through mechanical tests. However, as in any research stage of new nanocomposites, the amount of material available can be very small, making the use of miniature tests necessary for their mechanical characterization. Among these, the small punch test (SPT) has been widely used for many years to test mechanical properties, especially those of metallic materials. Recently, researchers have started exploring its potential to test polymeric materials as well. For example, Gidding *et al*. [10] applied the technique to UHMWPE, HDPE, PTFE, polyacetal and poly(methyl methacrylate) (PMMA) bone cement. Jaekel *et al*. [11] in PEEK. Rodriguez *et al*. [12] successfully employed SPT for testing the mechanical properties of different polymers: EVOH, PP, PET, PETg and PLA sheets. The SPT was also used to characterize PLA reinforced with organically modified nanoclay (o-MMT) films [13, 14].

The small punch test can be briefly described as follows. A thin specimen is clamped between two circular dies and stretched to failure point with a hemispherical head punch at a constant displacement rate. A load cell located above the head punch measures the reaction force of the sample to the punch displacement, while the actual specimen displacement is recorded using clip-gage knife-edge extensometers. From the obtained load-punch displacement, curves are analyzed, and several parameters to identify each deformation region (elastic, plastic and failure) are obtained.

From the load-punch displacement curves, the initial slope of the curve, $Slope_{ini}$, as a measure of the elastic modulus, and the load at the first maximum, P_y, usually related to the yield strength (σ_y), according to the Equations (1) and (2) with parameters obtained from tensile tests in the case of polymeric materials:

$$E = \alpha_1 \frac{Slope_{ini}}{t} + \alpha_2 \quad (1)$$

$$\sigma_y = \beta \frac{P_y}{t^2} \quad (2)$$

where t is the initial specimen thickness and α_1, α_2 and β are characteristic material coefficients when the same devices, sample geometries and testing conditions are used [12]. Thus, a pre-requisite for using this test technique is to know the values of these coefficients a priori.

Rodríguez *et al*. [12], working with several polymeric systems, determined the values of these characteristic coefficients using a linear fit of the correlation between the SPT parameter tests and their respective E and σ obtained from tensile tests. From the global adjustment, the values obtained were 12.439, 1426.3 and 0.0971 for α_1, α_2 and β, respectively.

The main aim of this work is to evaluate the effect of the addition of a surface-modified CNC compared with unmodified one, on mechanical properties of PLA to determine its viability as a sustainable biocomposite for packaging applications. In this paper, a correlation between tensile test and small punch test (SPT) technique will be evaluated, taking into consideration the different loading modes that each of them applies. In addition, a correlation with the deformation micromechanisms involved in each loading mode is carried out.

2. Experimental section

2.1. Materials

Poly(lactic acid) (PLA) (4032D grade) was purchased from Nature Works (Nebraska, USA). The ratio of l-lactic acid and D-lactic acid in PLA was 98.6/1.4. The number average (M_n) and weight average molecular weight (M_w) of the PLA were 90 and 181 kg·mol^{-1}, respectively [15]. Cellulose nanocrystals (CNC) (2013-FPL-CNC-049) were kindly provided by Forest Products Laboratory (FPL), (Madison, USA). A needle-like structure was observed for CNC. The width and length of the CNC lied in the range of 3–11 and 161–550 nm, respectively. L-lactide, stannous octoate ($Sn(Oct)_2$), toluene, dichloromethane, chloroform and *N*,*N*-dimethylformamide (DMF) were purchased from Sigma Aldrich (St. Louis, USA). Methanol, ethanol, 1,4-dioxane,

and acetone were supplied by VWR International (Leuven, Belgium). All the chemicals and solvents were ACS grade.

2.2. Surface modification of CNC using ring opening polymerization (ROP)

To get better dispersion of CNC in PLA matrix, the surface of CNC was modified. PLA chains were grafted on the surface of CNC by ROP of L-lactide. The procedure for surface modification as followed by Mujica-Garcia *et al*. [9] was used. In short, the aqueous suspension of CNC was solvent exchanged with acetone, dichloromethane and finally with dry toluene using centrifugation and re-dispersion cycles. L-lactide was dissolved in dry toluene in a three-neck round bottom flask connected to the condenser. After that, previously dispersed CNC was poured into the reaction flask, heated to 80 °C and stirred using a magnetic stirrer at 150 rpm. 0.2 g of $Sn(Oct)_2$ was added as a catalyst into the reaction flask dropwise using a syringe and the reaction was kept for 24 h. The product was recovered in toluene followed by redispersion cycles to remove the unreacted monomers using methanol, ethanol, and acetone. The grafting of CNC is illustrated in Figure 1. The effectiveness of this treatment was verified by FTIR as by Mujica-Garcia *et al*. [9]. In mCNC FTIR spectrum was observed the presence of an intense band at 1739 cm^{-1} corresponding to the carbonyl stretching frequency of the PLA, not present in the unmodified CNC. Moreover, the signals of L-lactide, *i.e.* 1212 and 1296 cm^{-1}, are absent, which provides the evidence that unreacted monomers are removed during washing.

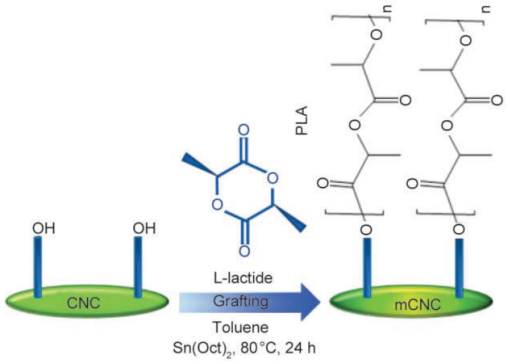

Figure 1. Scheme of PLA grafting on CNC surface via ring opening polymerization (ROP) technique.

2.3. Nanocomposites preparation

Nanocomposites of PLA with CNC and PLA with grafted CNC (mCNC) were prepared using a three-step solvent mixing technique. In the first step, PLA pellets were dissolved in 1,4 dioxane using a magnetic stirrer for 24 h. At the same time, 1 wt% CNC and 1 wt% mCNC were separately dispersed in DMF using a magnetic stirrer for 2 h and ultrasonication for 5 min. The dispersion of CNC was confirmed by flow birefringence. In step two, the dissolved PLA solution and the dispersed CNC suspensions were mixed and further stirred for 2 h and sonicated for 5 min, resulting in a homogeneous dispersion of the CNCs in the PLA matrix. In the third step, this suspension of PLA with CNC or mCNC was used to prepare microspheres by dropping the suspension in liquid nitrogen (see Figure 2). The obtained microspheres were freeze-dried and kept in sealed plastic bags for further processing. PLA nanocomposites were prepared by adding 1 wt% of unmodified and modified CNC, henceforth referred to as PLA/CNC and PLA/mCNC, respectively.

2.4. Extrusion-calendering of films

From these microspheres, extruded calandered films of approximately of 0.1 mm thick were obtained. A single screw extruder (Lab Tech Engineering Company Ltd., Samutprakan, Thailand) with $L/D = 30$ and $D = 10$ mm was used. The temperature profile ranged from 190 °C (feed zone) to 200 °C (die zone), and the screw speed was 40 rpm. During the calendering process, a hot stretching process was performed between two calendering rollers at a speed of 0.5 and 8 rpm, respectively, to obtain oriented films.

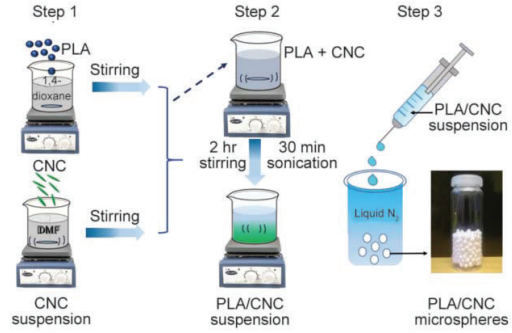

Figure 2. Schematic representation of PLA nanocomposites preparation by solvent mixing.

In order to assure a better surface quality of the samples to be tested and to keep the orientation imparted in the CNC's during the extrusion-calendering, from the 0.1 mm thick films thicker ones (0.3 mm) were prepared, stacking 3 extruded foils (films), of approximately 120 mm in length, using a compression press moulding machine (IQAP LAP PL-15; IQAP Masterbatch group SL, Barcelona, Spain). The moulding temperature was set at 190 °C, and 15 bars of pressure was applied for 30 s. After 3 minutes under pressure, the films were immediately cooled by immersing them in ice water.

To evaluate possible thermodegradation effects of this post-extrusion protocol, the viscosimetric molecular weight (M_v) was estimated through the determination of the intrinsic viscosity (IV) in chloroform at 30 °C, following the procedure described by Hakim *et al*. [16]. According to the results obtained, this processing causes a maximum loss of 8%, and there are practically no effects of degradation.

2.5. Tensile tests

The mechanical properties of the nanocomposite films were tested on a Galdabini Sun 2500 universal tensile machine (Galdabini, Cardano al Campo, Italy) equipped with a 1 kN load cell. The tensile tests were performed at room temperature with a crosshead speed of 2 mm·min^{-1}. ISO 527-2 type 1BA dumbbell test specimens were extracted from the compression moulded films using a ZCP 020 manual cutting press (Zwick, Ulm, Germany). The actual displacement of the calibrated zone was measured with a video extensometer (OS-65D CCD, Minstron, Taipei, Taiwan) coupled to a Windows-based software (Messphysik, Fürstenfeld, Austria).

Before obtaining the tensile specimens, the films were subjected to a 'physical de-aging' (rejuvenating) thermal treatment, as by Cailloux *et al*. [17], to release internal stresses present in the samples and to avoid defects during cutting. The samples were kept at room temperature with a controlled relative humidity of 50% for one week before testing.

The engineering stress-strain curves for every sample were recorded, and tensile modulus (E), tensile yield strength (σ_y), yield strain (ε_y) and strain at break (ε_b) were determined. The average values and corresponding standard deviation from five valid tests were calculated.

According to the first heating scan of DSC tests carried out on 5 mg samples taken from these dumbbell specimens, the materials showed a crystallinity of less than 6% after the first heating scan, regardless of the addition of CNC (or mCNC). Thus, they can be considered virtually amorphous, and with no crystallinity effect influencing the mechanical behaviour.

2.6. Small punch test (SPT)

Small punch tests were carried out on square samples of 10×10 mm^2 cut from the same heat-treated moulded plates as the tensile specimens. SPTs were performed using an experimental device designed and manufactured by the SIMUMECAMAT research group and mounted on a universal Instron testing machine equipped with a load cell of 5 kN. A punch diameter of 2.5 mm, a hole in the lower die with a diameter of 4 mm (with 0.2 mm corner radius) and a displacement rate of 0.2 mm·min^{-1}, were employed in all these tests. The punch displacement was measured using a COD extensometer attached between the upper and lower dies, as described by Rodríguez and coworkers [12, 18]. The thickness of the specimens was measured using a precision micrometre as the average of six measurements. Ten specimens of each material were used in the SPT characterization.

3. Results and discussions

3.1. Mechanical behaviour in the tensile test

Representative engineering stress-strain curves of all the materials are compared in Figure 3, and the characteristic parameters are summarized in Table 1. Following the usual classification in polymeric materials [19] three types of behaviour (in terms of the stress-strain traces), can be observed. Firstly, 'Ductile'

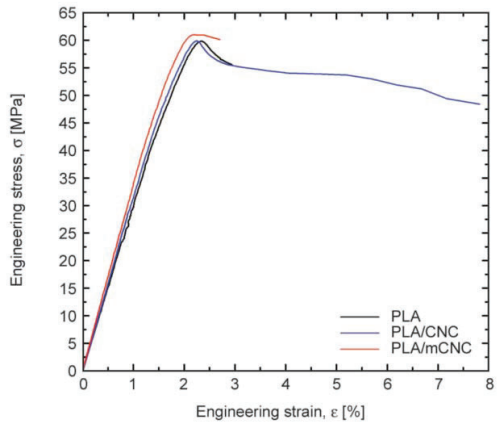

Figure 3. Engineering Stress-strain curves of PLA, PLA/CNC and PLA/mCNC.

Table 1. Tensile mechanical properties of PLA, PLA/CNC and PLA/mCNC.

		Material		
		PLA	**PLA/CNC**	**PLA/mCNC**
E	[GPa]	3.5±0.1	3.6±0.1	3.9±0.2
σ_y	[MPa]	60±1	60±2	61±2
ε_y	[%]	2.4±0.1	2.2±0.1	2.1±0.1
ε_b	[%]	3.0±0.9	8.0±1.0	2.7±0.4

behaviour for PLA: after reaching the local maximum associated with the yield, there is a decrease in the engineering stress, which could be associated with a localized necking and subsequent rupture. Secondly, in the case of PLA/CNC, 'Ductile with cold drawing' behaviour which is associated with polymers is observed: after yielding, and necking appear, the engineering stress stabilizes, usually associated with a localized neck propagation, to then break. Finally, the addition of surface-modified CNC (mCNC) drastically changes these behaviour patterns, generating the typical curve of a brittle material: after reaching the local maximum the rupture occurs without apparent generation of a neck.

A visual inspection of tested samples revealed no necking around the broken zone but rather crazes which are a highly localized yield phenomenon, confined to a very small volume of material [20]. The drop in engineering stress observed in the curves of figure 3 is due to the decrease in the load-bearing section of the specimen as a consequence of the formation of crazes. These structures are shown as a whitening area by adjusting the angle of incidence of a light beam to the fracture surface (Figure 4). It seems that the modification of the CNC drastically decreases the number of crazes (see Figure 4c) as a consequence of the expected restriction of the matrix mobility thanks to the greater PLA-CNC interaction. The best matrix interaction of PLA-CNC has an equivalent effect of increasing the density of molecular entanglements; thus the critical hydrostatic stress for craze initiation will be greater than that required in neat PLA, as have been reported with others materials [21]. During the tensile test (uniaxial solicitation), this stress is not reached, and therefore significant numbers of crazes do not appear (Figure 4c).

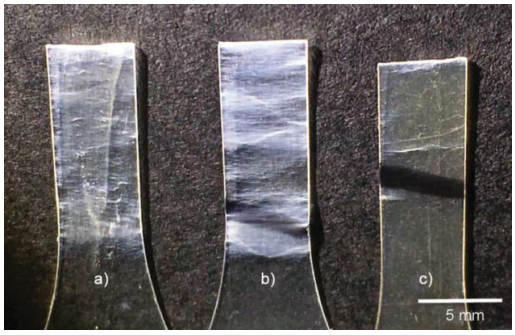

Figure 4. Photograph of broken zone from tensile specimens, (a) PLA, (b) PLA/CNC, and (c) PLA/mCNC.

In the case of unmodified CNC, a greater number of crazes are observed with respect to the PLA. The particles of CNC not adhered to the matrix may be acting as stress concentrators, thus promoting a greater number of crazes with a smaller size compared to neat PLA. This increases the volume of plastic deformation involved in the deformation process, providing a slight gain in ductility to the system [17, 20]. As can be seen in Table 1 there is an increase of 167% of the elongation at break (ε_b) with respect to neat PLA. Also, it can be observed that the addition of mCNC causes an increase of 11% in the elastic modulus of the PLA, with no apparent change when the CNC is unmodified. This may be related to a better matrix-CNC interaction promoted by the grafted PLA on the surface of the CNC.

Figure 5 shows the micrographs of the surfaces generated after a special sharp-notched dumbbell tensile sample tested at 2 mm·min^{-1}. This test was performed to view the situation without excessive tearing of the surface. It is observed that the addition of mCNC results in a greater number of cavitations of smaller size (Figure 5b) compared to those of unmodified CNC (Figure 5a). This can be attributed to the better dispersion and distribution of the CNC with PLA chain grafted on its surface. This better dispersion, together with the improved interaction with the PLA matrix, increases the reinforcement efficiency of mCNC.

3.2. Small punch test (SPT) results

It should be emphasized that in SPT a biaxial loading mode is applied. Thus, the deformation process of the sample may vary compared to the uniaxial loading mode (tensile test).

During the SPT all specimens generated a cap before the final break, typical of a ductile failure of the structure. However, two different types of breaks were observed, which have been classified as 'stable' and 'unstable'. These two different break behaviours can be detected through both the load (normalized by

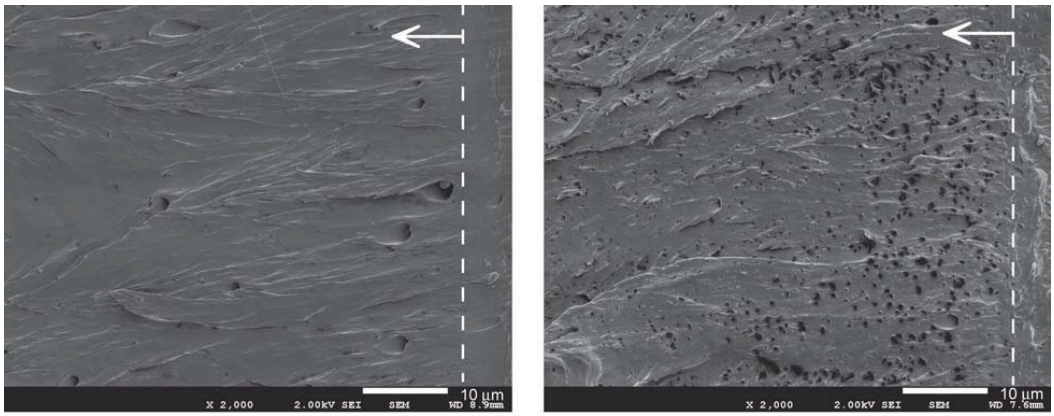

Figure 5. SEM micrographs of fracture surfaces taken from sharp-notched dumbbell tensile tests of: a) PLA/CNC and b) PLA/mCNC. Dashed line indicates the sharp-notch edge. Crack growth direction pointed with arrows.

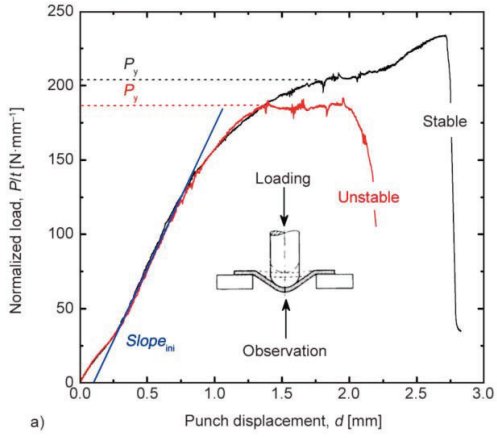

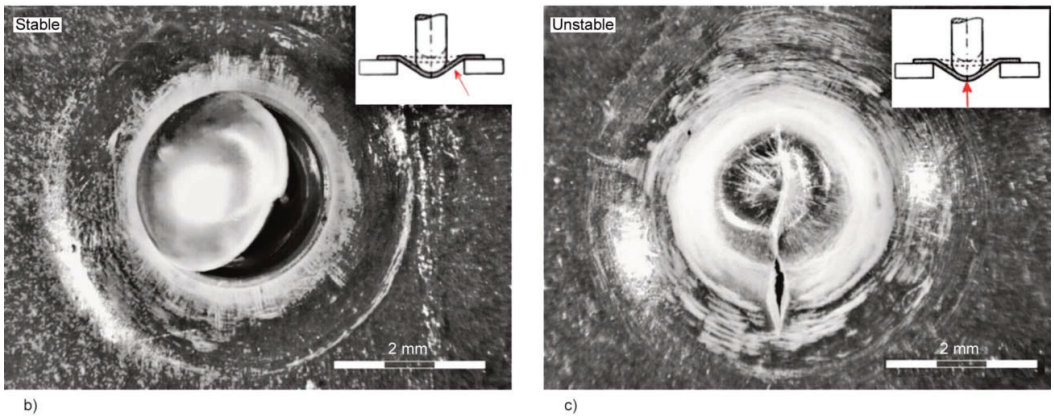

Figure 6. a) Representative thickness normalized load – punch displacement curves obtained for unstable and stable-ductile behaviour in PLA/mCNC. Inset: Simplified scheme of the loading solicitation mode during SPT. b) and c) optical micrographs of the tested samples with stable-ductile behaviour in PLA and unstable-ductile behaviour in PLA/mCNC, respectively. In upper right corner it is pointed with the arrow the location of the crack.

thickness) vs punch displacement curves (Figure 6a) and the appearance of the failure region (Figures 6b and 6c).

Figure 6a shows a schematic of the specimen during loading and the observation direction, by optical microscopy, after being tested. The traces of the normalized load-punch displacement curves in the initial zone, associated with elastic deformation, are similar for both types of failure. Differences occur once the plastic collapse stress is exceeded. In the ductile-stable behaviour, typical of the PLA and PLA/CNC, a decrease of the curve slope is observed before a new increase. This behaviour can be attributed to the combination of strain hardening of the material and friction between the specimen and the punch during its advance. In the case of unstable-failure, typical of PLA/mCNC, once a certain load level is reached, there is a sudden load drop followed by a plateau which is associated with the crack propagation.

In the case of the stable-ductile failure, the crack is located in the wall of the cap (Figure 6b) while those with unstable failure the crack is generated at the pole of the cap (Figure 6c). These facts are in agreement with the results obtained from a preliminary numerical simulation of SPT on an Ethylene Vinyl Alcohol copolymer, EVOH, (Figure 7) which has ductile behaviour in tensile tests [12]. In this case, an ideal elasto-plastic model with the EVOH tensile parameters (E and σ_y) was used. The location of the greatest stress was observed at the maximum necking region (yellow circle), where the crack appears in the materials that suffer stable-ductile failure.

However, when the capacity for plastic deformation of the material is restricted, the crack appears prematurely on the face opposite the contact with the punch (under a tensile field) and located at the pole of the cap, which is the region subjected to maximum stress values. The appearance of this new free surface limits the capacity of stress transfer in the system and restricts the propagation of the neck in the wall of the cap. Consequently, the curves do not show the zone associated with the hardening.

It should be noted that depending on the type of material, the proportion of stable-ductile to unstable-ductile failures varies. The addition of CNC in the PLA does not modify the type of failure, being 100% stable-ductile in both materials (PLA and PLA/CNC). However, after modifying the surface of the CNC, unstable-ductile failure becomes the typical mode of failure, present in more than 80% of the tested specimens. This observation could be associated with the capacity of plastic deformation of each material. The adhesion between mCNC and the matrix restricts the already limited deformation ability of PLA.

The different patterns of craze growth developed in each type of failure mode are shown in Figures 6b

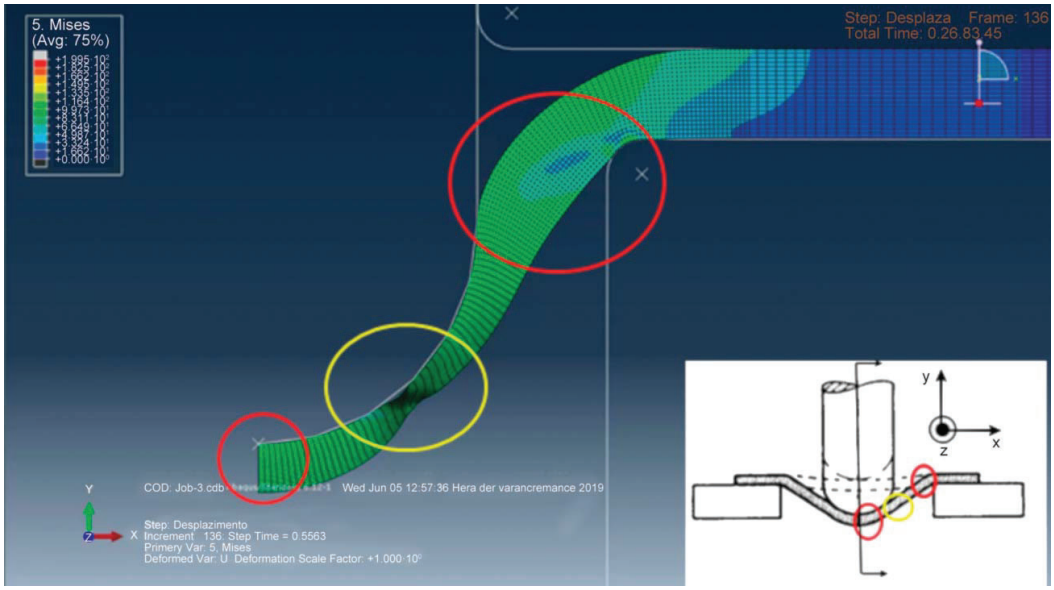

Figure 7. Image taken from a preliminary numerical simulation of the SPT test in EVOH, as an example of ductile behaviour in tensile test. Inset: Simplified scheme of the loading geometry and regions taken for monitoring the stress field involved during SPT.

and 6c. In PLA and PLA/CNC the crazes are mostly oriented in the radial direction (see Figure 6b corresponding to the PLA), concentrated in the necking area of Figure 7 (yellow circle). In the case of PLA/mCNC (Figure 6c) there is an increase in the number of crazes, and different orientation: tangential to the punch. This rise in the number of crazes increases the chances of unstable failure.

During SPT the generation of localized necking can act as a stress relief mechanism. In systems where the necking is restricted (PLA/mCNC), there is no such stress relief, so that the stress state in the red circle regions of Figure 7 can reach the critical hydrostatic stress to initiate crazes.

As it is well known, crazes appear and grow perpendicular to the resulting tensile component of the local stress field [17, 20]. In the case of PLA and PLA/CNC, this component seems to be oriented tangentially to the punch, perhaps induced by the local deformation constraint in that direction. In the case of PLA/mCNC, the tensile resultant is located radially, coinciding with the face of the sheet that is subjected to traction.

Once normalized by thickness, the obtained values of $Slope_{ini}$ and P_y ($Slope_{ini}/t$ and Py/t^2) are summarized in Table 2. The value of P_y has been defined differently for each type of breaking behaviour, *i.e.* stable-ductile and unstable-ductile. In the case of unstable failure, P_y coincides with the first registered load maximum. In the case of stable ductile behaviour, P_y is taken as the load value, after the elastic region, from which the first derivative of the load-displacement trace becomes constant again. It must be remembered that independently of the type of failure, the process involved is shear yielding, so this P_y value is related to the initiation of this process.

Table 2. SPT parameters of PLA, PLA/CNC and PLA/mCNC.

Parameter		Material		
		PLA	CNC	mCNC
$Slope_{ini}/t$	[MPa]	188±7	202±3	209±9
P_y/t_2	[MPa]	679±74	712±45	671±69
E (Predicted)	[GPa]*	3.6±0.2	3.7±0.3	3.9±0.3

*From Equation (1) and fitting values of Figure 8a.

Figures 8a and 8b show these SPT parameters ($Slope_{ini}/t$ and P_y/t^2) *versus* the corresponding experimental tensile properties (E and σ_y). These graphs also include the characteristic values of other polymeric materials reported in previous works [12] and their linear fitting coefficient by way of comparison. As can be seen in Figure 8a, the values obtained for $Slope_{ini}/t$ follow the expected trend and agree with the values of elastic modulus obtained in the tensile tests. Thus, these results corroborate that SPTs can predict the elastic modulus of polymeric materials in biaxial loading by means of Equation 1. Using the coefficients of the linear regression fit of previous work [12], the predicted values of E (Table 2) are in good agreement with the experimental ones reported in Table 1.

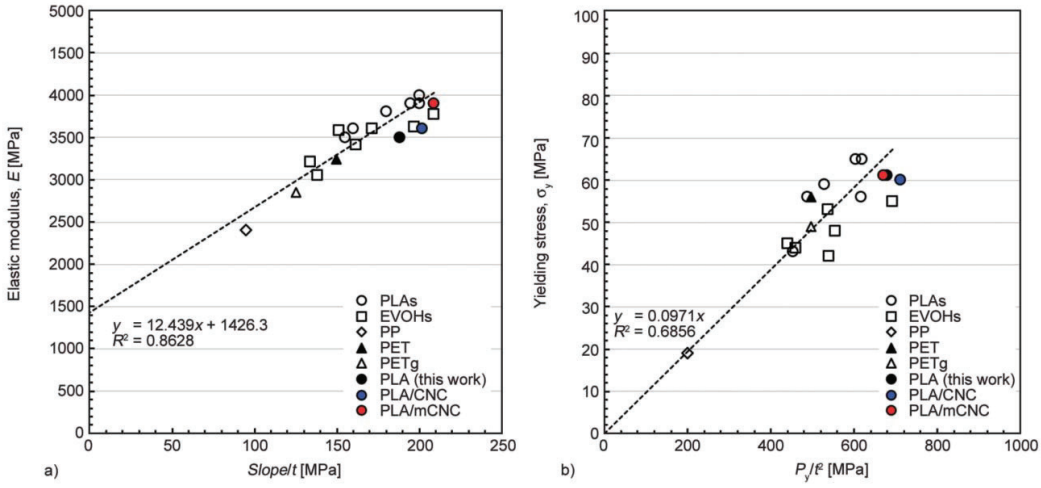

Figure 8. Graphical correlation between SPT and tensile parameters: a) $Slope_{ini}/t$ *vs.* E and b) P_y/t^2 *vs.* σ_y. Filled circles correspond to materials of this work (PLA in black, PLA/CNC in blue and PLA/mCNC in red). Other polymeric materials data are taken and adapted from [12].

However, the P_y/t^2 values do not follow any trend. Furthermore, the correlation shown in Figure 8b, corresponding to Equation 2, shows a poor linear regression fit. It must be taken into account that in this region of the mechanical behavior the viscoelastic effects take on importance. Not all polymeric materials have the same sensitivity with the deformation speed in this region.

Therefore, it may be impossible to obtain a universal β coefficient for the adjustment of different polymeric materials tested under the same conditions of displacement speeds of jaws and/or punch, since it is not guaranteed that the strain rates are the same between them. This aspect is not so critical in the elastic region of the material, where the consequences of the viscoelastic effects are minimized.

By the other side, it is necessary to clearly define how parameter P_y is determined in polymeric materials and its relationship with σ_y. Perhaps the parameter should not be P_y/t^2 but rather one which considers the punch displacement at the yield moment (d_y), $P_y/(t \cdot d_y)$, similar to that used to estimate the ultimate tensile strength in metals [18]. An extensive revision of the correlations in metallic materials has recently been proposed, as these are developed from a specified set of materials and testing conditions [22, 23].

4. Conclusions

Under uniaxial loading (tensile tests), the addition of CNC promotes multiple crazing in the PLA matrix that increases its ductility. The crazing process is reduced with the surface modification of CNC, which demonstrates better adhesion of the nanoparticle to the matrix. Under biaxial loading (SPT), depending on the type of material, the proportion of stable-ductile to unstable-ductile failures varies. The addition of CNC in the PLA does not modify the type of failure, being 100% stable-ductile in both materials (neat PLA and PLA/CNC). Adding modified CNC (mCNC), unstable-ductile failure becomes the typical mode of failure. Hence, the elastic modulus and embrittlement of PLA/mCNC increase slightly.

The applicability of the small punch test (SPT) to predict the tensile modulus, E, of nanocomposites of PLA and CNC has been shown. It is necessary to clearly define the correct way to calculate the SPT yield load, P_y, in polymeric materials as well as the correct SPT parameter that relates it with σ_y.

Acknowledgements

The authors would like to acknowledge the European Union for its financial support of Shikha Singh for the Joint European Doctoral Programme in Advanced Material Science and Engineering (DocMASE) and the Spanish Ministry of Economy and Competitiveness for the MAT2016-80045R project.

References

[1] Auras R. A., Lim L-T., Selke S. E. M., Tsuji H. T.: Poly(lactic acid): Synthesis, structures, properties, processing, and applications. Wiley, Hobodoken (2010). https://doi.org/10.1002/9780470649848

[2] Velazquez-Infante J. C., Gamez-Perez J., Franco-Urquiza E. A., Santana O. O., Carrasco F., Maspoch M. L.: Effect of the unidirectional drawing on the thermal and mechanical properties of PLA films with different L-isomer content. Journal of Applied Polymer Science, **127**, 2661–2669 (2013). https://doi.org/10.1002/app.37546

[3] Bondeson D., Syre P., Niska K. O.: All cellulose nanocomposites produced by extrusion. Journal of Biobased Materials and Bioenergy, **1**, 367–371 (2007). https://doi.org/10.1166/jbmb.2007.011

[4] Gray D. G.: Transcrystallization of polypropylene at cellulose nanocrystal surfaces. Cellulose, **15**, 297–301 (2008). https://doi.org/10.1007/s10570-007-9176-2

[5] Tanpichai S., Oksman K.: Crosslinked poly(vinyl alcohol) composite films with cellulose nanocrystals: Mechanical and thermal properties. Journal of Applied Polymer Science, **135**, 45710/1–45710/11 (2018). https://doi.org/10.1002/app.45710

[6] Mathew A. P., Oksman K., Sain M.: The effect of morphology and chemical characteristics of cellulose reinforcements on the crystallinity of polylactic acid. Journal of Applied Polymer Science, **101**, 300–310 (2006). https://doi.org/10.1002/app.23346

[7] Yu H-Y., Zhang H., Song M-L., Zhou Y., Yao J., Ni Q-Q.: From cellulose nanospheres, nanorods to nanofibers: Various aspect ratio induced nucleation/reinforcing effects on polylactic acid for robust-barrier food packaging. ACS Applied Materials and Interfaces, **9**, 43920–43938 (2017). https://doi.org/10.1021/acsami.7b09102

[8] Oksman K., Aitomäki Y., Mathew A. P., Siqueira G., Zhou Q., Butylina S., Tanpichai S., Zhou X., Hooshmand S.: Review of the recent developments in cellulose nanocomposite processing. Composites Part A: Applied Science and Manufacturing, **83**, 2–18 (2016). https://doi.org/10.1016/j.compositesa.2015.10.041

[9] Mujica-Garcia A., Hooshmand S., Skrifvars M., Kenny J. M., Oksman K., Peponi L.: Poly(lactic acid) melt-spun fibers reinforced with functionalized cellulose nanocrystals. RSC Advances, **6**, 9221–9231 (2016). https://doi.org/10.1039/C5RA22818B

[10] Giddings V. L., Kurtz S. M., Jewett C. W., Foulds J. R., Edidin A. A.: A small punch test technique for characterizing the elastic modulus and fracture behavior of PMMA bone cement used in total joint replacement. Biomaterials, **22**, 1875–1881 (2001). https://doi.org/10.1016/S0142-9612(00)00372-0

[11] Jaekel D. J., MacDonald D. W., Kurtz S. M.: Characterization of PEEK biomaterials using the small punch test. Journal of the Mechanical Behaviour of Biomedical Materials, **4**, 1275–1282 (2011). https://doi.org/10.1016/j.jmbbm.2011.04.014

[12] Rodríguez C., Cuesta I. I., Maspoch M. L., Belzunce F. J.: Application of the miniature small punch test for the mechanical characterization of polymer materials. Theoretical Applied Fracture Mechanics, **86**, 78–83 (2016). https://doi.org/10.1016/j.tafmec.2016.10.001

[13] Rodríguez C., Arencón D., Belzunce J., Maspoch M. L.: Small punch test on the analysis of fracture behaviour of PLA-nanocomposite films. Polymer Testing, **33**, 21–29 (2014). https://doi.org/10.1016/j.polymertesting.2013.10.013

[14] Maspoch M. L., Santana O. O., Cailloux J., Franco-Urquiza E., Rodriguez C., Belzunce J., Martínez A. B.: Ductile-brittle transition behaviour of PLA/o-MMT films during the physical aging process. Express Polymer Letters, **9**, 185–195 (2015). https://doi.org/10.3144/expresspolymlett.2015.20

[15] Cailloux J., Santana O. O., Franco-Urquiza E., Bou J. J., Carrasco F., Gámez-Pérez J., Maspoch M. L.: Sheets of branched poly(lactic acid) obtained by one step reactive extrusion calendering process: Melt rheology analysis. Express Polymer Letters, **7**, 304–318 (2012). https://doi.org/10.3144/expresspolymlett.2013.27

[16] Hakim R. H., Cailloux J., Santana O. O., Bou J., Sánchez-Soto M., Odent J., Raquez J. M., Dubois P., Carrasco F., Maspoch M. L.: PLA/SiO2 composites: Influence of the filler modifications on the morphology, crystallization behavior, and mechanical properties. Journal of Applied Polymer Science, **134**, 45367/1–45367/12 (2017). https://doi.org/10.1002/app.45367

[17] Cailloux J., Santana O. O., Franco-Urquiza E., Bou J. J., Carrasco F., Maspoch M. L.: Sheets of branched poly (lactic acid) obtained by one-step reactive extrusion–calendering process: Physical aging and fracture behavior. Journal of Materials Science, **49**, 4093–4107 (2014). https://doi.org/10.1007/s10853-014-8101-y

[18] García T. E., Rodríguez C., Belzunce F. J., Suárez C.: Estimation of the mechanical properties of metallic materials by means of the small punch test. Journal of Alloys and Compounds, **582**, 708–717 (2014). https://doi.org/10.1016/j.jallcom.2013.08.009

[19] Ward I. M., Sweeney J.: The mechanical properties of polymers: General considerations. in 'Mechanical properties of solid polymers: Third edition' (eds.: Ward I. M., Sweeney J.) Wiley, Chichester, 19–21 (2013). https://doi.org/10.1002/9781119967125.ch2

[20] Kinloch A. J., Young R. J.: Crazing. in 'Fracture behaviour of polymers' (eds.: Kinloch A. J., Young R. J.) Springer, Dordrecht, 147–181 (1995). https://doi.org/10.1007/978-94-017-1594-2_5

[21] Donald A. M.: Crazing. in 'The physics of glassy polymers' (eds.: Haward R. N., Young R. J.) Springer, Dordrecht, 295–339 (1997). https://doi.org/10.1007/978-94-011-5850-3_6

[22] Bruchhausen M., Austin T., Holmström S., Altstadt E., Dymacek P., Jeffs S., Lancaster R., Lacalle R., Matocha K., Petzová J.: European standard on small punch testing of metallic materials. in 'ASME 2017 Pressure Vessels and Piping Conference, Waikoloa, USA' PVP2017-65396/1–PVP2017-65396/14 (2018). https://doi.org/10.1115/PVP2017-65396

[23] Arunkumar S.: Overview of small punch test. Metals and Materials International, 26, 4545/1–4545/20 (2020). https://doi.org/10.1007/s12540-019-00454-5